Calibration of Numerical Models with Application to Groundwater Flow in the Willunga Basin, South Australia

Paul Edward Rasser

Thesis submitted for the degree of

Master of Science

in

Applied Mathematics

at

Adelaide University

(Faculty of Engineering, Computer and Mathematical Sciences)

Department of Applied Mathematics

June 1, 2001

Contents

List of Tables

List of Figures

Abstract

The process of calibrating a numerical model is examined in this thesis with an application to the flow of groundwater in the Willunga Basin in South Australia. The calibration process involves estimating unknown parameters of the numerical model so that the output obtained from the model is comparable with data that is observed in the field.

Three methods for calibrating numerical models are discussed, these being the steepest descent method, the nonlinear least squares method, and a new method called the response function method. The response function method uses the functional relationship between the model's output and the unknown parameters to determine improved estimates for the unknown parameters. The functional relationships are based on analytic solutions to simplified model problems or from previous experience.

The three calibration methods are compared using a simple function involving one parameter, an idealised steady state model of groundwater flow and an idealised transient model of groundwater flow. The comparison shows that the response function method produces accurate estimates in the least amount of iterations.

A numerical model of groundwater flow in the Willunga Basin in South Australia has been developed and the response function method used to estimated the unknown parameters for this model. The model of the Willunga Basin has been used to examine the sustainable yield of groundwater from the basin. The effect on groundwater levels in the basin using current and estimated extraction rates from the literature for sustainable yield has been examined.

The response function method has also been used to estimate the rate of extraction to return the groundwater levels at a specific location to a desirable level.

Signed Statement

This work contains no material which has been accepted for the award of any other degree or diploma in any university or other tertiary institution and, to the best of my knowledge and belief, contains no material previously published or written by another person, except where due reference has been made in the text.

I give consent to this copy of my thesis, when deposited in the University Library, being available for loan and photocopying.

SIGNED: ..... DATE: .....

Acknowledgements

I thank my supervisor, Dr Michael Teubner for his support, enthusiasm and guidance throughout this work.

Chapter 1

Introduction

Water that accumulates between the soil particles below the surface of the Earth is called groundwater. Precipitation is a contributor to a groundwater system with the water penetrating the surface and percolating downward under the influence of gravity until reaching the groundwater table or impermeable strata. Aquifers are geological units that permit the movement of groundwater, with this movement being from areas of high pressure to areas of low pressure at a rate that is dependent on such conditions as the aquifer material. Figure 1.1 shows the movement of the groundwater from the higher pressure and piezometric head at h_1 to the lower pressure and piezometric head h_2. Aquifers consisting of relatively large particles such as sand allow the groundwater to flow rapidly compared to aquifers consisting of clay. Geological units which greatly retard the movement of groundwater are called aquitards. Water is drawn from an aquifer by

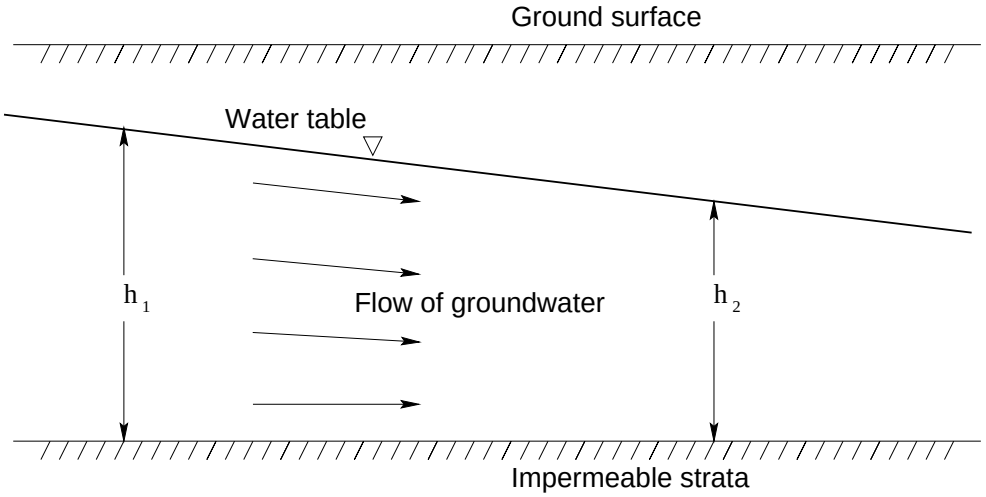

Figure 1.1: *Schematic representation of the flow of groundwater from the higher pressure h_1 to the lower pressure h_2.*

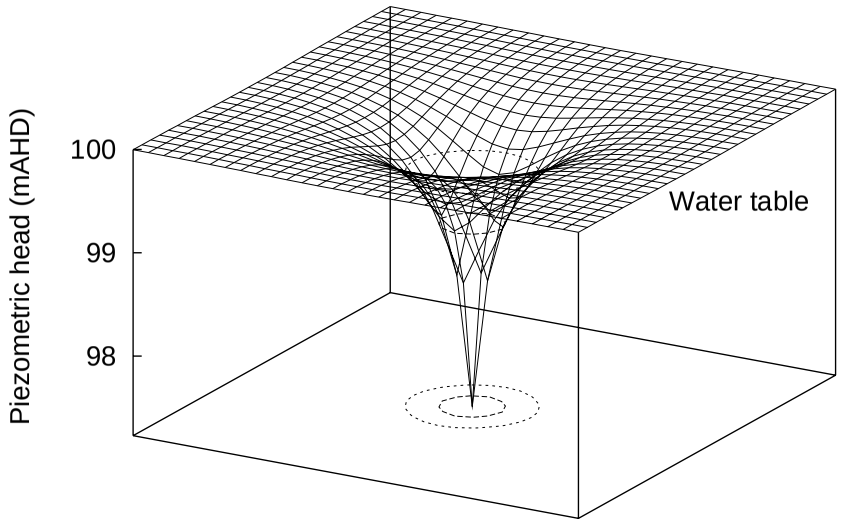

Figure 1.2: *Diagram of the effect on the water table in an aquifer resulting from extraction (mAHD = metres above head datum).*

drilling a bore or well into an aquifer where the water can be extracted. Pumping water from an aquifer has the local effect of producing a cone of depression in the groundwater table as shown in Figure 1.2. This cone of depression will gradually recede once extraction stops although the overall level of the water table may have decreased. Water can also be injected into an aquifer where it can be stored. This storage of water can then be reclaimed when needed from the aquifer. This practice is known as aquifer storage and recovery (ASR) and has all the benefits of surface water storage without the need for large areas of land together with minimising evaporation.

The flow of groundwater in an aquifer can be simulated by way of the process of numerical modelling [18, 25] which involves:

1. The development of the initial conceptual model of the site of interest.
2. The development of governing equations describing the physical system.
3. The development of the numerical solution to the governing equations.
4. Verification of the numerical solution against a known analytical solution.
5. Calibration of the numerical model.

6. Validation of the numerical model.

7. Application of the validated model.

Steps 2 and 3 of the process of numerical modelling have been well documented with many codes having being written to solve the governing equations, such as PLASM [19] and MODFLOW [9] which calculate the resulting groundwater levels. Chapter 2 of this thesis describes the groundwater flow equation and the numerical scheme used by PLASM for the numerical solution to this equation.

The main focus of this thesis is on the process of calibration of numerical models (Step 5). In the development of a numerical model, aspects of the physical system will be unknown. For the numerical modelling of groundwater flow an example of this is the transmissivity of an aquifer. The transmissivity (m^2/day) of an aquifer is a measure of the aquifer's ability to transmit water; materials such as sand have a high transmissivity whereas clay has a low transmissivity. While it is possible to determine experimentally the transmissivity of a soil type from a sample, it is impractical and highly expensive to perform this experiment on a regional scale. An important feature of groundwater in an aquifer is the standing water level. The standing water level is the level to which the water in an aquifer will rise due to pressure. Since bores or wells allow readings to be taken of standing water levels in an aquifer, they can be used to develop a time history of the water levels in the aquifer at various locations and at various times. Given the availability of standing water levels in an aquifer, the calibration of a numerical groundwater model requires the adjustment of the unknown parameters (such as transmissivity) until a satisfactory match is obtained between the output from the numerical model and what is observed in the field. In Chapter 3 of this thesis a review of some of the methods for solving the problem of calibration is provided, as well as a comparison of these methods with a new method, called the response function method, developed for the calibration process. This new method is then applied in Chapter 5 to a model of groundwater flow for the multi–aquifer system of the Willunga Basin, South Australia.

The Willunga Basin is approximately 30km south of Adelaide and is used extensively by the agricultural industry. This industry is heavily reliant on groundwater resources in the area for irrigation of grapes, almonds and olives. The Willunga Basin consists of three main water bearing units, the Port Willunga Formation aquifer, Maslin Sands aquifer and the Basement aquifer. Chapter 4 discusses these stratigraphic units and their

interactions, as well as highlighting the distribution of groundwater levels and amounts of extraction in the Basin.

Chapter 5 uses the calibration processes discussed in Chapter 3 to develop and calibrate a three-dimensional model of groundwater flow in the Willunga Basin.

The declining groundwater levels in the Willunga basin have resulted in local and state government agencies looking for new ways to manage the groundwater resource more effectively. One of the options for water allocation and management under consideration is estimating the sustainable yield for the basin. This management option is applied to the groundwater model of the Willunga Basin and appears in Chapter 6 together with an analysis of the results.

A summary and a set of conclusions are provided in Chapter 7 of this thesis.

Chapter 2

Mathematical Description of Groundwater Flow

2.1 Groundwater flow equation

The three-dimensional groundwater flow equation [8] is given by

$$\frac{\partial}{\partial x}\left(K_x\frac{\partial h}{\partial x}\right)+\frac{\partial}{\partial y}\left(K_y\frac{\partial h}{\partial y}\right)+\frac{\partial}{\partial z}\left(K_z\frac{\partial h}{\partial z}\right)=S^*\frac{\partial h}{\partial t}+Q^*, \tag{2.1}$$

where

x, y, z are Cartesian coordinates (m),

t is time (days),

h is the piezometric head (m),

S^* is the storage coefficient (m^{-1}),

K_x, K_y, K_z are conductivities in the x, y, z directions respectively (m/day),

Q^* is the net source/sink of water (m^3/day/m^3).

2.2 z-directional averaging

Groundwater systems, like the Willunga Basin in South Australia, are often made up of a collection of aquifers and aquitards. The boundaries of each hydrogeologic unit occur at significant changes in the geological material that define the particular unit. Schematically, the aquifers and aquitards generally overlay one another, with the majority of the flow of groundwater being contained within an aquifer. For this reason it is

deemed unnecessary to model the flow of groundwater in a fully three–dimensional way, and to accommodate the flow of groundwater that does occur between layers in a z–directional averaged manner. A two–dimensional layered approach to three–dimensional modelling uses the thickness and conductivity of an aquitard that separates the two aquifers to determine the leakance term which is defined to be the vertical hydraulic conductivity divided by the thickness of the aquitard [1]. From a conceptual point of view, the interaction between two aquifers through the aquitard is dependent on the piezometric head in each of the aquifers and the ability for the aquitard to transmit water between them. It is assumed that water will move from an aquifer with a high piezometric head to one with a lower piezometric head at a rate that is dependent on the conductivity of the aquitard.

To convert the full three–dimensional groundwater flow equation to a two–dimensional layered equation, Equation (2.1) can be integrated in the z-direction from the bottom of the aquifer, β metres Above Head Datum (m AHD), to the top of the aquifer, τ m AHD (head datum is taken to be Mean Sea Level). Integrating Equation (2.1) over z gives

$$\int_\beta^\tau \left\{ \frac{\partial}{\partial x}\left(K_x \frac{\partial h}{\partial x}\right) + \frac{\partial}{\partial y}\left(K_y \frac{\partial h}{\partial y}\right) + \frac{\partial}{\partial z}\left(K_z \frac{\partial h}{\partial z}\right) - S^* \frac{\partial h}{\partial t} - Q^* \right\} dz = 0. \tag{2.2}$$

Here

$$\int_\beta^\tau \frac{\partial}{\partial x}\left(K_x \frac{\partial h}{\partial x}\right) dz = \frac{\partial}{\partial x} \int_\beta^\tau \left(K_x \frac{\partial h}{\partial x}\right) dz, \tag{2.3}$$

and as K_x is assumed constant in the z–direction within an aquifer and $T_x = (\tau - \beta)K_x$, this reduces to

$$\frac{\partial}{\partial x}\left((\tau - \beta)K_x \frac{\partial h}{\partial x}\right) = \frac{\partial}{\partial x}\left(T_x \frac{\partial h}{\partial x}\right). \tag{2.4}$$

Similarly, as K_y is constant in the z–direction within an aquifer and $T_y = (\tau - \beta)K_y$ then,

$$\int_\beta^\tau \frac{\partial}{\partial y}\left(K_y \frac{\partial h}{\partial y}\right) dz = \frac{\partial}{\partial y}\left(T_y \frac{\partial h}{\partial y}\right). \tag{2.5}$$

Expanding Equation (2.2) and substituting Equations (2.4) and (2.5) gives

$$\frac{\partial}{\partial x}\left(T_x \frac{\partial h}{\partial x}\right) + \frac{\partial}{\partial y}\left(T_y \frac{\partial h}{\partial y}\right) = S\frac{\partial h}{\partial t} + Q - \left[K_z \frac{\partial h}{\partial z}\right]^\tau + \left[K_z \frac{\partial h}{\partial z}\right]^\beta \tag{2.6}$$

where

$Q = \int_\beta^\tau Q^* dz$ ($\mathrm{m}^3/\mathrm{day}/\mathrm{m}^2$) and

$S = \int_\beta^\tau S^* dz$ is the storativity.

Equation (2.6) can also be written as

$$\frac{\partial}{\partial x}\left(T_x \frac{\partial h}{\partial x}\right) + \frac{\partial}{\partial y}\left(T_y \frac{\partial h}{\partial y}\right) = S\frac{\partial h}{\partial t} + Q + K_z \frac{\partial h}{\partial z}|_{z=\beta} - K_z \frac{\partial h}{\partial z}|_{z=\tau}. \tag{2.7}$$

2.3 Methods of Solution

Equation (2.7) can be solved to estimate such quantities as the amount of draw down of the water table as a result of some extraction of groundwater, or the transmissivity when the extraction volume and draw down are known. For simple cases these solutions can be obtained analytically [28]. For confined aquifers, which are aquifers confined by an aquitard resulting in a pressure in the confined aquifer greater than atmospheric, the transmissivity is given by [28]

$$T = \frac{Q}{2\pi(h_2 - h_1)} \ln(\frac{r_2}{r_1}) \tag{2.8}$$

where T is the transmissivity (m^2/day), Q is the extraction rate (m^3/day)and h_1 and h_2 are the piezometric head (m) at two locations at distances r_1 and r_2 (m) away from the extraction well. For an unconfined aquifer, which are aquifers that are not confined by an aquitard, the conductivity K (m/day) is given by [28]

$$K = \frac{Q}{2\pi(h_2^2 - h_1^2)} \ln(\frac{r_2}{r_1}). \tag{2.9}$$

These solutions can only be used to estimate very simple groundwater scenarios. To estimate more complicated systems, numerical solutions of Equation (2.7) are needed.

2.4 Numerical Solution

A number of groundwater flow codes exist which can solve the partial differential equation (2.7) numerically. Of these, the groundwater flow code PLASM [14], which uses the method of finite–differences, is easy to modify and test, and has been extensively bench marked against various analytical solutions in it's documentation. Figure 2.1 shows the grid of the finite–difference method which is developed by discretising the solution domain by using a rectangular grid with spacings of Δx, Δy, Δz and Δt in the x, y, z and t directions respectively, where Δx, Δy and Δz are measured in metres and Δt is measured in days. Using the notation $x_i = i\Delta x$, $y_j = j\Delta y$, $z_k = k\Delta z$ and $t_n = n\Delta t$ for integer values of i, j, k and n, the piezometric head at the $(i, j, k)^{th}$ grid point at time t_n can be written as $h^n_{i,j,k} = h(x_i, y_j, z_k, t_n)$. The transmissivity in the x–direction between the grid point (i, j, k) and $(i + 1, j, k)$ can be written as $T_{i,j,k,2} = T_x(x_i, y_j, z_k)$ as shown in Figure 2.2(b). Similarly the transmissivity in the y–direction between the grid point (i, j, k) and $(i, j + 1, k)$ can be written as $T_{i,j,k,1} = T_y(x_i, y_j, z_k)$ also shown

in Figure 2.2(a). The groundwater flow code PLASM [19] uses the alternating direction implicit finite–difference scheme [14], by using block–centred finite–differences in space and a combination of forward and backward finite–differences in time. PLASM separates Equation (2.7) into the following two equations

$$\frac{\partial}{\partial x}\left(T_x\frac{\partial h}{\partial x}\right)\Big|^{n} + \frac{\partial}{\partial y}\left(T_y\frac{\partial h}{\partial y}\right)\Big|^{n+*} = S\frac{\partial h}{\partial t}\Big|^{n+*} + Q^n + K_z\frac{\partial h}{\partial z}\Big|^{n}_{z=\beta} - K_z\frac{\partial h}{\partial z}\Big|^{n}_{z=\tau}, \quad (2.10)$$

$$\frac{\partial}{\partial x}\left(T_x\frac{\partial h}{\partial x}\right)\Big|^{n+1} + \frac{\partial}{\partial y}\left(T_y\frac{\partial h}{\partial y}\right)\Big|^{n+*} = S\frac{\partial h}{\partial t}\Big|^{n+1} + Q^{n+*} + K_z\frac{\partial h}{\partial z}\Big|^{n+*}_{z=\beta} - K_z\frac{\partial h}{\partial z}\Big|^{n+*}_{z=\tau}, \quad (2.11)$$

where $n+*$ is an intermediate time step between n and $n+1$. By applying these finite–differences to Equation (2.10) gives

$$\begin{aligned}
T_{i,j,k,2}(h^n_{i+1,j,k} - h^n_{i,j,k})/(\Delta x)^2 &- T_{i-1,j,k,2}(h^n_{i,j,k} - h^n_{i-1,j,k})/(\Delta x)^2 \\
+T_{i,j,k,1}(h^{n+*}_{i,j+1,k} - h^{n+*}_{i,j,k})/(\Delta y)^2 &- T_{i,j-1,k,1}(h^{n+*}_{i,j,k} - h^{n+*}_{i,j-1,k})/(\Delta y)^2 \\
+K_z|_{i,j,k+1}(h^n_{i,j,k+1} - h^n_{i,j,k})/\Delta z &- K_z|_{i,j,k}(h^n_{i,j,k} - h^n_{i,j,k-1})/\Delta z \\
= S_{i,j,k}(h^{n+*}_{i,j,k} - h^n)/\Delta t &+ Q^n_{i,j,k}. \qquad (2.12)
\end{aligned}$$

Letting $\Delta x = \Delta y$ gives

$$\begin{aligned}
T_{i,j,k,2}(h^n_{i+1,j,k} - h^n_{i,j,k}) &- T_{i-1,j,k,2}(h^n_{i,j,k} - h^n_{i-1,j,k}) \\
+T_{i,j,k,1}(h^{n+*}_{i,j+1,k} - h^{n+*}_{i,j,k}) &- T_{i,j-1,k,1}(h^{n+*}_{i,j,k} - h^{n+*}_{i,j-1,k}) \\
+(\Delta x)^2 K_z|_{i,j,k+1}(h^n_{i,j,k+1} - h^n_{i,j,k})/\Delta z &- (\Delta x)^2 K_z|_{i,j,k}(h^n_{i,j,k} - h^n_{i,j,k-1})/\Delta z \\
= S_{i,j,k}(\Delta x)^2(h^{n+*}_{i,j,k} - h^n_{i,j,k})/\Delta t &+ Q^n_{i,j,k}(\Delta x)^2. \qquad (2.13)
\end{aligned}$$

Column calculations can be performed by moving spatially in increments of j and keeping i constant (Figure 2.1). For column calculations Equation (2.13) is written in the form

$$-T_{i,j-1,k,1}h^{n+*}_{i,j-1,k}$$

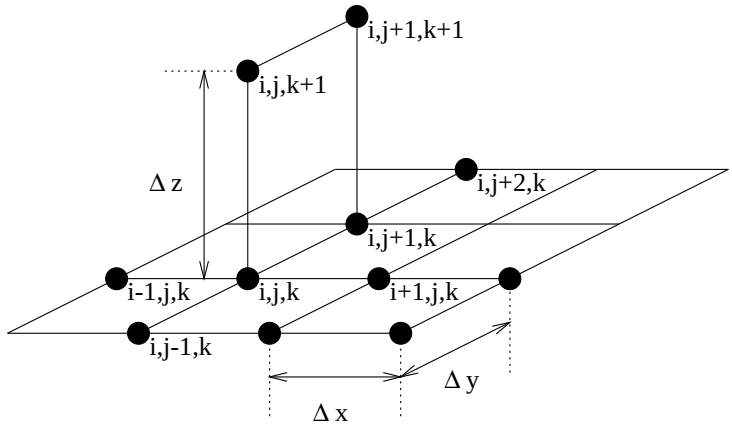

Figure 2.1: *The finite–difference grid for every time step.*

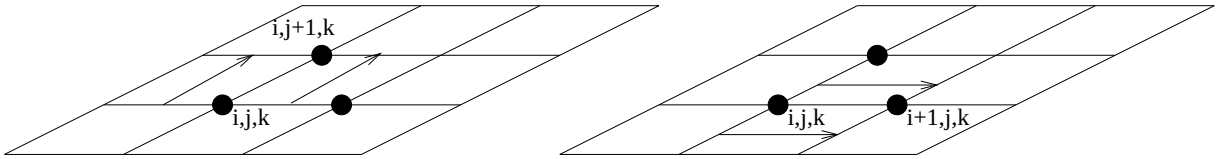

$T_{i,j,k,1}$ $T_{i,j,k,2}$

(a) (b)

Figure 2.2: *Two finite–difference grids showing* (a) *the transmissivity in the y–direction,* $T_{i,j,k,1}$ *and* (b) *the transmissivity in the x–direction,* $T_{i,j,k,2}$.

$$
\begin{aligned}
&+h^{n+*}_{i,j,k}(T_{i,j,k,1} + T_{i,j-1,k,1} + S_{i,j,k}(\Delta x)^2/\Delta t) \\
&-T_{i,j,k,1}h^{n+*}_{i,j+1,k} \\
&= S_{i,j,k}(\Delta x)^2 h^n_{i,j,k}/\Delta t - Q^n_{i,j,k}(\Delta x)^2 + T_{i-1,j,k,2}h^n_{i-1,j,k} + T_{i,j,k,2}h^n_{i+1,j,k} \\
&+L_{i,j,k+1}(h^n_{i,j,k+1} - h^n_{i,j,k}) + L_{i,j,k}(h^n_{i,j,k-1} - h^n_{i,j,k}) - h^n_{i,j,k}(T_{i-1,j,k,2} + T_{i,j,k,2})
\end{aligned} \tag{2.14}
$$

which reduces to

$$A_j h^{n+*}_{i,j-1,k} + B_j h^{n+*}_{i,j,k} + C_j h^{n+*}_{i,j+1,k} = D_j, \tag{2.15}$$

where

$A_j = -T_{i,j-1,k,1}$,

$B_j = T_{i,j,k,1} + T_{i,j-1,k,1} + SF1_{i,j,k}$,

$C_j = -T_{i,j,k,1}$ and

$D_j = SF1_{i,j,k}h^n_{i,j,k} - Q^n_{i,j,k}(\Delta x)^2 + T_{i-1,j,k,2}h^n_{i-1,j,k} + T_{i,j,k,2}h^n_{i+1,j,k} + L_{i,j,k+1}(h^n_{i,j,k+1} - h^n_{i,j,k}) + L_{i,j,k}(h^n_{i,j,k-1} - h^n_{i,j,k}) - h^n_{i,j,k}(T_{i-1,j,k,2} + T_{i,j,k,2})$,

and where

$L_{i,j,k+1} = (\Delta x)^2 K_z|_{i,j,k+1}/\Delta z$,

$L_{i,j,k} = (\Delta x)^2 K_z|_{i,j,k}/\Delta z$ and

$SF1_{i,j,k} = S_{i,j,k}(\Delta x)^2/\Delta t$.

Equation (2.15) can be solved using the Thomas algorithm [14] as the matrix generated from Equation (2.15) is tridiagonal, with all the terms in the vector generated by D_j assumed to be at the previous time level.

For row calculations Equation (2.11) in finite difference form is rearranged into

$$-T_{i-1,j,k,2}h^{n+1}_{i-1,j,k}$$

$$
\begin{aligned}
&+h^{n+1}_{i,j,k}(T_{i-1,j,k,2} + T_{i,j,k,2} + S_{i,j,k}(\Delta x)^2/\Delta t) \\
&-T_{i,j,k,2}h^{n}_{i+1,j,k} \\
&= S_{i,j,k}(\Delta x)^2 h^{n+*}_{i,j,k}/\Delta t - Q^{n+*}_{i,j,k}(\Delta x)^2 + T_{i,j-1,k,1}h^{n+*}_{i,j-1,k} + T_{i,j,k,1}h^{n+*}_{i,j+1,k} \\
&+L_{i,j,k+1}(h^{n+*}_{i,j,k+1} - h^{n+*}_{i,j,k}) + L_{i,j,k}(h^{n+*}_{i,j,k-1} - h^{n+*}_{i,j,k}) - h^{n+*}_{i,j,k}(T_{i,j,k,1} + T_{i,j-1,k,1}) \qquad (2.16)
\end{aligned}
$$

rewriting this equation as

$$
E_i h^{n+1}_{i-1,j,k} + F_i h^{n+1}_{i,j,k} + G_i h^{n+1}_{i+1,j,k} = H_i, \qquad (2.17)
$$

where

$E_i = -T_{i-1,j,k,2}$,
$F_i = T_{i-1,j,k,2} + T_{i,j,k,2} + SF1_{i,j,k}$,
$G_i = -T_{i,j,k,2}$,
$H_i = SF1_{i,j,k}h^{n+*}_{i,j,k}Q^{n+*}_{i,j,k}(\Delta x)^2 + T_{i,j-1,k,1}h^{n+*}_{i,j-1,k} + T_{i,j,k,1}h^{n+*}_{i,j+1,k} + L_{i,j,k+1}(h^{n+*}_{i,j,k+1} - h^{n+*}_{i,j,k}) +$
$L_{i,j,k}(h^{n+*}_{i,j,k-1} - h^{n+*}_{i,j,k}) - h^{n+*}_{i,j,k}(T_{i,j,k,1} + T_{i,j-1,k,1})$.

Similarly Equation (2.17) can be solved using the Thomas algorithm.

This numerical scheme is used by PLASM for the calculation of the piezometric head h when all other parameters (e.g. transmissivity and storativity) are know. This is defined to be the **forward model** for groundwater flow. This is in contrast to an **inverse model** of groundwater flow which would use known values of piezometric head to estimate values for unknown parameters such as transmissivity and storativity. In the following chapter, an inverse technique is described and later used to develop a quasi three–dimensional model of groundwater flow for the Willunga Basin in South Australia.

Chapter 3

Calibration of Numerical Models

3.1 Introduction

In Chapter 2, the forward model of groundwater flow in an aquifer was defined to be solution of h from the groundwater flow equation (2.1). This solution for h can be obtained when transmissivity, storativity, leakance, extraction and injection of water from wells, and initial and boundary conditions are known. In reality, however, the information available from the field consists of the geological boundaries, the annual injection and extraction volumes of water from the aquifers, and the sparsely distributed piezometric head. The aquifer properties such as transmissivity, storativity, and leakance are generally poorly known for confident use in the forward model.

In order to develop a forward model of a groundwater system, the unknown quantities will need to be estimated in some way, such that, when these estimates are included in the forward model, values for h can be determined at the same locations as the sparsely distributed groundwater levels observed in the field. A model that estimates the values for the unknown parameters to produce an accurate match between results from the forward model and the field data is defined to be an inverse model.

3.1.1 Trial and error

One method for solving the inverse problem of calibration for groundwater flow models is trial and error. The method of trial and error initially involves selecting values for the unknown parameters. Using these, the forward model is run and a comparison is made between the recorded piezometric head and the output from the forward model.

Generally this comparison is made using some mathematical measure such as the sum of squares or root mean square of differences between the recorded field values and output from the forward model. If the match is satisfactory, i.e. the sum of squares is less than some acceptable threshold value, then an acceptable solution has been obtained. If the match is unsatisfactory, then a second estimation is made for the unknown parameters, and so on until a satisfactory match is reached. When many parameters are sought the method of trial and error can be time consuming and so is generally not efficient in reaching an acceptable result for calibration. Despite the fact that the method of trial and error is generally slow for refinement of unknown parameter values, it does enable the modeller to assess some of the assumptions made about the model being calibrated.

3.1.2 Direct methods

Other methods for solving the inverse problem of calibration include direct methods which have been classified in reviews of inverse techniques [2, 33]. Direct methods in groundwater flow modelling assume the water levels throughout the flow domain are known, and by rearranging the groundwater flow equation (2.1), the unknown parameters can be found [24]. For example, consider the two–dimensional isotropic steady–state groundwater flow equation with no source or sink term:

$$\frac{\partial}{\partial x}\left(T\frac{\partial h}{\partial x}\right)+\frac{\partial}{\partial y}\left(T\frac{\partial h}{\partial y}\right)=0. \tag{3.1}$$

If the transmissivity can vary spatially, expanding Equation (3.1) gives

$$\frac{\partial T}{\partial x}\frac{\partial h}{\partial x}+T\frac{\partial^2 h}{\partial x^2}+\frac{\partial T}{\partial y}\frac{\partial h}{\partial y}+T\frac{\partial^2 h}{\partial y^2}=0. \tag{3.2}$$

By writing this in finite–difference form and letting $\Delta x=\Delta y$ and $T_{i,j}=T(i\Delta x, j\Delta y)$, Equation (3.2) becomes

$$\begin{aligned}(T_{i,j}-T_{i-1,j})(h_{i,j}-h_{i-1,j})/(\Delta x)^2+T_{i,j}(h_{i-1,j}-2h_{i,j}+h_{i+1,j})/(\Delta x)^2\\ +(T_{i,j}-T_{i,j-1})(h_{i,j}-h_{i,j-1})/(\Delta x)^2+T_{i,j}(h_{i,j-1}-2h_{i,j}+h_{i,j+1})/(\Delta x)^2=0,\end{aligned} \tag{3.3}$$

which gives, after reordering,

$$-(h_{i,j}-h_{i-1,j})T_{i-1,j}+(h_{i+1,j}-2h_{i,j}+h_{i,j+1})T_{i,j}-(h_{i,j}-h_{i,j-1})T_{i,j-1}=0. \tag{3.4}$$

For a solution for $T_{i,j}$, boundary conditions for $T_{i,j}$ will need to be known as well as values of $h_{i,j}$ everywhere in the computational domain. Unfortunately, the field data

regarding the piezometric head, $h_{i,j}$, are almost always very sparse and irregularly distributed making this solution method generally unusable without extensive interpolation and extrapolation [3].

Flownets are another form of inverse method. Flownets involve developing a mesh of the groundwater surface from the piezometric head surface to develop stream lines. The stream lines represent the velocities of flows within the aquifer. While flownets can be effective in estimating the transmissivity of an aquifer they are generally limited to unconfined, surficial aquifers, so that this technique requires information about the surface topology and vegetation to make an assessment of the piezometric head everywhere within the aquifer boundary [21].

3.1.3 Indirect methods

An alternative to the method of trial and error and direct methods are indirect methods. Indirect methods use the output from the forward model as a component of the inverse solution method. Indirect methods have been classified by Sun [24] to be search, gradient, or second order methods. Search methods are those that use an objective function E (e.g. least–squares) for the determination of the search sequence. Gradient methods are classified as those that use the gradient of the objective function for the determination of the search sequence, while second order methods are those that use the second order derivative of the objective function for the determination of the search sequence [24].

Indirect methods typically use an algorithm that contains the following steps:

1. Find or guess an initial value for the unknown parameters.

2. Use one of the methods, search, gradient or second order, to generate a search sequence $\mathbf{p}^1$, $\mathbf{p}^2, \ldots$, where $\mathbf{p}^1$, $\mathbf{p}^2, \ldots$, are iterate parameter sets of m unknown parameters such that $\mathbf{p}^t = (p_1^t, p_1^t, ..., p_m^t)$ and where $E(\mathbf{p}^t) > E(\mathbf{p}^{t+1})$ for some t. Here, $E(\mathbf{p}^t)$ and $E(\mathbf{p}^{t+1})$ are objective functions (mathematical measures) that compare the observed field data and the output from the forward model using the parameter sets $\mathbf{p}^t$ and $\mathbf{p}^{t+1}$ respectively.

3. Continue Step 2 until the value of the objective function (mathematical measure) has reached a minimum.

Method of steepest descent

The method of steepest descent is a gradient method that minimises the sum of squares of differences between the observed standing water levels from the field and the output from the model at corresponding locations [24]. It is based on finding the minimum of a function, f [13]. The minimum is found by determining the value of τ and $\mathbf{z}(\tau) = \mathbf{p}^t - \tau\nabla f(\mathbf{p}^t)$, for which $f(\mathbf{z}(\tau))$ has a minimum. This value of $\mathbf{z}(\tau)$ is then taken as the next approximation for $\mathbf{p}$ and the process repeated.

The sum of squares of differences between the n field observations h_i^{obs} for $i = 1, \ldots, n$ and the results from the forward model H_i using the parameter set $\mathbf{p}^t = (p_1^t, \ldots p_m^t)$, in the forward model is given by

$$E(\mathbf{p}^t) = \sum_{i=1}^{n} [h_i^{obs} - H_i(\mathbf{p}^t)]^2, \tag{3.5}$$

so that

$$[\nabla E(\mathbf{p}^t)]_j = -2\sum_{i=1}^{n} [h_i^{obs} - H_i(\mathbf{p}^t)](\partial H_i(\mathbf{p}^t)/\partial p_j) \qquad \text{for } j = 1, \ldots, m, \tag{3.6}$$

where $\nabla E(\mathbf{p}^t) = (\partial E(\mathbf{p}^t)/\partial p_1, \partial E(\mathbf{p}^t)/\partial p_2, \ldots, \partial E(\mathbf{p}^t)/\partial p_m)$. Let the $n \times m$–dimensional matrix $\mathbf{A} = [\partial H_i(\mathbf{p}^t)/\partial p_j]_{n,m}$ and the n–dimensional vector $\mathbf{h} = [h_i^{obs} - H_i(\mathbf{p}^t)]_{n,1}$, so that

$$\nabla E(\mathbf{p}^t) = -2\mathbf{A}^{\mathbf{T}}\mathbf{h}. \tag{3.7}$$

Define

$$\mathbf{z}(\tau) = \mathbf{p}^t - \tau(\nabla E(\mathbf{p}^t)), \tag{3.8}$$

so that

$$\mathbf{z}(\tau) = \mathbf{p}^t + 2\tau(\mathbf{A}^{\mathbf{T}}\mathbf{h}). \tag{3.9}$$

Substitution of Equation (3.9) for $\mathbf{p}^t$ in Equation (3.5) yields

$$E(\mathbf{z}(\tau)) = \sum_{i=1}^{n} [h_i^{obs} - H_i(\mathbf{p}^t + 2\tau(\mathbf{A}^{\mathbf{T}}\mathbf{h})]^2. \tag{3.10}$$

and differentiation with respect to τ gives

$$dE(\mathbf{z}(\tau))/d\tau = -2\sum_{i=1}^{n} [h_i^{obs} - H_i(\mathbf{p}^t + 2\tau(\mathbf{A}^{\mathbf{T}}\mathbf{h})](dH_i(\mathbf{p}^t + 2\tau(\mathbf{A}^{\mathbf{T}}\mathbf{h})/d\tau). \tag{3.11}$$

E will be a minimum when Equation (3.11) equals zero. Setting $dE(\mathbf{z}(\tau))/d\tau = 0$ and assuming $(dH_i(\mathbf{p}^t + 2\tau(\mathbf{A}^{\mathbf{T}}\mathbf{h})/d\tau) \neq 0$, which must be the case otherwise the model output will be constant for all parameter values, gives

$$\sum_{i=1}^{n} [h_i^{obs} - H_i(\mathbf{p}^t + 2\tau(\mathbf{A}^{\mathbf{T}}\mathbf{h})] = 0. \tag{3.12}$$

Since $A_{i,j} = \partial H_i(\mathbf{p}^t)/\partial p_j$ then $H_i(\mathbf{p}^t) = A_{i,j}p_j + c_i$ for $i = 1, \ldots, n$ and $j = 1, \ldots, m$. Both $A_{i,j}$ and c_i can be determined from $m + 1$ runs of the forward model, where each parameter p_j is perturbed in turn from its initial value. Therefore Equation (3.12) leads to, in matrix form

$$\mathbf{h}^{obs} - \mathbf{A}(\mathbf{p}^t + 2\tau(\mathbf{A}^\mathbf{T}\mathbf{h})) - \mathbf{c} = 0. \tag{3.13}$$

Multiplying through by $\mathbf{A}^\mathbf{T}$ gives

$$\mathbf{A}^\mathbf{T}\mathbf{h}^{obs} - \mathbf{A}^\mathbf{T}\mathbf{A}(\mathbf{p}^t + 2\tau(\mathbf{A}^\mathbf{T}\mathbf{h})) - \mathbf{A}^\mathbf{T}\mathbf{c} = 0. \tag{3.14}$$

Assuming $\mathbf{A}^\mathbf{T}\mathbf{A}$ is non–singular then multiplying though by $(\mathbf{A}^\mathbf{T}\mathbf{A})^{-1}$ gives

$$(\mathbf{A}^\mathbf{T}\mathbf{A})^{-1}\mathbf{A}^\mathbf{T}\mathbf{h}^{obs} - (\mathbf{A}^\mathbf{T}\mathbf{A})^{-1}\mathbf{A}^\mathbf{T}\mathbf{A}(\mathbf{p}^t + 2\tau(\mathbf{A}^\mathbf{T}\mathbf{h})) - (\mathbf{A}^\mathbf{T}\mathbf{A})^{-1}\mathbf{A}^\mathbf{T}\mathbf{c} = 0, \tag{3.15}$$

so that

$$2\tau\mathbf{A}^\mathbf{T}\mathbf{h} = (\mathbf{A}^\mathbf{T}\mathbf{A})^{-1}\mathbf{A}^\mathbf{T}(\mathbf{h}^{obs} - \mathbf{A}\mathbf{p}^t - \mathbf{c}). \tag{3.16}$$

Substitution of Equation (3.16) into Equation (3.9) gives

$$\mathbf{z}(\tau) = \mathbf{p}^t + (\mathbf{A}^\mathbf{T}\mathbf{A})^{-1}\mathbf{A}^\mathbf{T}(\mathbf{h}^{obs} - \mathbf{A}\mathbf{p}^t - \mathbf{c}), \tag{3.17}$$

where $\mathbf{z}(\tau)$ is taken to be the next approximation for the parameter set $\mathbf{p}$, so that

$$\mathbf{p}^{t+1} = \mathbf{p}^t + (\mathbf{A}^\mathbf{T}\mathbf{A})^{-1}\mathbf{A}^\mathbf{T}(\mathbf{h}^{obs} - \mathbf{A}\mathbf{p}^t - \mathbf{c}). \tag{3.18}$$

Using the forward model and initial and perturbed values for the unknown parameters, the matrix $\mathbf{A}$ and the vector $\mathbf{c}$ can be determined and used in Equation (3.18). In this way, a new estimate for the unknown parameter set $\mathbf{p}^{t+1}$ can be determined. This iteration technique is repeated until the objective function reaches a minimum.

Gauss–Newton method

The Gauss–Newton method or the generalised least squares method is a second order indirect inverse technique that can be applied to groundwater flow model calibration [5, 15, 24, 27]. It is derived from the multivariable Taylor series [6] for a function F:

$$F(\mathbf{p}^{t+1}) = F(\mathbf{p}^t) + (\mathbf{p}^{t+1} - \mathbf{p}^t)^\mathbf{T}\nabla F(\mathbf{p}^t) + HOT, \tag{3.19}$$

where $\mathbf{p}^t$ and $\mathbf{p}^{t+1}$ are parameter sets and HOT are second and higher order terms. Let the objective function E be equal to the sum of squares of differences between the n field

observations h_i^{obs} for $i = 1, \ldots, n$ and the results from the forward model H_i using the parameter set $\mathbf{p}^t = (p_1^t, \ldots p_m^t)$, that is,

$$E(\mathbf{p}^t) = \sum_{i=1}^{n} [h_i^{obs} - H_i(\mathbf{p}^t)]^2. \tag{3.20}$$

The values for $\mathbf{p}^{t+1}$ such that $E(\mathbf{p}^{t+1})$ is a minimum occurs when $\nabla E(\mathbf{p}^{t+1}) = 0$, so by letting $F(\mathbf{p}^{t+1}) = \nabla E(\mathbf{p}^{t+1})$ in Equation (3.19) the minimum occurs when

$$\nabla E(\mathbf{p}^t) + (\mathbf{p}^{t+1} - \mathbf{p}^t)^T \nabla^2 E(\mathbf{p}^t) \approx 0. \tag{3.21}$$

Differentiating Equation (3.20) with respect to each of the unknown parameters gives

$$\partial E(\mathbf{p}^t)/\partial p_j = -2 \sum_{i=1}^{n} [h_i^{obs} - H_i(\mathbf{p}^t)](\partial H_i(\mathbf{p}^t)/\partial p_j) \qquad \text{for } j = 1, \ldots, m. \tag{3.22}$$

Define the $n \times m$–dimensional matrix $\mathbf{A} = [\partial H_i(\mathbf{p}^t)/\partial p_j]_{n,m}$ and the n–dimensional vector $\mathbf{h} = [h_i^{obs} - H_i(\mathbf{p}^t)]_{n,1}$, so that Equation (3.22) becomes

$$\nabla E(\mathbf{p}^t) = -2\mathbf{A}^\mathbf{T}\mathbf{h}. \tag{3.23}$$

Differentiating Equation (3.20) twice with respect to each of the unknown parameters gives

$$\nabla^2 E(\mathbf{p}^t) \approx 2 \sum_{i=1}^{n} (\partial H_i(\mathbf{p}^t)/\partial p_j)(\partial H_i(\mathbf{p}^t)/\partial p_k) \quad \text{for } j = 1, \ldots, m, \text{ and } k = 1, \ldots, m, \tag{3.24}$$

where the second order terms are assumed to be small compared with the first order terms, and have been omitted, leading to.

$$\nabla^2 E(\mathbf{p}^t) = 2\mathbf{A}\mathbf{A}^\mathbf{T}. \tag{3.25}$$

Substituting Equations (3.23) and (3.25) into Equation (3.21) gives

$$-2\mathbf{A}^\mathbf{T}\mathbf{h} + (\mathbf{p}^{t+1} - \mathbf{p}^t)^\mathbf{T}(2\mathbf{A}\mathbf{A}^\mathbf{T}) \approx 0, \tag{3.26}$$

so that

$$2\mathbf{A}^\mathbf{T}\mathbf{h} - 2(\mathbf{A}^\mathbf{T}\mathbf{A})(\mathbf{p}^{t+1} - \mathbf{p}^t) \approx 0, \tag{3.27}$$

and by simplifying and multiplying through by $(\mathbf{A}^\mathbf{T}\mathbf{A})^{-1}$ gives

$$(\mathbf{A}^\mathbf{T}\mathbf{A})^{-1}\mathbf{A}^\mathbf{T}\mathbf{h} - (\mathbf{A}^\mathbf{T}\mathbf{A})^{-1}(\mathbf{A}^\mathbf{T}\mathbf{A})(\mathbf{p}^{t+1} - \mathbf{p}^t) \approx 0. \tag{3.28}$$

This can be reduced to

$$\mathbf{p}^{t+1} \approx \mathbf{p}^t + (\mathbf{A}^\mathbf{T}\mathbf{A})^{-1}\mathbf{A}^\mathbf{T}\mathbf{h}. \tag{3.29}$$

Using the forward model and initial and perturbed values for the unknown parameters, the matrix $\mathbf{A}$ and the vector $\mathbf{h}$ can be determined and used in Equation (3.29). In this way, a new estimate for the unknown parameter set $\mathbf{p}^{t+1}$ can be determined. This re–estimation is repeated until the objective function E reaches a minimum.

Non–linear least squares

In defining the matrix $\mathbf{A} = [\partial H_i(\mathbf{p}^t)/\partial p_j]_{n,m}$ in the previous section, it is easiest to assume a linear relationship between $H_i(\mathbf{p})$ and $\mathbf{p}$ which might be written as

$$H_i = A_{i,j}p_j + c_i \qquad \text{for } i = 1, \ldots, n, j = 1, \ldots, m, \tag{3.30}$$

where H_i is the set of solutions from the forward model using the set of parameters p_j. However, non–linear relationships can be assumed between the unknown parameters and the observed field data [27]. For instance, the relationship between H_i and p_j may take a quadratic form, viz

$$H_i = B_{i,j}p_j^2 + c_i \tag{3.31}$$

where $B_{i,j}$ and c_i can be estimated using two simulations of the forward model. Then

$$\partial H_i/\partial p_j = 2B_{i,j}p_j, \tag{3.32}$$

and this can be used to formulate the matrix $\mathbf{A}$ in Equation (3.29). These non–linear relationships can be determined from analytic solutions to simple groundwater flow scenarios as in Equation (2.9), or from previous experience [27].

Levenberg–Marquardt method

Using indirect methods such as linear and non–linear least squares can cause the iterate solution to move away from the true solution if the relationship between the unknown parameters and the output from the forward model is non–linear [16]. Using a Levenberg–Marquardt parameter [24], Marquardt [16] developed an algorithm that would force the linear solution to approximate the non–linearity of the unknown parameter [12, 22]. The Levenberg–Marquardt parameter, λ, is used in the non–linear least squares formulation of Equation (3.29) in the method described by Sun [24] as the Gauss–Newton–Levenberg–Marquardt method. This is also the method used by the inverse code MODFLOWP [10]. This method is used when the estimations determined from the Gauss–Newton method result in $E(\mathbf{p}^{t+1}) > E(\mathbf{p}^t)$, where $\mathbf{p}^{t+1}$ and $\mathbf{p}^t$ are successive estimated parameter sets.

By incorporating the Levenberg–Marquardt parameter λ into the Gauss–Newton formula (3.29), the value of λ can be increased by factors of 10 whenever $E(\mathbf{p}^{t+1}) > E(\mathbf{p}^t)$. The addition of the Levenberg–Marquardt parameter λ into the Gauss–Newton formula (3.29) gives

$$\mathbf{p}^{t+1} \approx \mathbf{p}^t + (\mathbf{A^T A} + \lambda \mathbf{I})^{-1} \mathbf{A^T h} \tag{3.33}$$

where $\mathbf{I}$ is the $n \times n$ identity matrix. It can be seen that as λ is increased the elements of matrix $(\mathbf{A^T A} + \lambda \mathbf{I})^{-1}$ decrease, so that the step size in moving from $\mathbf{p}^t$ to $\mathbf{p}^{t+1}$ is reduced.

3.2 Response functions and calibration

With the indirect methods described above, the objective function E is used for the determination of the search sequence. The method that follows, while it can be classified as an indirect method as it uses the forward model as part of the inverse solution, approaches the inverse problem of calibration by assuming that the response from the forward model for each parameter can be represented using either a linear or a non-linear function [20, 27]. To further expand on this idea, assume that the forward model has one unknown parameter (eg. transmissivity) and there exists one recorded head value with which to compare the forward model. If the forward model is run a large number of times with different values for the unknown parameter, a relationship between the unknown parameter and the output from the forward model will become evident. Figure 3.1 shows a pointwise relationship that may occur between the unknown parameter and the model output. This relationship can be approximated using some function known as a response function. As it is desirable to reduce the number of runs of the forward model, by assuming a relationship of the form

$$h = af(p) + c, \tag{3.34}$$

where h is the output from the forward model, p is the unknown parameter and $f(p)$ is either an exponential function (i.e. $f(p) = \mathrm{e}^p$ or $f(p) = p^{q/r}$ where q and r are integers with $r \neq 0$) or a logarithmic function (i.e. $f(p) = \log(p)$), only two runs of the forward model are required to determine the coefficients a and c. In this way a relationship between the unknown parameter and the forward model output is formed. Given this relationship and the recorded value that is wished to be matched by the forward model, the recorded value can be substituted into Equation (3.34) and the unknown parameter

value p determined. That is, if the recorded piezometric head is written as h^R, then the unknown parameter value p^R will satisfy the equation

$$p^R = f^{-1}\left(a^{-1}(h^R - c)\right). \tag{3.35}$$

The response functions f are based on past experience, or on existing analytic solutions to simplified groundwater flow problems [27] such as those suggested by Equations (2.8) and (2.9).

Applying this same principle to n recorded head values and m different parameter values, results in the following formulation. By assuming the water levels, h_i, at the n recorded head locations can be expressed as functional combinations of the m unknown parameters, p_j, where $n \geq m$ then,

$$h_i = \sum_{j=1}^{m} A_{ij} f_j(p_j) + c_i \qquad \text{for } i = 1, \ldots, n, \tag{3.36}$$

where $f_j(p_j)$ are the predetermined response functions, with c_i and A_{ij} the functional coefficients. In matrix form, Equation (3.36) can be written as:

$$\mathbf{h} = \mathbf{A}\mathbf{f}(\mathbf{p}) + \mathbf{c}, \tag{3.37}$$

where $\mathbf{f}(\mathbf{p}) = (f_1(p_1), \ldots, f_m(p_m))^{\mathrm{T}}$. The $n \times m$–dimensional matrix, $\mathbf{A}$ and the n–dimensional vector $\mathbf{c}$, can be found by running the model $m+1$ times using initial values, $\mathbf{p}^I = (p_1^I, \ldots, p_m^I)^{\mathrm{T}}$, and perturbed estimates, $\mathbf{p}^* = (p_1^*, \ldots, p_m^*)^{\mathrm{T}}$, for the unknown parameters, where the first perturbed run would use the parameter set $\mathbf{p}^{*1} = (p_1^*, p_2^I \ldots, p_m^I)^{\mathrm{T}}$

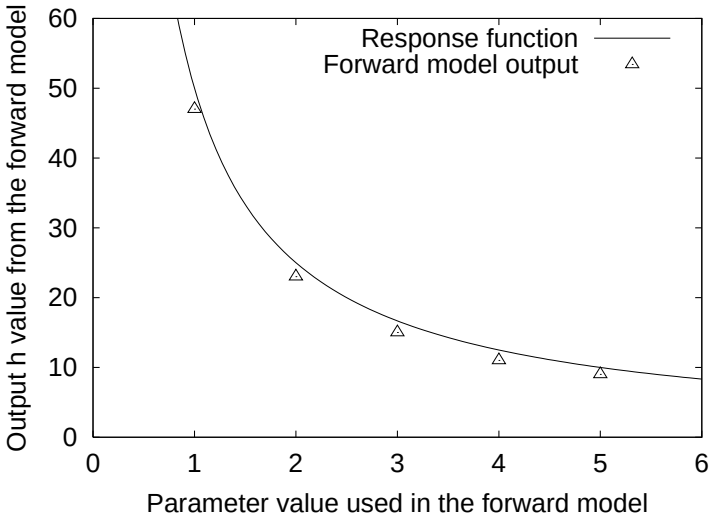

Figure 3.1: *Diagram of model output and approximate response function.*

[27]. Multiplying Equation (3.37) through by $(\mathbf{A^T A})^{-1}\mathbf{A^T}$, assuming $(\mathbf{A^T A})^{-1}$ is non–singular, gives

$$(\mathbf{A^T A})^{-1}\mathbf{A^T h} = (\mathbf{A^T A})^{-1}\mathbf{A^T A f(p)} + (\mathbf{A^T A})^{-1}\mathbf{A^T c}, \tag{3.38}$$

which simplifies to

$$(\mathbf{A^T A})^{-1}\mathbf{A^T h} = \mathbf{f(p)} + (\mathbf{A^T A})^{-1}\mathbf{A^T c}. \tag{3.39}$$

It is known that $\mathbf{h}^I$ is the solution from the model when the parameter values $\mathbf{p}^I$ are used and so

$$\mathbf{h}^I = \mathbf{A f}(\mathbf{p}^I) + \mathbf{c}, \tag{3.40}$$

i.e.

$$\mathbf{c} = \mathbf{h}^I - \mathbf{A f}(\mathbf{p}^I). \tag{3.41}$$

Upon substitution of $\mathbf{c}$ from Equation (3.41) into Equation (3.39) gives

$$(\mathbf{A^T A})^{-1}\mathbf{A^T h} = \mathbf{f(p)} + (\mathbf{A^T A})^{-1}\mathbf{A^T}(\mathbf{h}^I - \mathbf{A f}(\mathbf{p}^I)), \tag{3.42}$$

so that

$$(\mathbf{A^T A})^{-1}\mathbf{A^T h} = \mathbf{f(p)} + (\mathbf{A^T A})^{-1}\mathbf{A^T h}^I - \mathbf{f}(\mathbf{p}^I), \tag{3.43}$$

and after rearranging yields

$$\mathbf{f(p)} = \mathbf{f}(\mathbf{p}^I) + (\mathbf{A^T A})^{-1}\mathbf{A^T}(\mathbf{h} - \mathbf{h}^I). \tag{3.44}$$

Using the vector of recorded heads $\mathbf{h^R}$ as the "true solution" and solving Equation (3.44) for $\mathbf{p}$ gives the iterate equation:

$$p_j^1 = f_j^{-1}\left(f_j(p_j^I) + (\mathbf{A^T A})^{-1}\mathbf{A^T}(\mathbf{h^R} - \mathbf{h}^I)\right) \qquad \text{for } j = 1, \ldots, m, \tag{3.45}$$

where p_j^1 are the new values for the unknown parameters. It should be noted that $n \geq m$ is a necessary condition for the existence of $(\mathbf{A^T A})^{-1}$.

In some instances when using Equation (3.45), the estimated parameter values can exceed realistic bounds as described in the section on the Levenberg–Marquardt method; this can be controlled by changing the form of the response function or adding a Levenberg–Marquardt parameter [24] so that Equation (3.45) becomes

$$p_j^{t+1} = f_j^{-1}\left(f_j(p_j^t) + (\mathbf{A}^T\mathbf{A} + \lambda\mathbf{I})^{-1}\mathbf{A^T}(\mathbf{h^R} - \mathbf{h}^t)\right) \qquad \text{for } j = 1, \ldots m, \tag{3.46}$$

where $\mathbf{I}$ is the identity matrix and λ is the Levenberg–Marquardt parameter that reduces the descent length, and $\mathbf{h}^t$ is the model output from using the parameter set $\mathbf{p}^t$. From

Equation (3.46) it can be seen that as λ tends to infinity, p_j^{t+1} tends to p_j^t. In this way the length of the step size taking p_j^t to p_j^{t+1} can be reduced. This reduction in step size by increasing the Levenberg–Marquardt parameter is also used when a parameter set from the inverse model results in a value from the objective function that is greater than the value produced from the previous parameter set, that is when

$$E(\mathbf{p}^{t+1}) > E(\mathbf{p}^t), \tag{3.47}$$

where the measure of error $E(\mathbf{p}^t)$ is chosen to be

$$\text{error} = \sum_{i=1}^{n} \frac{100}{n} \left| \frac{h_i^{obs} - H_i(\mathbf{p})}{h_i^{obs}} \right| \%, \tag{3.48}$$

This error measure has been chosen because it gives a weighted error at each location and so is less reflective of the magnitude of values being used.

3.3 Comparison of indirect methods

When linearity is assumed between the model output and the unknown parameter, the methods of steepest descent, least squares and the response function method are equivalent. The differences occur when the relationship is non–linear.

To compare the effectiveness of each of these methods for determining an unknown parameter value, a simple model consisting of two equations has been used to represent the model output at two locations (r_1 and r_2) from one unknown parameter (x). The equations given by Fletcher [7] are

$$\begin{aligned} r_1(x) &= x + 1 \\ r_2(x) &= Lx^2 + x - 1 \end{aligned} \tag{3.49}$$

where L is a constant that can be altered to increase or decrease the non–linearity of $r_2(x)$. In this case, the model's output are the values for r_1 and r_2 when a value for the unknown parameter x is used.

Using this set of two functions, several simulations have been performed using $L = 0.1, 1.0$ and 10.0; in this way the degree of non–linearity for $r_2(x)$ can be adjusted.

For the first simulation the value of L has been set to 0.1. The recorded value has been set to $x = 10.0$ and the values of $r_1(x)$ and $r_2(x)$ assumed to be known at $x = 10.0$. The inverse problem then becomes: what is the value of x that will give the "true values"

of $r_1(10.0)$ and $r_2(10.0)$. To set up the matrices and vectors for each of the methods, initial (x^I) and perturbed (x^t) values for the unknown parameter x have been used to determine $r_1(x^I)$, $r_2(x^I)$ and $r_1(x^t)$, $r_2(x^t)$. In this case the initial value for the unknown parameter was set to be 5 and the perturbed value a 10% increase to 5.5 [20]. For the linear least squares method the relationship between the unknown parameter and the output is linear, which can be written as $r_1 = A_1 x + c_1$ and $r_2 = A_2 x + c_2$. Using $r_1(x^I)$ and $r_1(x^t)$ the values of A_1 and c_1 have been determined. Similarly using $r_2(x^I)$ and $r_2(x^t)$ the values of A_2 and c_2 have been determined. The linear least squares equation (3.18) then becomes

$$x^{t+1} = x^t + (\mathbf{A^T A})^{-1}\mathbf{A}(\mathbf{h}^{obs} - \mathbf{A}x^t - \mathbf{c}) \tag{3.50}$$

where

x^{t+1} is the estimated value of the unknown parameter,

$\mathbf{A}$ is the vector (A_1, A_2),

$\mathbf{h}^{obs}$ is the vector $(r_1(10.0), r_2(10.0))^T$ and

$\mathbf{c}$ is the vector $(c_1, c_2)^T$.

For the non-linear least squares and the response function method the relationship has been chosen to be quadratic, so that $r_1 = A_1 x^2 + c_1$ and $r_2 = A_2 x^2 + c_2$. For the non-linear least squares method equation (3.33) becomes

$$x^{t+1} = x^t + (\mathbf{A^T A} + \lambda \mathbf{I})^{-1}\mathbf{A}(\mathbf{h}), \tag{3.51}$$

where

x^{t+1} is the estimated value of the unknown parameter,

$\mathbf{A}$ is the vector $(2A_1 x^t, 2A_2 x^t)$ and

$\mathbf{h}$ is the vector $(r_1(10.0) - r_1(x^t), r_2(10.0) - r_2(x^t))^T$.

For the response function method equation (3.46) becomes

$$x^{t+1} = ((x^t)^2 + (\mathbf{A^T A} + \lambda \mathbf{I})^{-1}\mathbf{A}(\mathbf{h}))^{1/2}, \tag{3.52}$$

where

x^{t+1} is the estimated value of the unknown parameter,

$\mathbf{A}$ is the vector (A_1, A_2) and

$\mathbf{h}$ is the vector $(r_1(10.0) - r_1(x^t), r_2(10.0) - r_2(x^t))^T$.

3.3.1 Results

The results shown in Tables 3.1–3.3 use (a) linear least squares, (b) non–linear least squares and (c) the response function approach to estimate the unknown parameter. For methods (b) and (c), a quadratic function was chosen as the response function for the relationship between the recorded values and the unknown parameter. The measure of

Table 3.1: *Results from the simple one–parameter model with two recorded (known) values and with $L = 0.1$, showing the estimated parameter values using (a) linear least squares, (b) non–linear least squares and (c) the response function method.*

no. of iter.	(a) Linear least squares		(b) Non-linear least squares		(c) Response function method	
	estimated parameter value	error (%)	estimated parameter value	error (%)	estimated parameter value	error (%)
0	5.000	55.62	5.000	55.62	5.000	55.62
1	8.679	15.97	14.200	56.86	10.820	10.32
2	9.779	2.73	10.580	7.31	9.942	0.72
3	9.970	0.38	9.975	0.31	10.000	0.06
4	9.996	0.05	10.000	0.03	10.000	0.01
5	9.999	0.01	10.000	0.00	10.000	0.00
exact	10.000		10.000		10.000	

error is chosen to be

$$\text{error} = \sum_{i=1}^{2} \frac{100}{2} \left| \frac{h_i^{obs} - H_i(\mathbf{p})}{h_i^{obs}} \right| \%, \tag{3.53}$$

so that error=0 when the model output and the recorded values are equal. From Tables 3.1–3.3 it can be seen that as L is increased, i.e., as the degree of non–linearity of the equation set is increased, the linear least squares method decreases in performance. The non–linear least squares method ultimately performs better than the linear least squares in each case; however the response function method performs the best. The results show that as the value L is increased so that the term Lx^2 dominates the equation set, the response function method converges increasingly faster. Also to be noted is that the linear least squares method performs better than the non-linear least squares method for only the first iteration but not for later iterations in each case.

Table 3.2: *Results from the simple one–parameter model with two recorded (known) values and with $L = 1.0$, showing the estimated parameter values using (a) linear least squares, (b) non–linear least squares and (c) the response function method.*

no. of iter.	(a) Linear least squares		(b) Non-linear least squares		(c) Response function method	
	estimated parameter value	error (%)	estimated parameter value	error (%)	estimated parameter value	error (%)
0	5.000	59.42	5.000	59.42	5.000	59.42
1	8.080	25.53	12.700	41.62	10.100	1.41
2	9.490	7.12	10.280	3.96	9.999	0.01
3	9.892	1.53	10.000	0.02	10.000	0.00
4	9.979	0.30	10.000	0.00	10.000	0.00
5	9.996	0.06	10.000	0.00	10.000	0.00
exact	10.000		10.000		10.000	

Table 3.3: *Results from the simple one–parameter model with two recorded (known) values and with $L = 10.0$, showing the estimated parameter values using (a) linear least squares, (b) non–linear least squares and (c) the response function method.*

no. of iter.	(a) Linear least squares		(b) Non-linear least squares		(c) Response function method	
	estimated parameter value	error (%)	estimated parameter value	error (%)	estimated parameter value	error (%)
0	5.000	60.14	5.000	60.14	5.000	60.14
1	8.008	26.93	12.520	39.70	10.010	0.15
2	9.445	7.90	10.250	3.70	10.000	0.00
3	9.877	1.77	10.000	0.04	10.000	0.00
4	9.975	0.36	10.000	0.00	10.000	0.00
5	9.995	0.07	10.000	0.00	10.000	0.00
exact	10.000		10.000		10.000	

3.4 Application to idealised steady–state groundwater model

To continue further with the testing of the indirect inverse techniques, an idealised steady–state groundwater flow model from Segerlind [23] is used and shown in Figure 3.2. The indirect approaches presented have been applied to the following groundwater model. A

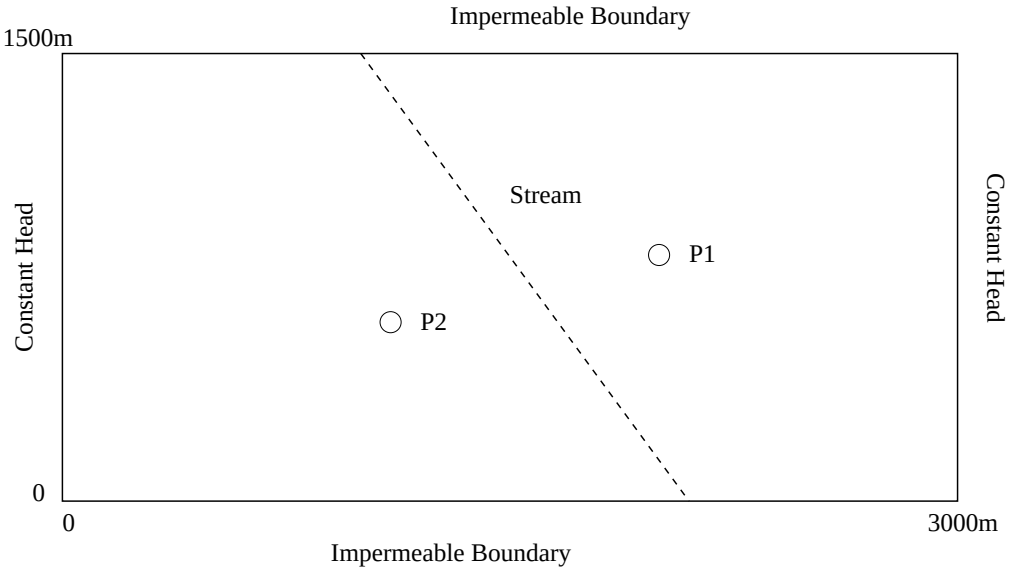

Figure 3.2: *Diagram of the idealised model of the steady–state aquifer of Segerlind [23].*

rectangular region 3000 m by 1500 m is bounded on the north and south by impermeable boundaries, and on the east and west by a constant piezometric head of 200 m. A stream runs through the region beginning at the point (1000,1500) m and ending at (2000,0) m and is adding water to the region at a rate of 0.24 m^3/day/m of length. Two wells P1 and P2 are removing water from the aquifer at a rate of 1200 m^3/day and 2400 m^3/day and are located at (2000,830) and (1100,600) respectively. The transmissivities are T_x = 40 m^2/day and T_y = 20 m^2/day.

For application of the indirect inverse methods, it is assumed that the transmissivities T_x and T_y are unknown and that the piezometric head at the 11 observation wells shown in Figure 3.3 is known at steady–state. These 11 heads are determined by running the forward model with the true parameter values. Here $\Delta x = \Delta y = 100$ m. Using grid steps of this size resulted in the well P1 not lying on a grid point. For the purposes of modelling this well on the finite difference grid it has been split into two adjacent wells which extract a combined volume equivalent of 1200 m^3/day. These two wells are shown

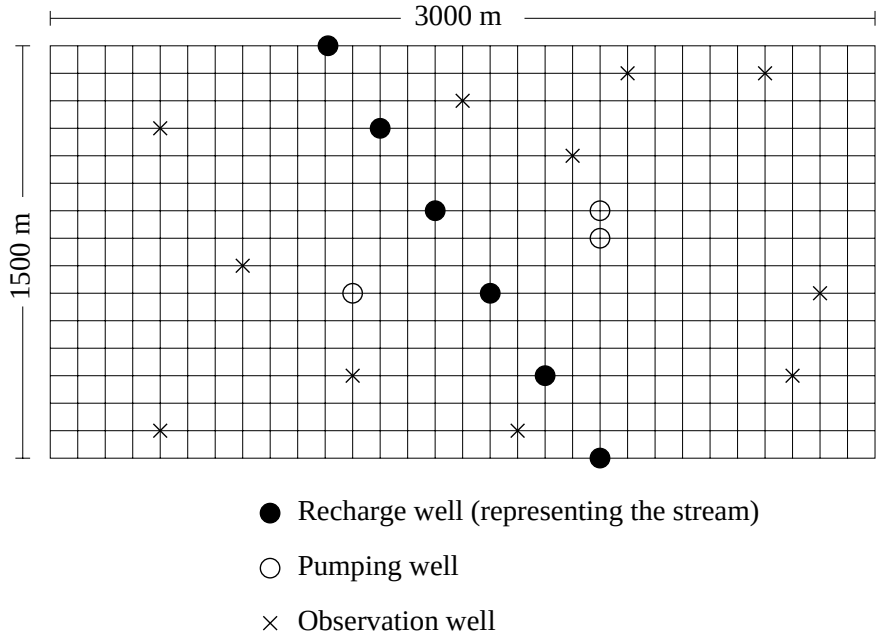

Figure 3.3: *Diagram of the finite–difference grid used to model the idealised steady–state aquifer of Segerlind [23].*

in Figure 3.3. The stream is modelled using injection wells as shown in Figure 3.3.

As there are two unknown parameters, the forward model must be run three times using initial values for T_x and T_y, which are set to 10 m^2/day, and then perturbing T_x and T_y in turn. The perturbed value used for T_x and T_y is set to 11 m^2/day, i.e. an increase of 10% [20]. The three inverse techniques (a) linear least squares, (b) non–linear least squares and (c) the response function approach were used to solve the inverse problem. In cases (b) and (c) the response functions were of the type $f(p) = 1/\sqrt{p}$ based on the analytic solution given in Equation (2.9).

3.4.1 Results

Table 3.4 shows the number of iterations, the transmissivities T_y and T_x and the error from the calibration of the Segerlind model [23], using linear least squares, non–linear least squares and the response function method respectively. The error has been calculated using Equation (3.48). By comparing the error columns in these tables, it can be seen that the response function method performs best with convergence to the exact values occurring within 11 iterations. The non–linear least squares also performs well with convergence achieved in 12 iterations; however the linear least squares method requires a far greater number of iterations for convergence. It should be noted with the non–

Table 3.4: *Results from the Segerlind model with 11 recorded (known) values, showing the estimated values for T_y and T_x using (a) linear least squares, (b) non–linear least squares and (c) the response function method.*

no. of iter.	(a) Linear least squares			(b) Non-linear least squares			(c) Response function method		
	T_y	T_x	error (%)	T_y	T_x	error (%)	T_y	T_x	error (%)
0	10.000	10.000	11.71	10.000	10.000	11.71	10.000	10.000	11.71
1	9.331	21.918	4.15	9.378	21.092	4.50	9.406	50.413	2.37
2	11.297	26.319	2.82	10.863	34.571	0.73	16.073	38.417	0.22
3	12.473	29.264	2.04	13.823	40.189	0.54	17.889	40.297	0.18
4	13.458	31.409	1.54	16.815	39.942	0.21	19.269	39.958	0.04
5	14.302	33.040	1.19	18.552	40.019	0.09	19.702	40.011	0.02
6	15.034	34.314	0.94	19.411	40.004	0.04	19.890	40.001	0.01
7	15.671	35.326	0.75	19.770	40.003	0.01	19.958	40.000	< 0.01
8	16.228	36.140	0.61	19.912	40.001	0.01	19.984	40.000	< 0.01
9	16.716	36.801	0.49	19.966	40.000	< 0.01	19.993	40.000	< 0.01
10	17.143	37.342	0.40	19.987	40.000	< 0.01	19.996	40.000	< 0.01
11	17.518	37.787	0.33	19.995	40.000	< 0.01	19.999	40.000	< 0.01
12	17.846	38.154	0.27	19.998	40.000	< 0.01			
13	18.134	38.458	0.22						
exact	20.000	40.000		20.000	40.000		20.000	40.000	

linear least squares method that the value for the error for the first iteration is greater than the error for the linear–least squares method. This can also be seen in Tables 3.1–3.3. However, after the second iteration the non–linear least squares method produces parameters that result in a smaller error than the least squares method.

3.4.2 Further considerations

An additional test has been performed to determine if the order in which the parameters are estimated has any bearing on the predicted values from the inverse model. Using the steady–state groundwater flow model for the Segerlind test case , the order of perturbation

of the parameters T_x and T_y has been reversed and the inverse model run. This simulation results in no change in the predicted values for the unknown parameters.

In steady–state problems with no extraction or injection, the groundwater flow equation in 2–dimensions becomes

$$\frac{\partial}{\partial x}\left(T_x\frac{\partial h}{\partial x}\right)+\frac{\partial}{\partial y}\left(T_y\frac{\partial h}{\partial y}\right)=0 \tag{3.54}$$

From examination of Equation (3.54) it can be seen that it is the ratio between T_x and T_y that determines the rate of flow through the aquifer. This being the case, only one parameter needs to be determined by the inverse technique. By holding one of the unknown parameters constant and using the indirect inverse methods to approximate the other, this ratio can be found [20] and the model calibrated even more quickly.

3.5 Application to idealised transient groundwater flow model

A third test of the indirect inverse methods has been performed using the idealised aquifer from Sun [24]. This aquifer simulation is transient with recorded values being collected at the 10 observation times of 0.05, 0.1, 0.2, 0.4, 0.6, 1.0, 2.0, 6.0, and 10.0 days. The aquifer is 600 m by 1200 m with the boundary AB having a constant head of 100 m, with the other boundaries BC, CD and AD being impermeable (see Figure 3.4). The modelled region consists of two hydrogeologic zones of equal area. Zone 1 covers the left hand half and Zone 2 covers the right hand half of the aquifer. The initial head in the aquifer is assumed to be 100 m. A recharge well located at (240,300) m is injecting water into the aquifer at a rate of 500 m^3/day and another well located at (960,300) m is pumping water from the aquifer at a rate of 4000 m^3/day. Four observation wells located at (480, 300), (720,150), (720,450) and (960,300) record the piezometric head at the 10 times. Zone 1 has an isotropic (constant in all directions) transmissivity of 250 m^2/day and for Zone 2 it is 500 m^2/day. The storativity for Zone 1 has been set to 0.001 and 0.002 for Zone 2. Grid spacings of Δx and Δy have been set to 30 m. To apply the indirect inverse method it is assumed that the transmissivities in Zones 1 and 2 are unknown, and that the storativity in Zone 1 is also unknown. The values for h at the 4 locations for the 10 times are known and have been determined by the forward model.

To set up the matrix $\mathbf{A}$ of Equation (3.46), the storativity in Zone 1 has been set to an

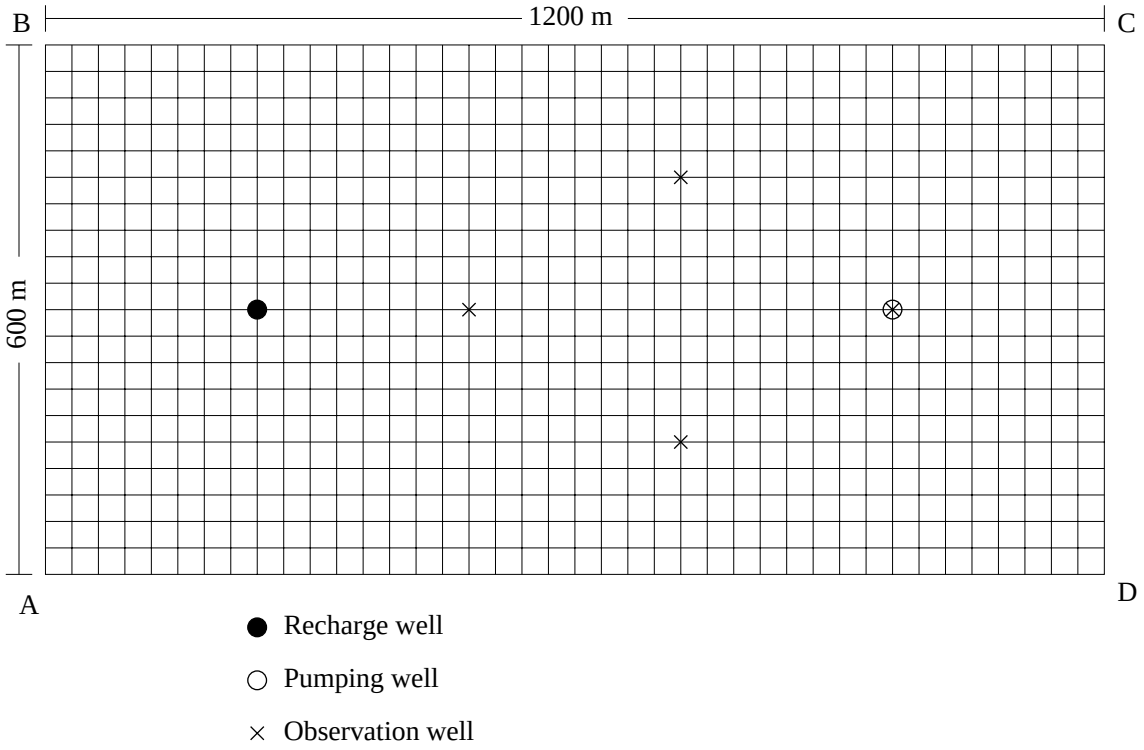

Figure 3.4: *Diagram of the finite–difference grid used to model the idealised confined aquifer from Sun [24].*

initial value of 0.003 and the perturbed value has been taken to be 0.0033, a 10% increase of the initial value [20]. Similarly the transmissivities have been set to 150 m^2/day and 400 m^2/day for Zone 1 and 2 respectively and the perturbed estimate 165 m^2/day and 440 m^2/day for each zone.

3.5.1 Results

A linear relationship is assumed between the model output and the unknown parameters based on the symmetric nature of the observation wells. In assuming a linear relationship, the three methods of linear least squares, non–linear least squares and the response function produce identical results; only one set of results is shown in Table 3.5. These results show that the indirect inverse methods converge rapidly to the true solution, with very good agreement achieved after 4 iterations.

3.6 Summary

For the numerical experiments shown in this chapter, it can be seen that the indirect inverse methods are effective and efficient for unknown parameter estimation. It can

Table 3.5: *Results from the Sun model [24] with 30 recorded (known) values over 10 times, showing the estimated values for S and T of Zone 1 and T of Zone 2. In this case a linear relationship has been assumed, so that the linear least squares, non–linear least squares and the response function method are equivalent.*

no. of iter.	Zone 1 S	Zone 1 T	Zone 2 T	error (%)
0	0.00300	150.00000	400.00000	0.9930
1	0.00163	235.17212	485.53855	0.0985
2	0.00121	247.52445	494.92850	0.0249
3	0.00105	250.10987	498.18223	0.0083
4	0.00101	250.30470	499.38438	0.0029
5	0.00100	250.12256	499.81035	0.0008
6	0.00100	250.01691	499.94064	0.0002
7	0.00100	249.99160	499.96667	0.0001
8	0.00100	249.99247	499.97460	0.0001
9	0.00100	249.99351	499.98244	0.0001
10	0.00100	249.99642	499.98599	0.0001
11	0.00100	249.99842	499.98999	< 0.0001
exact	0.00100	250.0000	500.00000	

also be seen by way of the results from using the function given by Equation (3.49) and the steady–state model from Segerlind, that the response function method performs better than linear and non–linear least squares methods when the relationship between the observed piezometric head and the unknown parameters is non–linear. The indirect inverse method using response functions is used in Chapter 5 to develop and calibrate a model of the flow of groundwater in the Willunga Basin, South Australia.

Chapter 4

The Willunga Basin, South Australia

4.1 Introduction

The Willunga Basin is situated approximately 30km south of Adelaide, South Australia. The boundaries of the basin are defined by the coast of the Gulf St. Vincent in the west, the Onkaparinga River in the north, and the Willunga Fault which runs north–east from the coast to the Onkaparinga River (Figure 4.1). The Willunga Basin is

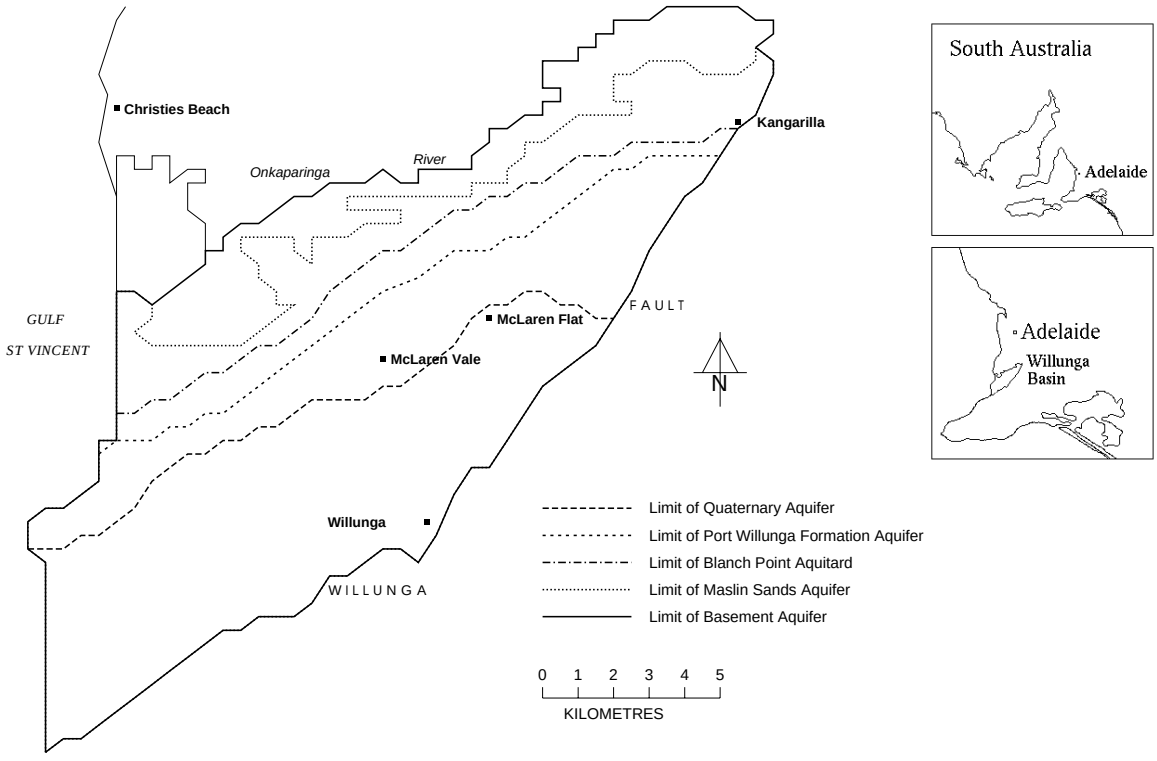

Figure 4.1: *Location map of the Willunga Basin, South Australia.*

a multi–aquifer system consisting of 5 main hydrogeologic units [4]. From the surface in a vertical direction downward the formations are the Quaternary aquifer, the Port Willunga Formation aquifer, the Blanch Point aquitard, the Maslin Sands aquifer and the Basement aquifer (see Section 4.2). Approximately 7380 ML of groundwater from the basin is used annually as irrigation for the production of grapes, almonds and olives [17]. The last few decades have seen groundwater levels within the Willunga Basin declining. Figure 4.2 shows the decline of piezometric head over the 10 year period 1988–1998. This decline in piezometric head is indicative of groundwater levels throughout the basin. Although 10 years of piezometric head data exists for the period 1989–1998, the scale on the x–axis of both hydrographs in Figure 4.2 has been set to 1970–1998 for consistency with other hydrographs from the Willunga Basin. It has been suggested [17] that the

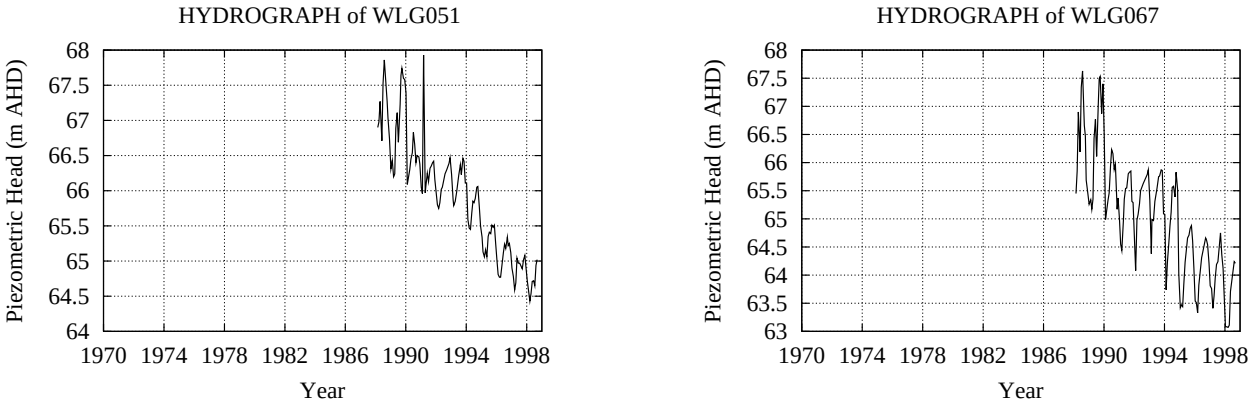

Figure 4.2: *Hydrographs of observation wells WLG051 and WLG067 from the Willunga Basin showing declining piezometric heads over the period 1988–1998.*

longer term effect of declining groundwater levels will be greater costs for the extraction of groundwater, and potential degradation of the quality of the groundwater, particularly in the coastal regions where salt water intrusion may occur.

Rainfall can recharge the groundwater in the Willunga Basin by penetrating the surface of the basin and percolating downwards. Figure 4.1 shows the outcrop areas for each aquifer. It is in the areas where the aquifers outcrop that the recharge of groundwater from precipitation can occur. It is estimated [17] that approximately 4,050 ML/yr of water recharges the groundwater system of the Willunga Basin by way of precipitation over the basin, and that approximately 4040 ML/yr of lateral inflow recharges the basin along the north–eastern margins of the basin. It has also been stated [17] that some water recharges the Willunga Basin from across the Willunga Fault.

Some of the management options to reverse the declining groundwater trends include the development of a groundwater flow model which could be applied for the determination of sustainable annual groundwater yields from the basin, and the potential use of aquifer storage and recovery (ASR) within the basin [17].

ASR for the Willunga Basin may involve the injection of storm water runoff and treated waste water from the Christies Beach Waste Water Treatment Plant, situated approximately 4km north of the Basin, into one or more of the aquifers during the winter period. This water could then be used during the drier months when the demand for water is at its greatest. ASR has the additional benefits of not needing large amounts of land and of minimising evaporation, two problems associated with surface water storage.

4.2 Hydrogeology of the Willunga Basin

Using well logs personally obtained from Primary Industries and Resources South Australia (PIRSA), stratigraphic cross–sections of the basin have been developed. From Figure 4.3(b) it can be seen that the basin rises in elevation from the coast, north–east to the Onkaparinga River. The Quaternary aquifer and the Port Willunga Formation aquifer appear to be relatively constant in thickness with the Blanch Point aquitard and Maslin Sands aquifer thinning near well WLG099. Figure 4.3(d) shows the stratigraphic cross–section from the Onkaparinga River south-east along the line CD to the Willunga Fault; in this direction each of the hydrogeologic units appear to be reasonably constant in thickness, except where each outcrops. As each of the aquifers lies over the top of another, the rainfall recharge for each of the aquifers will occur in the section where the aquifer outcrops at the surface. Also because of this reason it has be suggested [17] that the effects of evapotranspiration are negligible. The quaternary aquifer is not considered an important source of groundwater, and is not used by irrigators [17].

4.2.1 Port Willunga Formation Aquifer

The Port Willunga Formation aquifer is bounded by the Willunga Fault and the region along which it outcrops. The area of recharge from rainfall is limited by the Quaternary aquifer, which overlays a majority of the southerly section of the Port Willunga Formation. It is estimated that approximately 1050 ML/yr of rainfall recharges the Port

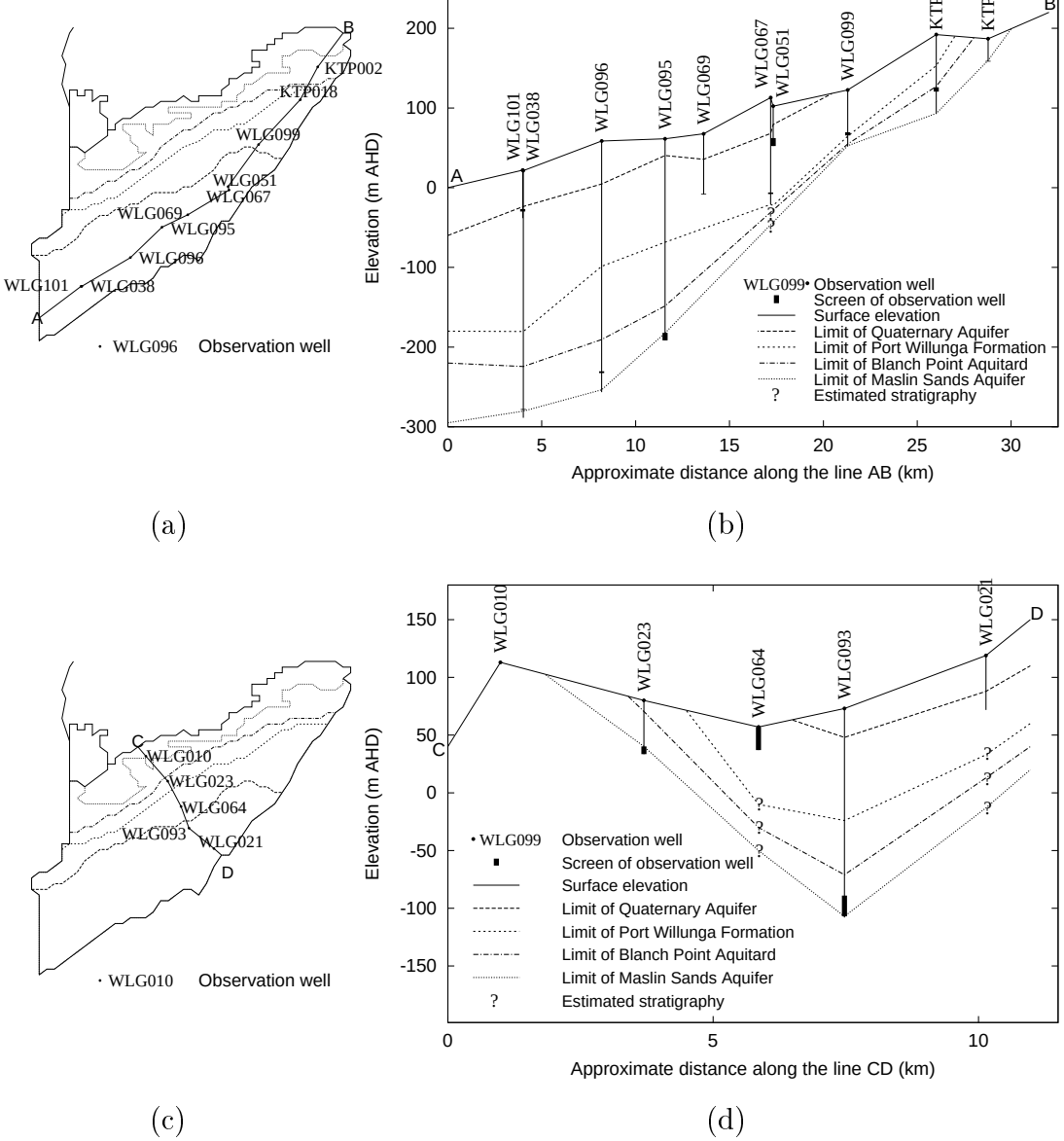

Figure 4.3: (a) *The location of observation wells along the line* AB *used to develop* (b) *the cross–sectional view of stratigraphy of the Willunga Basin along the line* AB. (c) *The location of observation wells along the line* CD *used to develop* (d) *the cross–sectional view of stratigraphy of the Willunga Basin along the line* CD. *The well log for WLG010 had no details beyond land elevation.*

Willunga Formation aquifer via the outcrop region [17]. Recharge may also enter the aquifer through leakance from the Blanch Point aquitard. Some testing of the soil properties has been performed for the Port Willunga Formation aquifer. This has included estimating the transmissivity and storativity values at various locations [32] in the Port Willunga Formation aquifer; these values range from 45 to 5560 m^2/day for transmissivity and 2.7×10^{-4} to 0.011 for storativity.

4.2.2 Observation wells within the Port Willunga Formation aquifer

A network of 16 observation wells has been developed within the Port Willunga Formation aquifer [11] with the location of each well being shown in Figure 4.4. Piezometric head data from these wells has been collected spasmodically since December 1973.

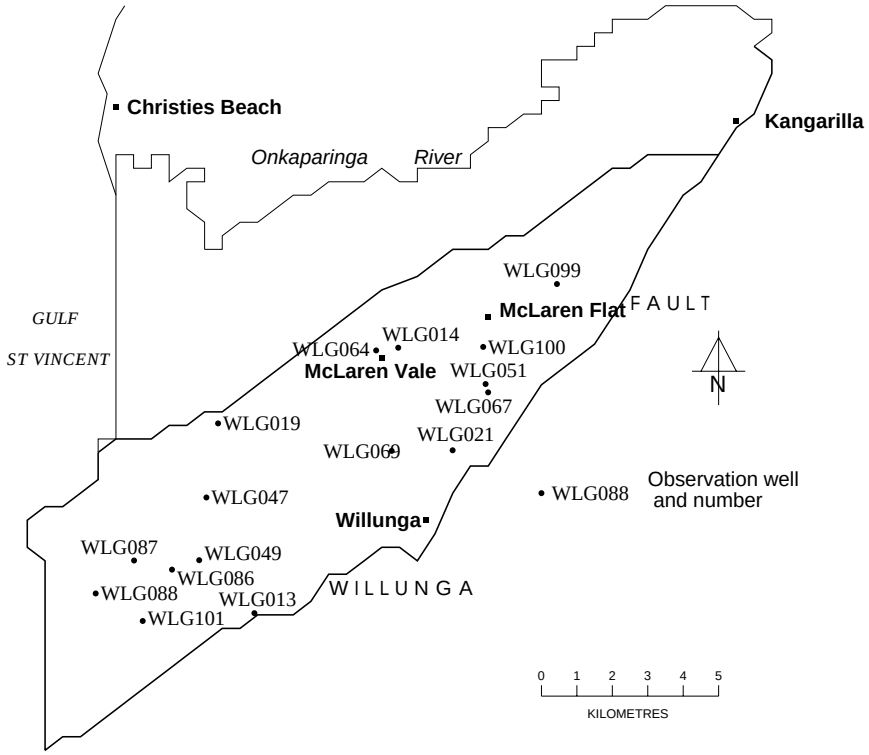

Figure 4.4: *Location of observation wells for the Port Willunga Formation aquifer.*

4.2.3 Groundwater levels within the Port Willunga Formation aquifer

The flow of groundwater within the Port Willunga Formation aquifer is from the north-eastern corner to the coast. Figure 4.5(b) represents a cross–sectional view of the piezometric head on 14/8/1995 and shows an almost linear relationship between the piezometric head and the location of the observation wells relative to the line AB. This date was chosen as it is a time at which a large amount of data exists, and for which the aquifer has had sufficient time over the winter period to return to its natural state after the summer extraction for irrigation. This date is also used in the calibration process in Chapter 5 for the development of the steady–state groundwater flow model of the

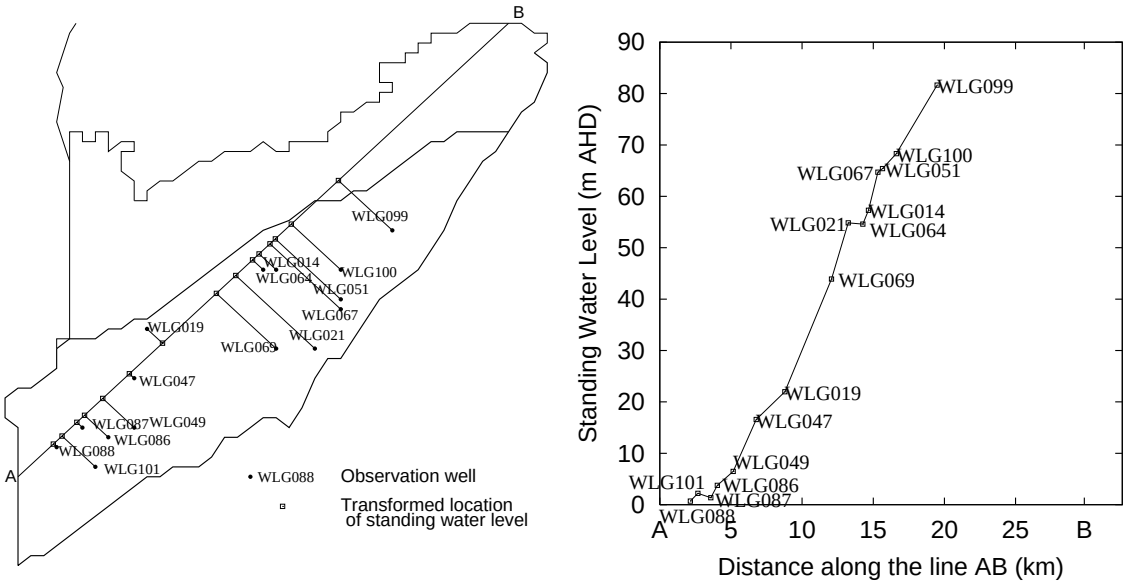

(a) (b)

Figure 4.5: (a) *The spatial location of the observation wells for the Port Willunga aquifer relative to the line* AB. (b) *1-dimensional view of piezometric head in the Port Willunga aquifer as of 14/8/1995 projected onto the line* AB.

Willunga Basin. It should also be noted that observation well WLG013 does not appear in Figure 4.5; this observation well was removed as the piezometric head recorded at this location (see Figure 4.4) was judged to be inconsistent with the groundwater levels recorded elsewhere in the Basin. Given the proximity of observation wells WLG049, WLG086 and WLG101, and their recorded piezometric head, shown in Figure 4.6, it was concluded that the water levels in WLG013 did not give a true representation of the piezometric head in the Port Willunga Formation aquifer due to the proximity of WLG013 to the Willunga Fault.

From the hydrographs of the observation wells of the Port Willunga Formation aquifer shown in Figure 4.6 and Appendix A, it can be seen that there has been a steady decline in groundwater levels for this aquifer of between 1 to 4 m over the last 10 years. The largest declines are observed in wells WLG051 and WLG067 as shown in Figure 4.2, with these wells all located near the townships of McLaren Vale, McLaren Flat and Willunga (see Figure 4.4). All the hydrographs also show the typical annual oscillation due to extraction in summer and recovery in winter.

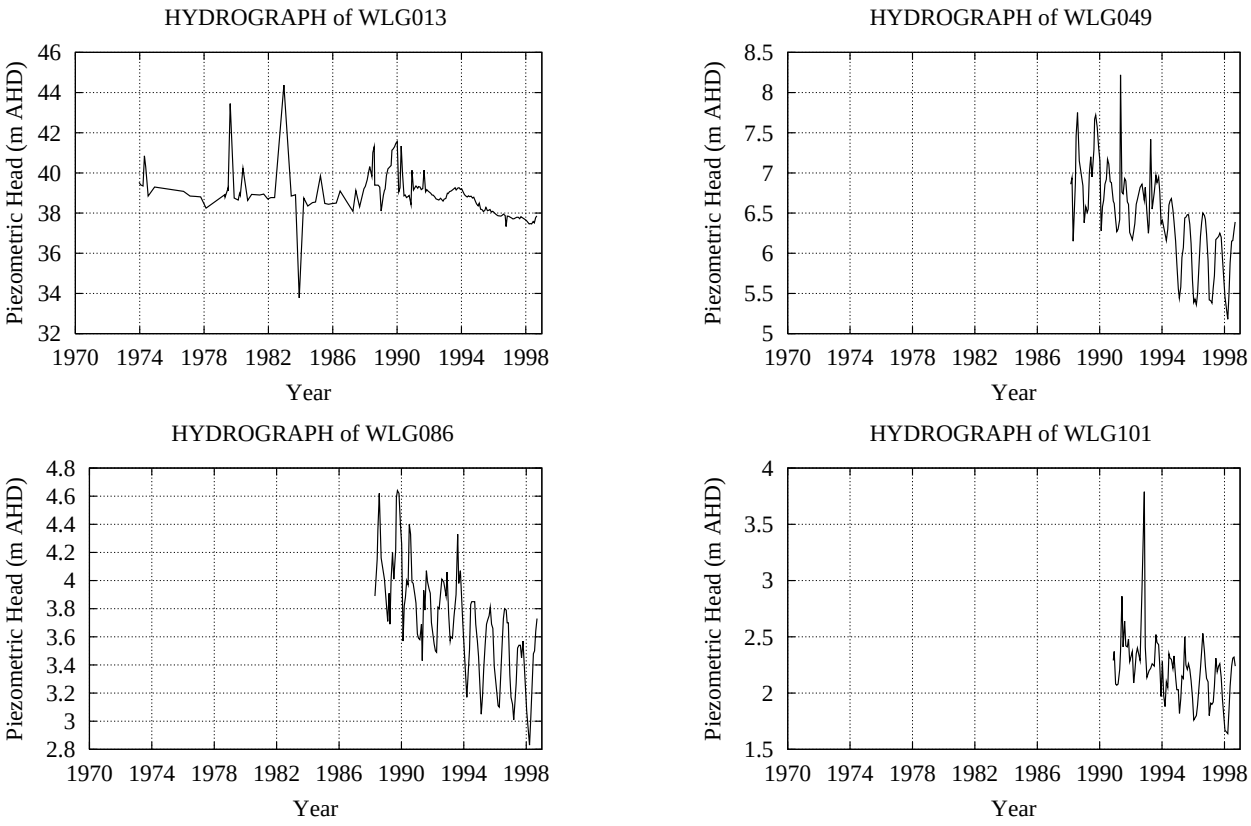

Figure 4.6: *Hydrographs of observation wells WLG013, WLG049, WLG086 and WLG101 of the Port Willunga Formation aquifer showing the inconsistency in piezometric head of WLG013 with the other nearby wells.*

4.2.4 Maslin Sands Aquifer

The Maslin Sands aquifer is similar to the Port Willunga Formation aquifer as it is bounded by the Willunga Fault and the region along which it outcrops. It is connected vertically above to the Blanch Point aquitard and below to the Basement aquifer. Rainfall recharge can enter the Maslin Sands aquifer via the section of the aquifer that is exposed at the surface; this has been estimated to be 900 ML/yr [17]. Some testing of the soil properties has been performed for the Maslin Sands aquifer. This has included estimating the transmissivity and storativity values at various locations [32] in the Maslin Sands aquifer with these values ranging between 16 and 49 m^2/day for transmissivity and 7.7×10^{-5} and 8.6×10^{-5} for storativity.

4.2.5 Observation wells within the Maslin Sands aquifer

There are 17 observation wells used to monitor the piezometric head within the Maslin Sands aquifer [11], with the majority of these wells being located in the northern half of

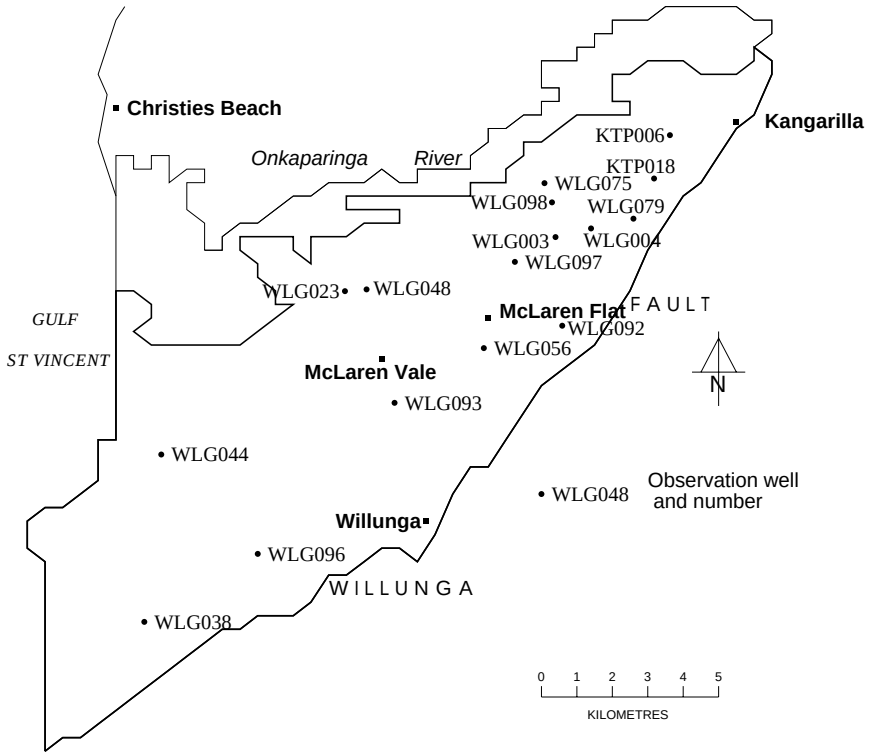

Figure 4.7: *Location of observation wells for the Maslin Sands aquifer.*

the basin as shown in Figure 4.7.

4.2.6 Groundwater levels within the Maslin Sands aquifer

Figure 4.8(b) is a cross–sectional view of piezometric head on 14/8/1995, and shows the flow of groundwater is from the north–east to the coast. In Figure 4.8, observation wells KTP006 and WLG096 have been removed. Well KTP006 has been removed as a piezometric head has not been recorded at the date 14/8/1995. Well WLG096 has also been removed as the piezometric head recorded at its location was negative (Figure 4.9), which is inconsistent with the groundwater levels elsewhere in the aquifer and seems to be anomalous. This is highlighted by observation well WLG038 (Figure 4.9) which has a higher piezometric head even though it is closer to the coast, where it can be assumed that groundwater levels are at their lowest. Figure 4.10 and Appendix B show hydrographs of the observation wells of the Maslin Sands aquifer where it can be seen that there has been a steady decline in groundwater levels for this aquifer of between 1 to 6 m over approximately the last 10 years. The largest declines are observed in wells WLG023 and WLG092 as shown in Figure 4.10. All the hydrographs also show the typical annual oscillation due to extraction in summer and recovery in winter.

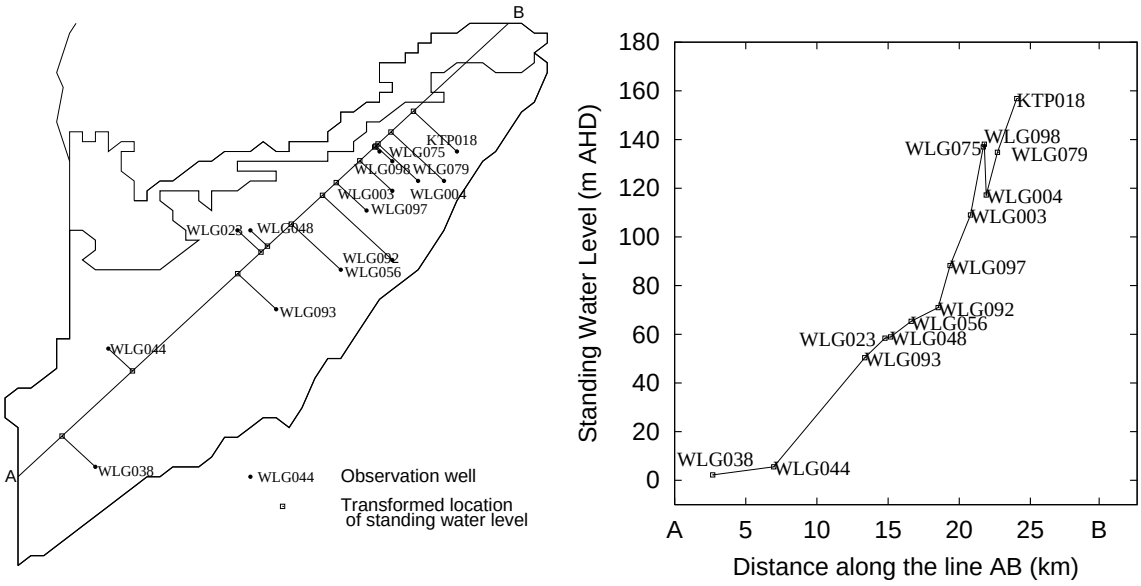

(a) (b)

Figure 4.8: (a) *The spatial location of the observation wells for the Maslin Sands aquifer relative to the line* AB. (b) *1-dimensional view of piezometric head in the Maslin Sands aquifer as of 14/8/1995 projected onto the line* AB.

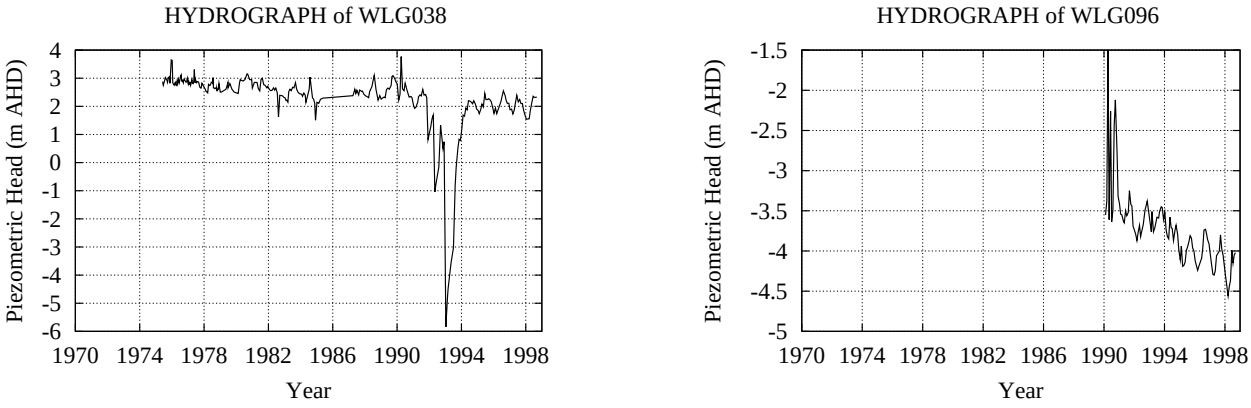

Figure 4.9: *Hydrographs of observation wells WLG038 and WLG096 of the Maslin Sands aquifer.*

4.2.7 Basement Aquifer

The Basement aquifer is bounded by the Willunga Fault and the Onkaparinga River. Recharge to the aquifer is from the Onkaparinga River and from rainfall which enters the Basement aquifer where it is exposed at the surface (see Figure 4.1); it has been estimated that 2100 ML/yr recharge the Basement aquifer [17]. The Basement aquifer also has a direct connection with the Maslin Sands aquifer, whereby groundwater can pass from one aquifer to the other depending on the groundwater levels in each aquifer.

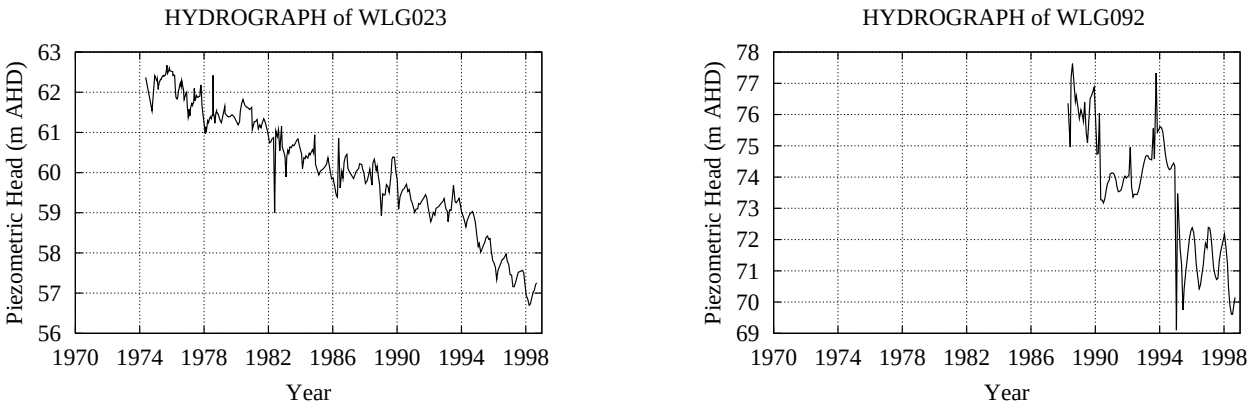

Figure 4.10: *Hydrographs of observation wells WLG023 and WLG092 of the Maslin Sands aquifer showing the declining piezometric head over the last decade.*

From Figure 4.3(b), the total depth of the Basement aquifer is uncertain, but, because of the direct connection between the Basement aquifer and the Maslin Sands aquifer and progressively through the Blanch Point aquitard to the Port Willunga Formation aquifer, maintaining high groundwater levels in the Basement aquifer is imperative to sustaining overall groundwater levels in the basin. Some testing of the soil properties has been performed for the Basement aquifer. This has included estimating the transmissivity and storativity values at 2 locations [32] in the Basement aquifer with these values being 44 m^2/day for transmissivity and range between 1.3×10^{-5} and 2.8×10^{-4} for storativity.

4.2.8 Observation wells within the Basement aquifer

The Basement aquifer has a network of 16 observation wells with all the wells located in the upper region of the Basin [11]. This is to be expected due to the depth of drilling that is required to reach the Basement aquifer near the coastal region as suggested by Figure 4.3(b). The locations of the observation wells for the Basement aquifer are shown in Figure 4.11.

4.2.9 Groundwater levels within the Basement aquifer

Figure 4.12(b) shows the variation in piezometric head projected onto the line AB, with groundwater levels highest in the north–eastern corner and reducing somewhat constantly toward the coast. Observation wells KTP007 and WLG017 show groundwater levels that appear to be inconsistent with levels elsewhere within the Willunga Basin, and so these wells were excluded from Figure 4.12. To justify their exclusion, Figure 4.13

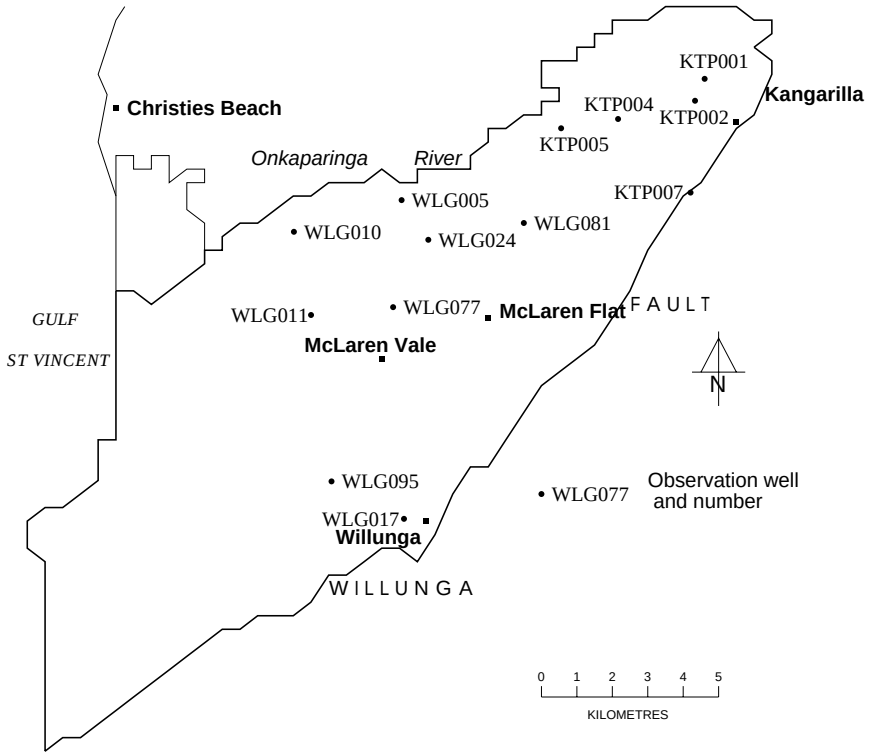

Figure 4.11: *Location of observation wells for the Basement aquifer.*

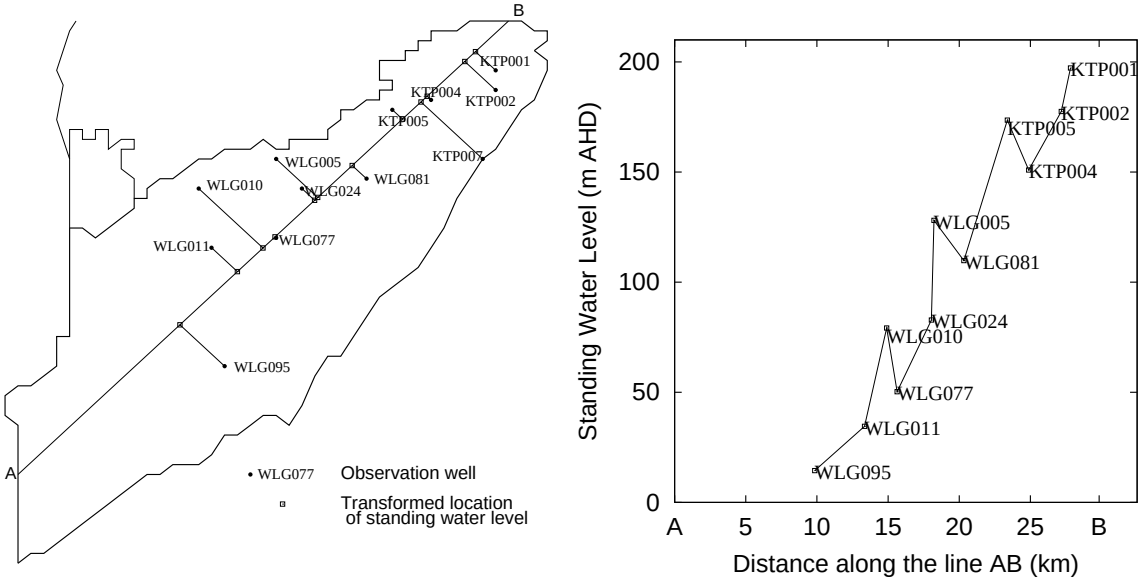

(a) (b)

Figure 4.12: (a) *The spatial location of the observation wells for the Basement aquifer relative to the line* AB. (b) *1-dimensional view of piezometric head in the Basement aquifer as of 14/8/1995 projected onto the line* AB.

shows the hydrographs of the observation wells KTP007 within the Basement aquifer and WLG079 within the Maslin Sands aquifer. If the levels observed in KTP007 are representative of the piezometric head at its location, then the piezometric head seen in the Maslin Sands aquifer at the observation well WLG079 should also be higher. This is the case because of the direct connection between the Basement and Maslin Sands aquifers and their similar spatial position within the Willunga Basin. Figure 4.14 shows

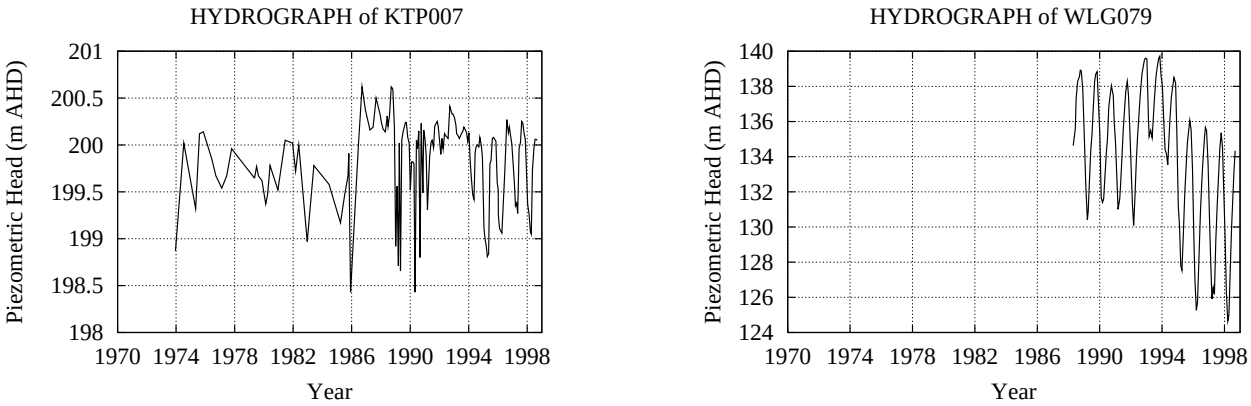

Figure 4.13: *Hydrographs of observation wells KTP007 within the Basement aquifer and WLG079 within the Maslin Sands aquifer.*

the hydrographs of WLG017 and WLG095 within the Basement aquifer. Similarly if WLG017 is representative of the groundwater levels in the Basement aquifer in that vicinity, then observation well WLG095 of the Basement aquifer should also show higher water levels. Figure 4.15 and Appendix C show hydrographs of the observation wells of the Basement aquifer where it can be seen that there has been a steady decline in

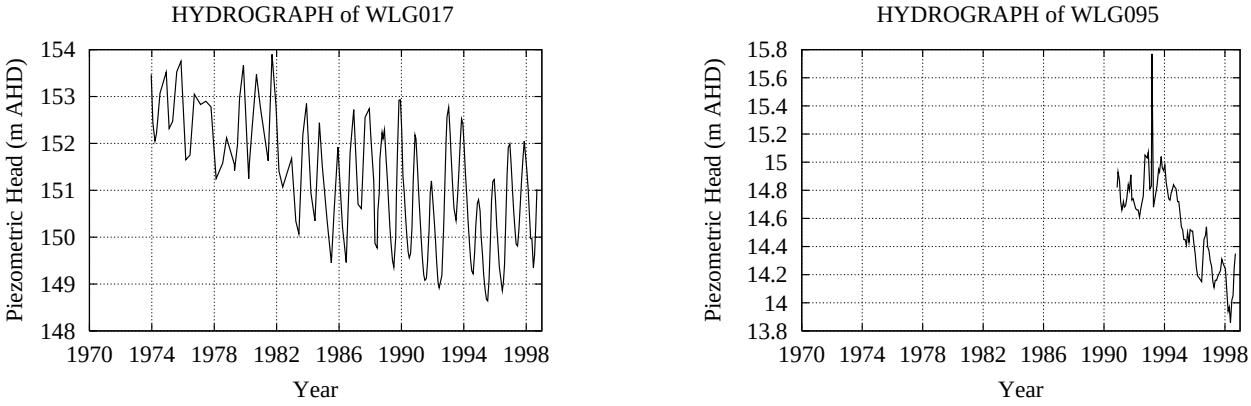

Figure 4.14: *Hydrographs of observation wells WLG017 and WLG095 within the Basement aquifer.*

groundwater levels for this aquifer of between 1 to 10 m over approximately the last 10 years. The largest declines are observed in wells WLG005 and WLG024 as shown in

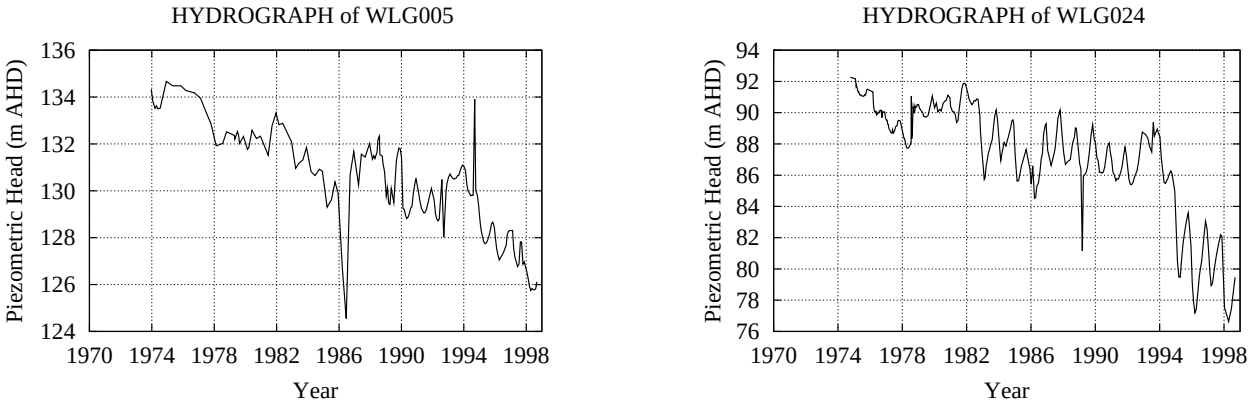

Figure 4.15: *Hydrographs of observation wells WLG005 and WLG024 within the Basement aquifer showing the declining piezometric head.*

Figure 4.15.

4.3 Production Wells within the Willunga Basin

Figure 4.16 shows the location of production wells within the Willunga Basin for the 1995–1996 season [30]. From this figure it can be seen that the production wells are evenly distributed throughout the basin, although only a few wells are present near the coastal region. Figure 4.17 shows the well locations as a function of the amount of water withdrawn from the basin [30]. It can be seen that most of the water is extracted from the McLaren Vale and McLaren Flat areas. This also is in agreement with the hydrographs of WLG051 and WLG067 from the Port Willunga Formation aquifer (Figure 4.2) which are located near these townships and for which some of the largest declines have been observed for this aquifer. The information presented in Figure 4.17 is somewhat suspect, though; personal contact with a major grape producer in the area [29] has suggested that meters to record the amount of groundwater extracted from some production wells had not been installed before the 1995–1996 extraction period. If this is generally the case, then the amounts extracted for the 1995–1996 period as shown in Figure 4.17 are likely to be based on estimated groundwater usage rather than metered usage.

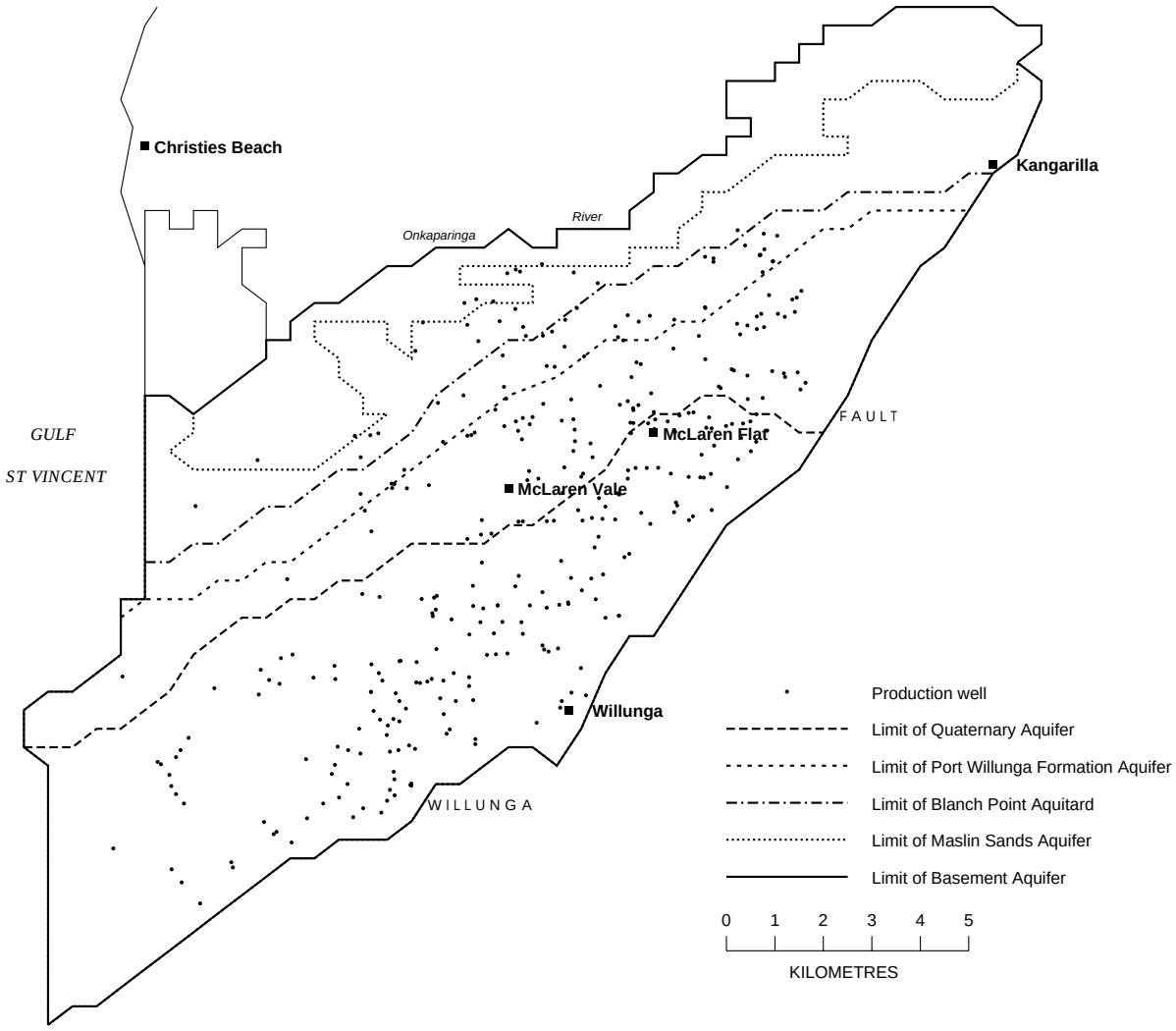

Figure 4.16: *Location of production wells in the Willunga Basin for the 1995–1996 season [30].*

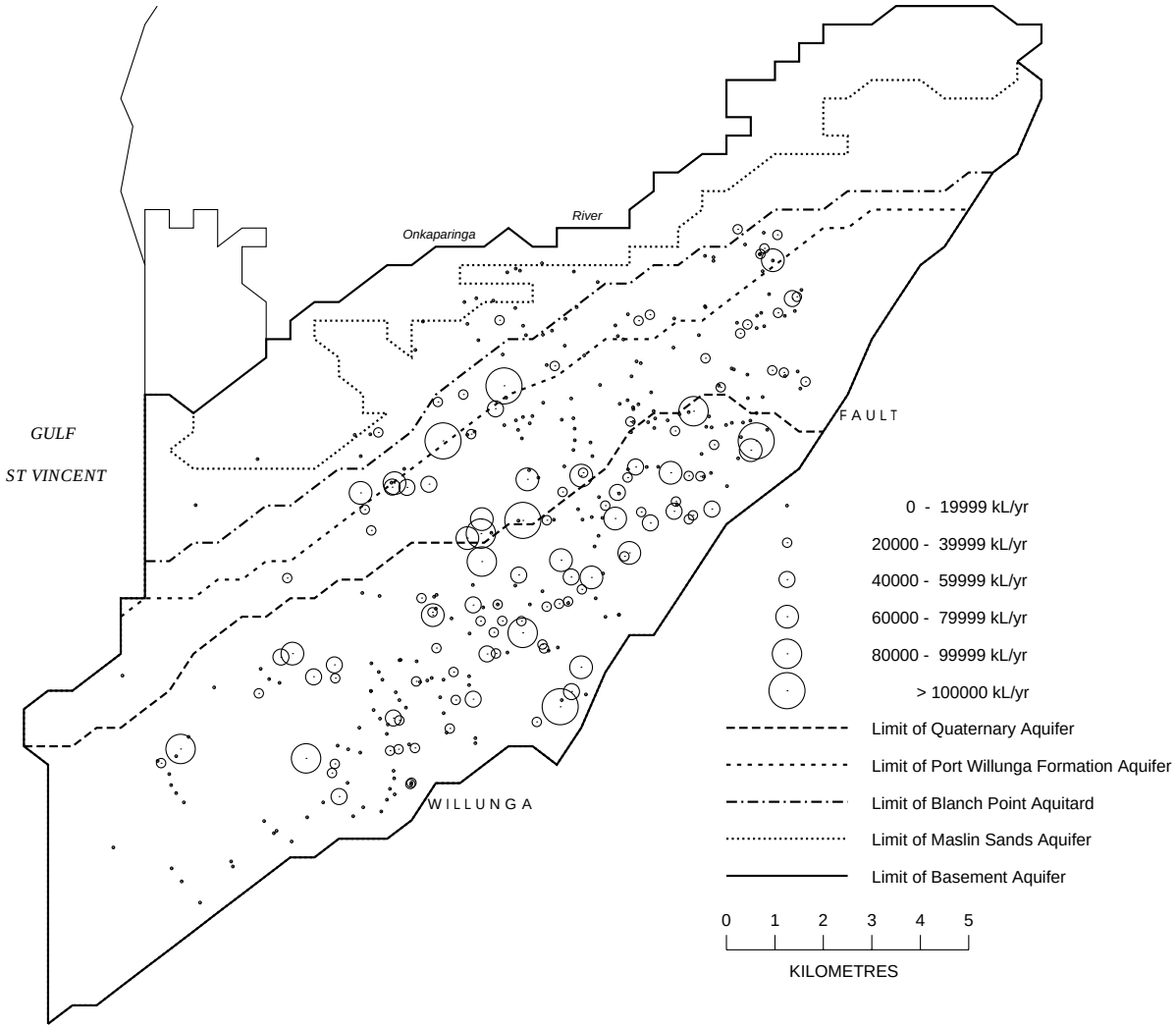

Figure 4.17: *Yield (kL/yr) and location of production wells in the Willunga Basin for the 1995–1996 season [30].*

Chapter 5

Model of Groundwater Flow in the Willunga Basin

5.1 Introduction

As described in Chapter 1, the process of numerical modelling involves the development of an initial conceptual model. In this chapter, conceptual models for steady–state and

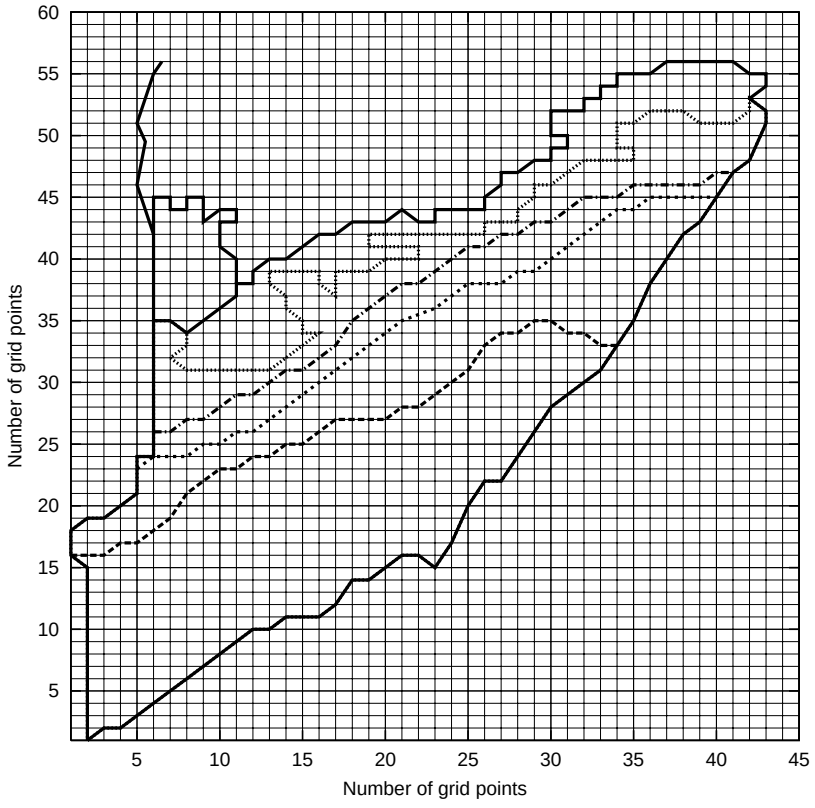

Figure 5.1: *The finite–difference grid applied to the Willunga Basin.*

time dependent scenarios of groundwater flow in the Willunga Basin are presented, as well as the method of implementation of these conceptual models into a numerical model. The method of trial and error and the response function inverse method (Section 3.2) are applied to the problem of calibrating the steady–state and transient aspects of the numerical model of groundwater flow in the Willunga Basin.

To model the groundwater flow in the Willunga Basin numerically, a finite–difference grid has been applied to the basin as shown in Figure 5.1. A grid of $\Delta x = \Delta y = 500$ m has been used. As described in Chapter 2, each aquifer is considered as a 2D layer with a leakance term that allows water to pass between the Port Willunga and Maslin Sands aquifers.

5.2 Model for steady–state simulations

Figure 5.2 shows the finite–difference grid and the points which define the boundary of the Port Willunga Formation aquifer, with a piezometric head of 0 m(AHD) at the coast and 55 m(AHD) on the Willunga Fault at the grid points (23,16), (24,18), and (25,20). These

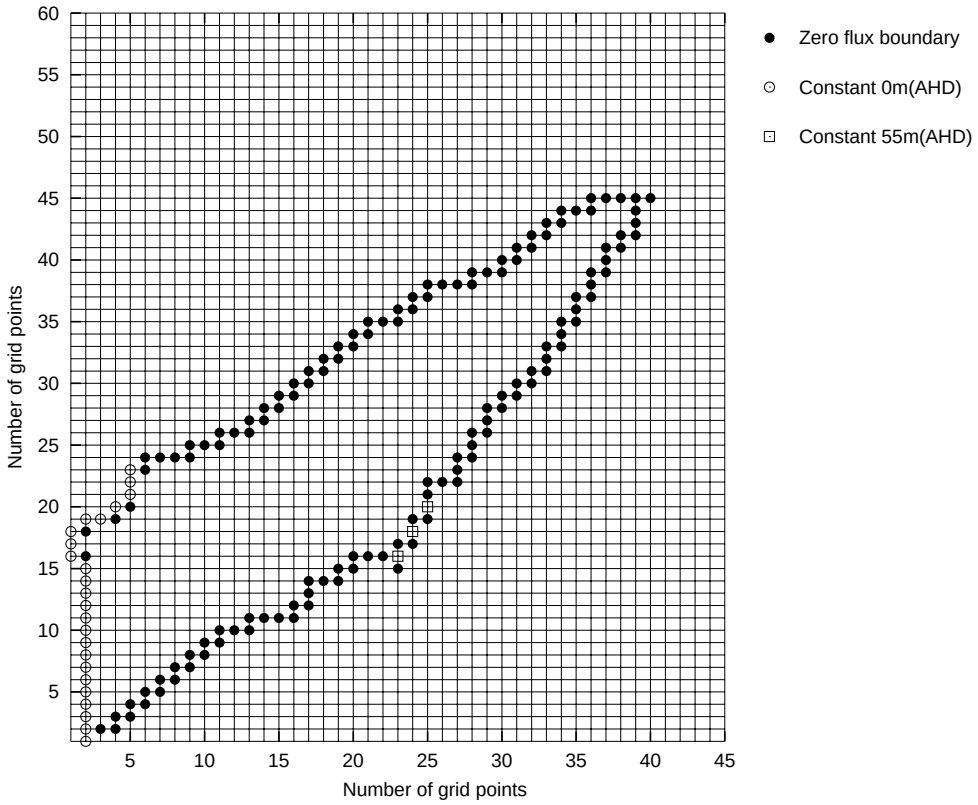

Figure 5.2: *The finite–difference grid boundaries of the Port Willunga Formation aquifer.*

points along the Willunga Fault have been selected as they lie close to the observation well WLG021 (see Figure 4.5(a)). The piezometric head at WLG021 is at a level more consistent with levels north–east of its location as shown in Figure 4.5(b). This suggests that some water from across the fault is recharging the area near WLG021 to a level of approximately 55 m (AHD).

The unknown parameters for the Port Willunga Formation aquifer are the transmissivity in the x and y directions (PWF T_x and PWF T_y) and the leakance between the Port Willunga Formation aquifer and the Maslin Sands aquifer (PWF-MS L).

Figure 5.3 shows the finite–difference grid and the points which define the boundary

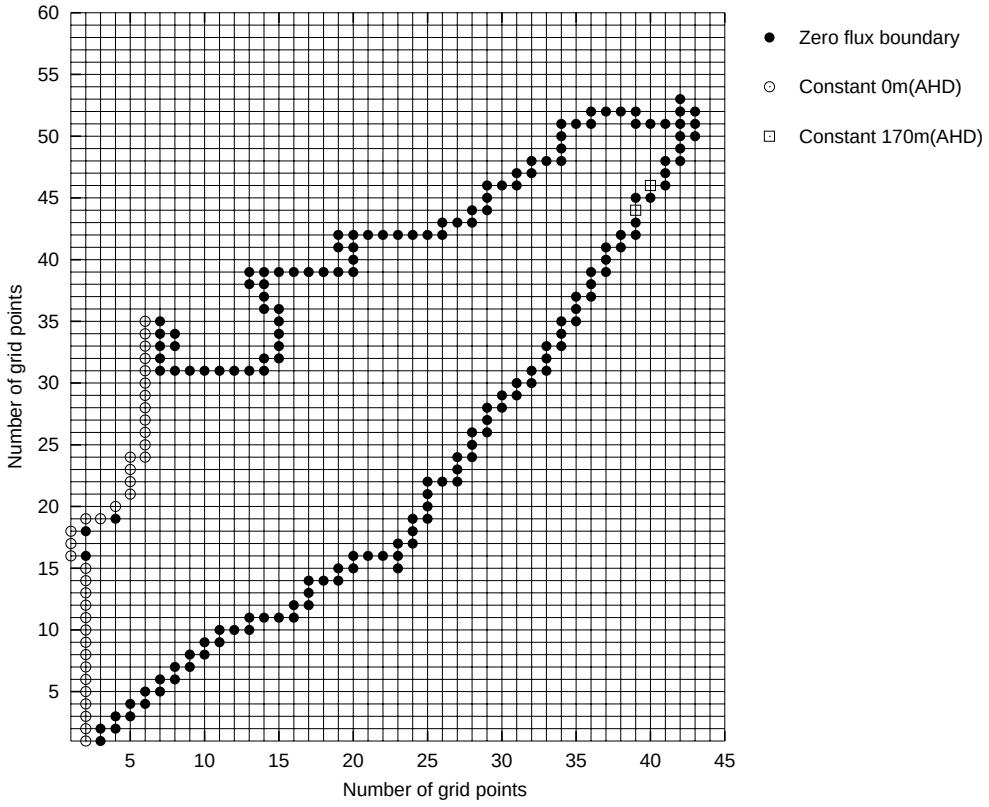

Figure 5.3: *The finite–difference grid boundaries of the Maslin Sands aquifer.*

of the Maslin Sands aquifer, with a piezometric head of 0 m (AHD) at the coast and 170 m (AHD) on the Willunga Fault at the grid locations (39,44) and (40,46). These points along the Willunga Fault have been selected as they lie close to Kangarilla (see Figure 4.1) where, it has been suggested [17], water may enter the basin. Figure 5.4 shows the piezometric head for observation well KTP006 which is located near Kangarilla (see Figure 4.7). From Figure 5.4 it can be seen that piezometric head levels at KTP006 are consistently around 170 m(AHD) which suggests this area is being recharged from across

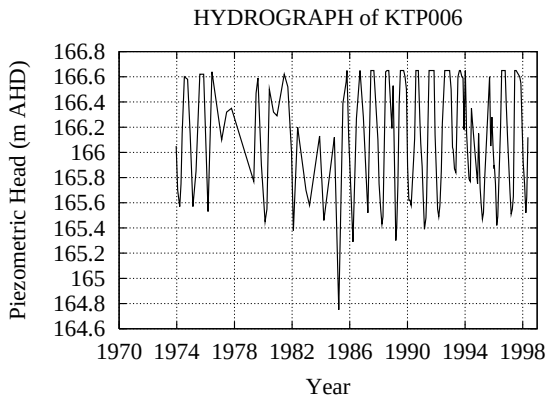

Figure 5.4: *Hydrograph of observation well KTP006 from the Maslin Sands aquifer.*

the fault.

The unknown parameters for the Maslin Sands aquifer are the transmissivity in the x and y directions (MS T_x and MS T_y) and the leakance between the Port Willunga Formation and Maslin Sands aquifer (PWF-MS L). As there is no aquitard between the Maslin Sands and Basement aquifers the leakage is simply a function of the piezometric head in each of these aquifers.

Figure 5.5 shows the finite–difference grid and the points which define the boundary of the Basement aquifer with a piezometric head of 0 m (AHD) at the coast and various piezometric head values along the north–eastern boundary. It has been suggested [17] that water enters the basin along the northern and eastern boundaries of the basin. From Figure 5.6 it can be seen that the values of piezometric head chosen around the north–eastern boundary in Figure 5.5 reflect the groundwater levels seen in observation wells KTP004 and KTP005 which are both located in the north–eastern section of the basin (see Figure 4.11).

The unknown parameters for the Basement aquifer are the transmissivity in the x and y directions (B T_x and B T_y).

For the steady–state model, no injection or extraction of water from the production wells, as well as no evapotranspiration is assumed.

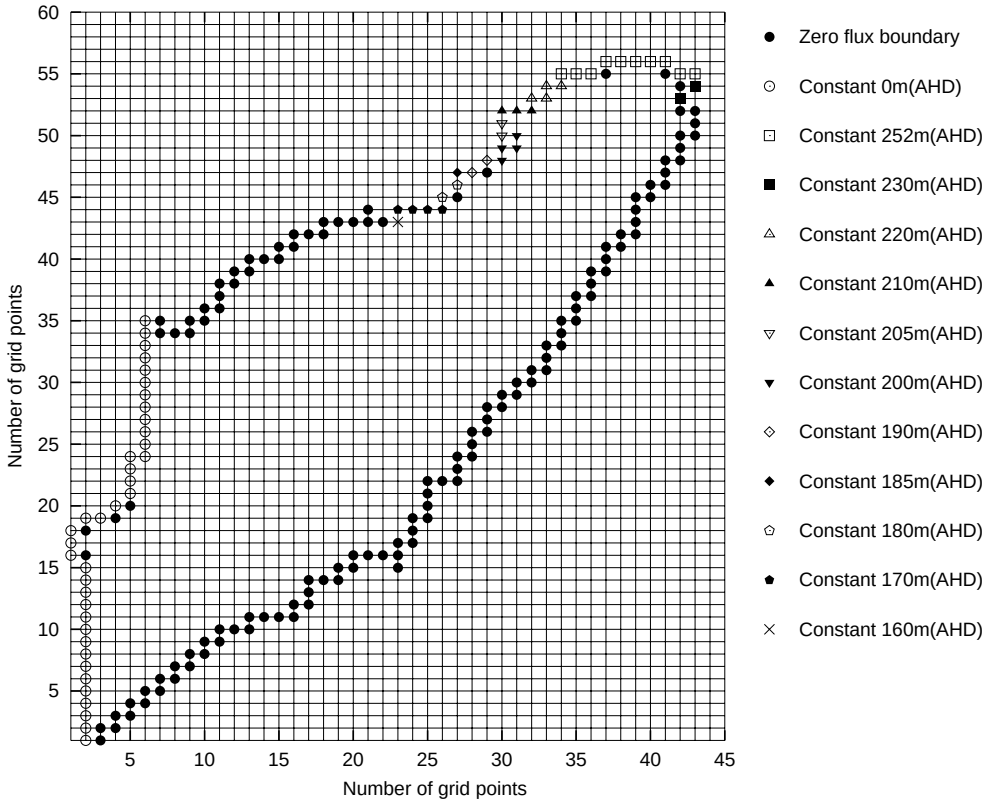

Figure 5.5: *The finite–difference grid boundaries of the Basement aquifer.*

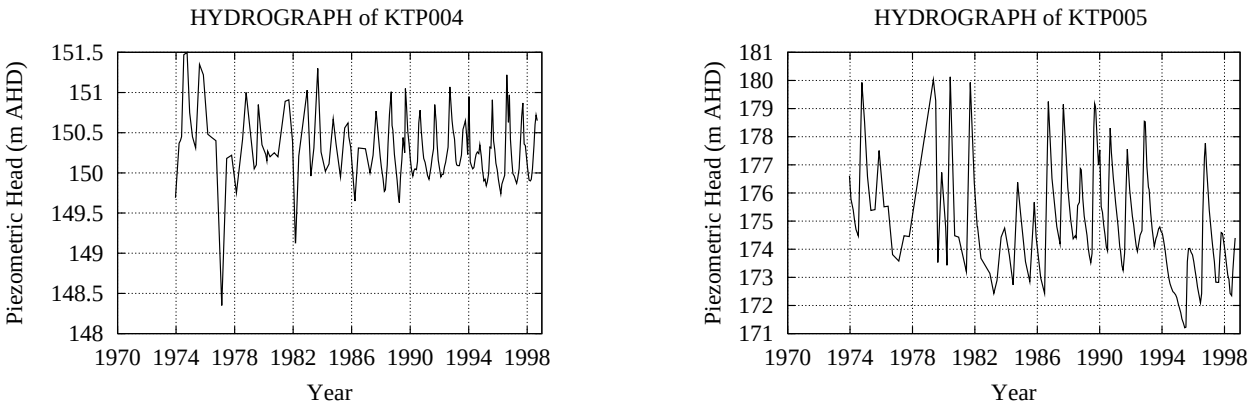

Figure 5.6: *Hydrographs of observation wells KTP004 and KTP005 of the Basement aquifer.*

5.3 Steady–state calibration using the trial and error method.

Using the method of trial and error, initial values of 600 m^2/day for transmissivity in the x and y directions for each of the aquifers, and a value of 100 for the leakance between

the Port Willunga and Maslin Sands aquifers have been used in the forward model. A total of 39 observation wells have also been used for the calibration with 15 from the Port Willunga Formation aquifer, 14 from of the Maslin Sands aquifer and 10 from the Basement aquifer. Any observation well that did not lie exactly on a point of the finite–difference grid has been projected to the nearest grid point.

The results from the forward model have been compared with the measured heads along the line AB (Figures 4.5, 4.8 and 4.12) using the mathematical measure

$$\text{error} = \sum_{i=1}^{39} \frac{100}{39} \left| \frac{h_i^{obs} - H_i(\mathbf{p})}{h_i^{obs}} \right| \%, \tag{5.1}$$

where h_i^{obs} is the recorded piezometric head at the 39 observation locations, and $H_i(\mathbf{p})$ is the output from the forward model at the corresponding 39 locations.

Seven unknown parameters have been identified for the steady–state Willunga Basin model, these being transmissivity in the y and x–directions for the Port Willunga Formation aquifer (PWF T_y, PWF T_x), Maslin Sands aquifer (MS T_y, MS T_x) and the Basement aquifer (B T_y, B T_x) and the leakance between the Port Willunga and Maslin Sands aquifer (PWF-MS L). As described in Section 3.4.2, for steady–state problems with no injection or extraction of groundwater it is the ratio between the transmissivities and leakance that determines the rate of flow within the aquifers. As a result of this, the transmissivity in the y–direction for the Port Willunga Formation aquifer (PWF T_y) has been fixed at 600 m^2/day. The process of calibrating the steady–state groundwater model of the Willunga Basin has therefore involved the estimation of the other 6 parameters.

Having performed the initial run of the forward model (i.e. 600 m^2/day for transmissivity in the x and y–directions for each of the aquifers, 100 m/day/m for the leakance between the Port Willunga and Maslin Sands aquifers) the unknown transmissivity parameters have been increased by 50 m^2/day which produced an error higher than that from the initial run. Because of this, the unknown transmissivity parameters have been decreased, one at a time, by 50 m^2/day, while the leakance parameter was decreased by 10 m/day/m. Each of the parameters have been reduced in this way until a minimum error was obtained. Having achieved a reasonable match, the leakance parameter has been further decreased by amounts of 1 m/day/m. Table 5.1 shows the values for the unknown parameters for each of the aquifers resulting from the trial and error calibration. In this table PWF T_y refers to the transmissivity in the y–direction for the Port Willunga Formation aquifer, etc. The value of the error as calculated by Equation (5.1) for the

parameter values in Table 5.1 has been found to be 48%. Although this value for the error seems relatively large, it was considered that sufficient effort has been made to calibrate the model. Figure 5.7 shows the cross–sectional view of the comparison between the

Table 5.1: *Values for the transmissivity parameters T_y and T_x for each of the aquifers and the leakance PWF-MS L between the Port Willunga Formation and the Maslin Sands aquifers after calibration using the method of trial and error.*

PWF T_y	PWF T_x	MS T_y	MS T_x	B T_y	B T_x	PWF-MS L
600.0	400.0	350.0	500.0	50.0	500.0	4.0

observed and modelled piezometric head on 14/8/1995 for each of the aquifers projected onto the line AB of Figure 4.5(a). From Figure 5.7 it can be seen that a good match has been obtained between the modelled and observed data. Even though this is the case, the response function inverse technique has been used to attempt to improve the calibration for the unknown parameter values, with the results described in the following section.

5.4 Steady–state calibration using response function method.

For the response function method the same set of parameters have been assumed unknown as for the trial and error calibration method (i.e. PWF T_x, MS T_y, MS T_x, B T_y, B T_x and PWF-MS L, with PWF T_y fixed at 600 m^2/day). As discussed in Chapter 3, initial and perturbed values for the unknown parameters are required. The initial values have been chosen to be the values found using the method of trial and error, shown in Table 5.1.

Using these initial values, the forward model has been run and the resulting piezometric head values at the 39 observation locations recorded. This initial run has been followed by an additional 6 runs wherein each of the unknown parameters has been increased by 10% in turn. For example, the second run has been performed using the values 440.0, 350.0, 500.0, 50.0, 500.0, 4.0 for the parameters PWF T_x, MS T_y, MS T_x, B T_y, B T_x and PWF-MS L respectively.

Having performed these 7 (initial + 6 perturbed) runs of the forward model the

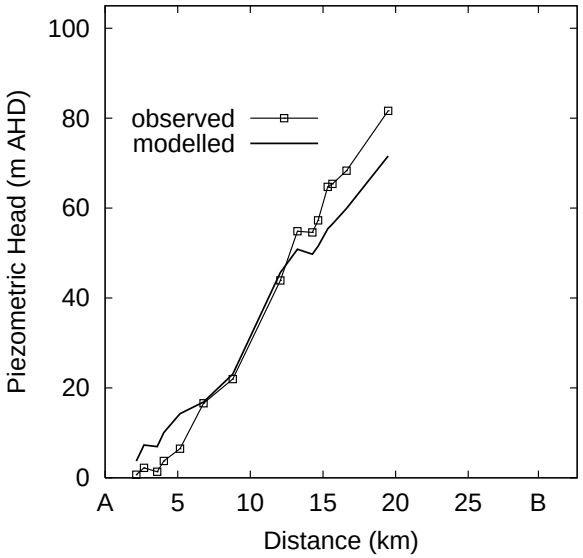

(a) Port Willunga Formation aquifer

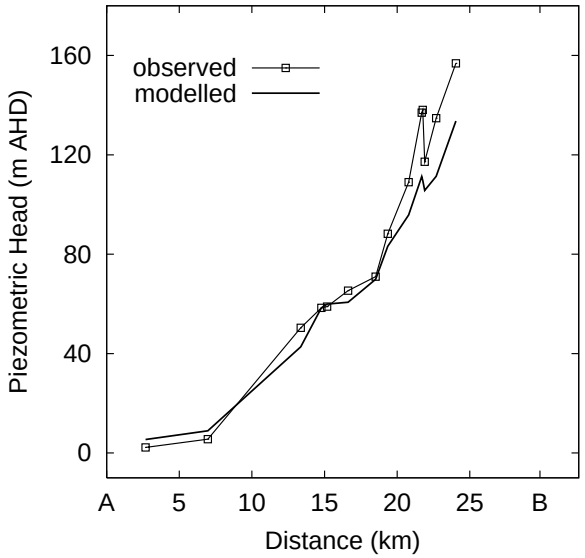

(b) Maslin Sands aquifer

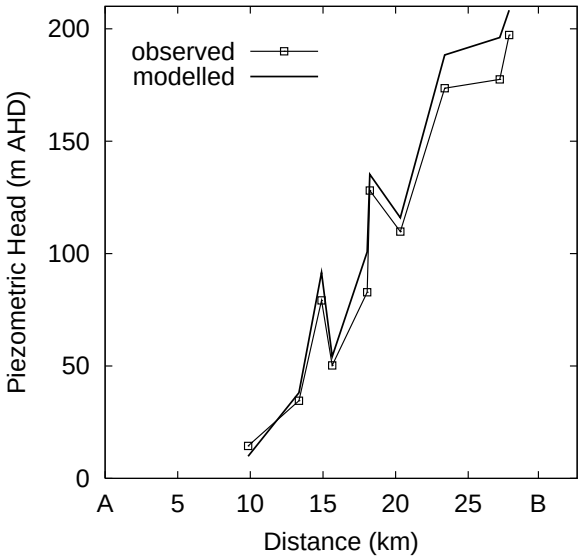

(c) Basement aquifer

Figure 5.7: *A comparison between the observed and modelled piezometric head on 14/8/1995 for (a) the Port Willunga Formation aquifer, (b) the Maslin Sands aquifer and (c) the Basement aquifer along the line AB (see Figure 4.5), after calibration using the method of trial and error.*

response functions were initially chosen to be $1/\sqrt{p}$. For transmissivity, this corresponded with the analytical solution of Equation 2.9. An upper and lower limit has also been applied to the unknown transmissivity parameters so that the ranges that were estimated experimentally in the field [32] could be conserved. Any estimated parameter value greater than the upper bound was restricted to the upper bound value and similarly any value that was less than the lower bound was restricted to the lower bound value. An upper bound value of 5560 m^2/day and a lower bound of 16 m^2/day for transmissivity

have been used [32]. These upper and lower bound values are the largest and smallest values found for transmissivity over the entire Basin. While restrictions to the upper and lower bounds could be made that reflect the values found for the individual aquifers (e.g. 45 to 5560 m^2/day for the Port Willunga Formation aquifer, 16 to 49 m^2/day for the Maslin Sands aquifer and 44 m^2/day for the Basement aquifer) it has been decided that too few locations have been sampled, particularly for the Maslin Sands and Basement aquifers, for tighter bounds.

After an initial run of the inverse response function method it has been found that the new estimated values resulted in an error larger than that obtained from the trial and error method. By changing the response functions to linear for each parameter in turn and re–running the response function method it has been found that linear response functions for the T_x parameter for both the Maslin Sands and Basement aquifers (i.e. MS T_x and B T_x) resulted in a smaller error.

The response function method has been applied 21 times resulting in the values shown in Table 5.2. Figure 5.8 shows the very good comparison between the observed and modelled piezometric head for each of the aquifers in the Willunga Basin for 14/8/1995.

Using the response function method the error has been found to be 27 % compared to an error of 48 % using the method of trial and error. This indicates that the response function method has reduced the error between the modelled and observed piezometric heads considerably, improving the calibration of the steady–state model.

5.5 Model for the transient simulations.

The transient model for the Willunga Basin uses the same boundary conditions as for the steady–state model, together with the transmissivities and leakance determined during calibration of the steady–state model. While some records are kept as to the amount of groundwater that is extracted from the Willunga Basin over each year, no data exists as to when specifically amounts are extracted. Similarly, no records exist as to which of the production wells take water from each aquifer.

Figure 5.9 shows the grid points that lie in the outcrop regions for the Port Willunga Formation, Maslin Sands and Basement aquifers. It has been estimated [17] that 1050 ML/year, 900 ML/year and 2100 ML/year of rainfall recharge the aquifers respectively. It is also assumed that the rainfall only infiltrates each aquifer during the months May to

Table 5.2: *Values for the transmissivity parameter T_y and T_x for each of the aquifers and the leakance PWF-MS L between the Port Willunga Formation and the Maslin Sands aquifers after calibration using the response function method.*

no. of iter.	PWF T_y	PWF T_x	MS T_y	MS T_x	B T_y	B T_x	PWF-MS L	error (%)
0	600.0	400.0	350.0	500.0	50.0	500.0	4.0	48.7135
1	600.0	53.2	297.0	500.3	28.1	499.4	1.0	37.1826
2	600.0	62.6	521.4	2882.3	16.0	16.0	1.6	27.5672
3	600.0	79.9	123.2	5169.8	16.0	16.0	3.4	28.2297
4	600.0	31.9	5560.0	2882.6	16.0	16.0	0.9	59.5945
5	600.0	51.9	1281.6	2882.3	16.0	16.0	1.6	32.2420
6	600.0	60.5	602.6	2882.3	16.0	16.0	1.6	27.2233
7	600.0	76.1	124.4	5178.0	16.0	16.0	3.3	28.1480
8	600.0	30.8	5560.0	2882.6	16.0	16.0	0.8	59.4330
9	600.0	50.7	1388.5	2882.3	16.0	16.0	1.6	33.3030
10	600.0	58.6	691.1	2882.3	16.0	16.0	1.6	27.2378
11	600.0	60.2	611.5	2882.3	16.0	16.0	1.6	27.1912
12	600.0	75.8	124.5	5179.0	16.0	16.0	3.3	28.1436
13	600.0	30.7	5560.0	2882.6	16.0	16.0	0.8	59.4172
14	600.0	50.6	1398.5	2882.3	16.0	16.0	1.6	33.3986
15	600.0	58.4	700.7	2882.3	16.0	16.0	1.6	27.2533
16	600.0	60.1	620.5	2882.3	16.0	16.0	1.6	27.1592
17	600.0	75.4	124.7	5180.1	16.0	16.0	3.2	28.1351
18	600.0	30.6	5560.0	2882.6	16.0	16.0	0.8	59.4005
19	600.0	50.5	1408.2	2882.3	16.0	16.0	1.6	33.4923
20	600.0	58.2	710.4	2882.3	16.0	16.0	1.6	27.2677
21	600.0	59.9	629.5	2882.3	16.0	16.0	1.6	27.1564

October, with May and October having half the infiltration of June through to September. As there are 190 grid points that outcrop the Port Willunga Formation aquifer this results in 18 m^3/day/grid point for May and October and 36 m^3/day/grid point for the months of June through September. For the Maslin Sands aquifer, there are 145 grid points that

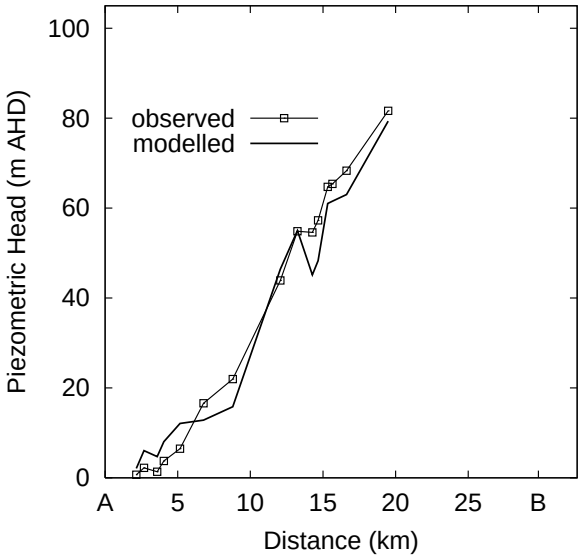

(a) Port Willunga Formation aquifer

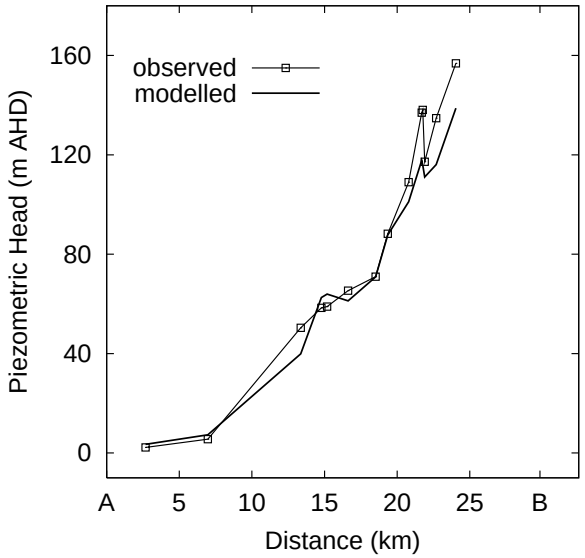

(b) Maslin Sands aquifer

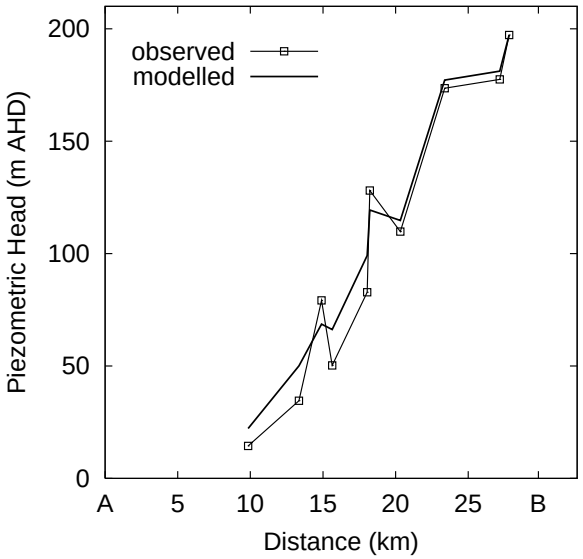

(c) Basement aquifer

Figure 5.8: *A comparison between the observed and modelled piezometric head on 14/8/1995 for (a) the Port Willunga Formation aquifer, (b) the Maslin Sands aquifer and (c) the Basement aquifer along the line AB (see Figure 4.5) from applying the response function method.*

lie in the outcrop region; this results in 20 m^3/day/grid point for May and October and 41 m^3/day/grid point for the months of June through September. For the Basement aquifer 132 grid points lie in the outcropping region, which results in 52 m^3/day/grid point for May and October and 104 m^3/day/grid point for the months of June through September.

Figure 5.10 shows the grid points for which it is believed water is extracted from the Port Willunga Formation, the Maslin Sands and Basement aquifers by the production

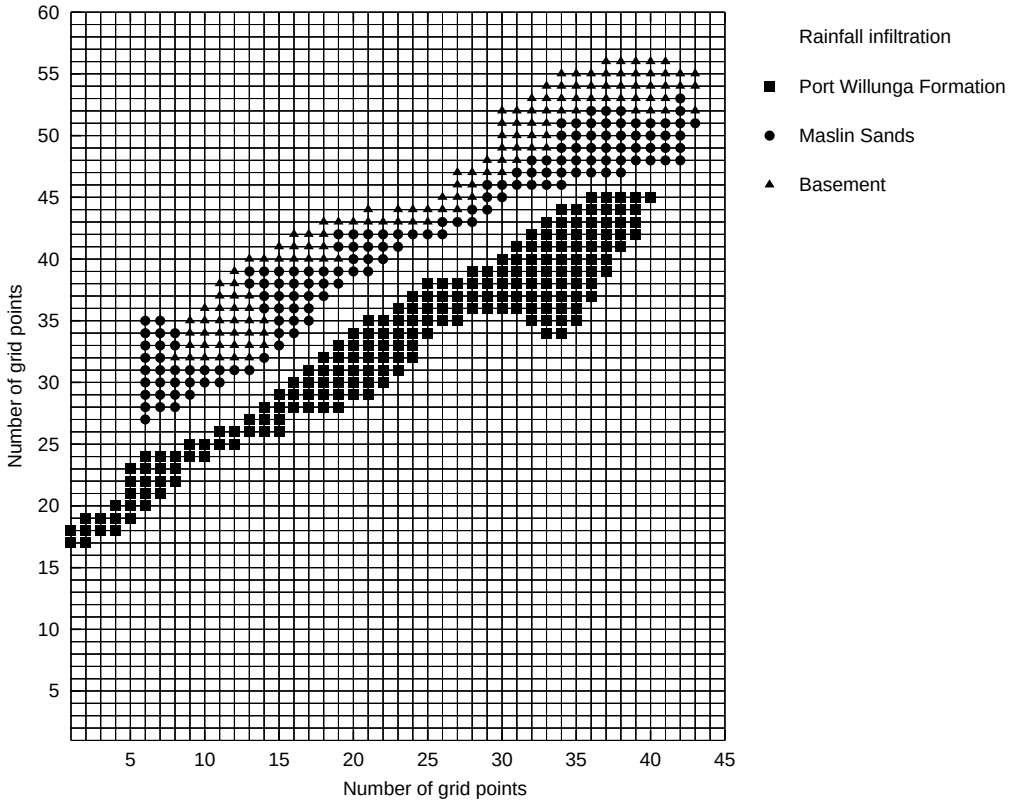

Figure 5.9: *The grid points representing rainfall infiltration for the Port Willunga Formation, Maslin Sands and Basement aquifers.*

wells [31]. This distribution of wells for each of the aquifers is based on the wells spatial location within the Willunga Basin and not on the stratigraphy. As mentioned in Section 4.3, it is quite likely that this information is inaccurate [26]. It is assumed that extraction occurs over the period December to March, with January and February having twice the extraction rates of December and March.

5.6 Transient calibration using the response function method

Using the values found for transmissivity and leakance for each of the aquifers from the steady–state response function method (Table 5.2), a transient calibration has been performed to determine the storativity for the Port Willunga Formation aquifer (PWF S).

As the storativity controls the steepness of the draw down curve and the rate of

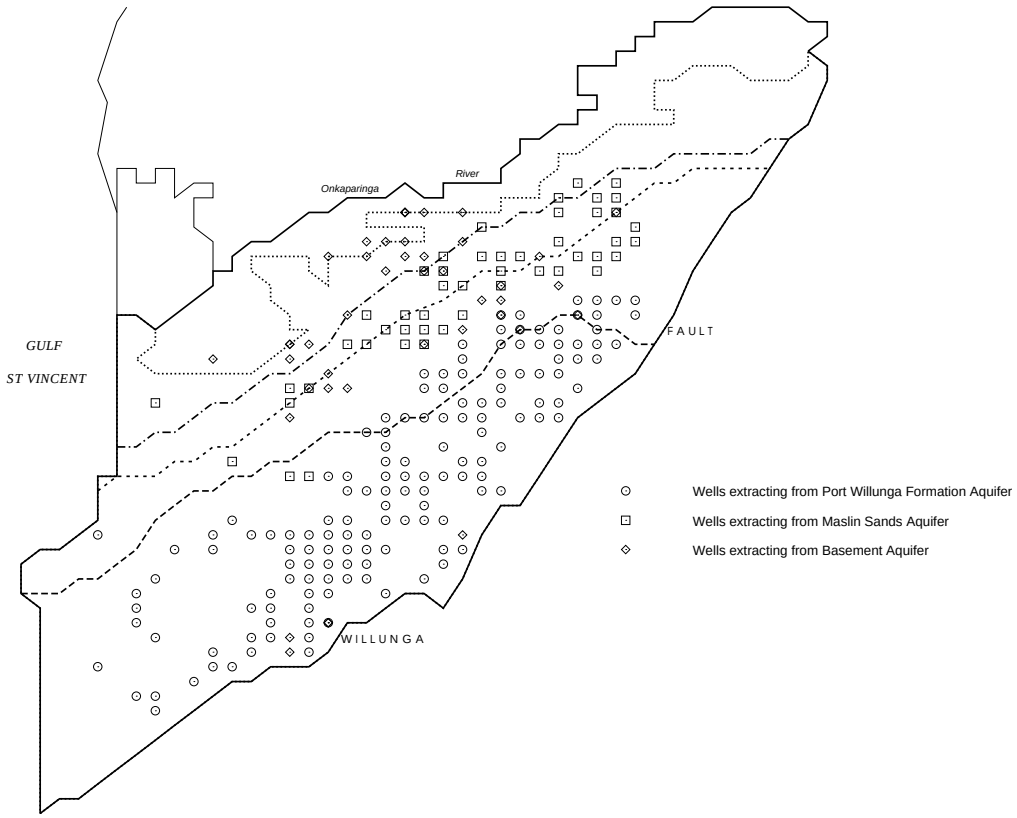

Figure 5.10: *Modelled location of production wells for the year 1995–1996.*

recovery of the groundwater table once extraction has stopped, two calibration dates, 11/1/1996 and 8/4/1996, have been used. 13 observation wells have piezometric head levels recorded for 11/1/1996 and 15 for 8/4/1996. This gives a total of 28 recorded head values. The error equation then becomes

$$\text{error} = \sum_{i=1}^{28} \frac{100}{28} \left| \frac{h_i^{obs} - H_i(\mathbf{p})}{h_i^{obs}} \right| \%, \tag{5.2}$$

where h_i^{obs} is the 28 recorded piezometric heads, and $H_i(\mathbf{p})$ is the output from the forward model at the corresponding locations and times.

An initial value of 0.0062 has been estimated to be the average value of storativity from Section 4.2.1. For the Maslin Sands and Basement aquifers the storativity was also taken from Sections 4.2.4 and 4.2.7. The perturbed parameter value for the storativity for the Port Willunga aquifer has been selected to be 0.0092; an additional 10 % of the initial value was shown to have no effect at several observation wells, indicating that the storativity parameter is insensitive to small changes. This insensitivity has also been found to a greater extent with the storativity for the Maslin Sands and Basement aquifers. For this reason, they have not been included in the transient calibration process but given constant values and are shown in Table 5.3.

Using the response function method with a linear response function the value for storativity for the Port Willunga aquifer was found to be 0.0046 as shown in Table 5.3. This value for storativity was found after 10 iterations. The initial error value

Table 5.3: *Values for the storativity parameter S for the Port Willunga Formation (PWF), the Maslin Sands aquifer (MS), and the Basement aquifer (B) after calibration using the response function method.*

No. of iter.	PWF S	MS S	B S	error (%)
0	0.004600	000086	0.00015	32.5055
1	0.024147	000086	0.00015	46.5922
2	0.004603	000086	0.00015	32.5103
3	0.004600	000086	0.00015	32.5049
4	0.024147	000086	0.00015	46.5922
5	0.004603	000086	0.00015	32.5104
6	0.004601	000086	0.00015	32.5045
7	0.024147	000086	0.00015	46.5922
8	0.004603	000086	0.00015	32.5100
9	0.004601	000086	0.00015	32.5053
10	0.004601	000086	0.00015	32.5044
11	0.024146	000086	0.00015	46.5922
12	0.004603	000086	0.00015	32.5100
13	0.004601	000086	0.00015	32.5053
14	0.004601	000086	0.00015	32.5055
15	0.004601	0.000086	0.00015	32.5044

was calculated to be 32.5055 %, while the converged value of the error was found to be 32.5044 % as calculated using Equation (5.2). These two error values are very similar which suggests that the initial value used for the storativity was relatively accurate. It also indicates a significant lack of sensitivity of the simulated piezometric head to changes in storativity.

5.7 Validation of the transient model

With all the unknown parameter values estimated, the forward model has been used to simulate groundwater levels from 14/8/1995 until 14/8/2000 to verify the values estimated by the response function calibration method.

Figure 5.11 shows the location of the observation wells used for the validation of the

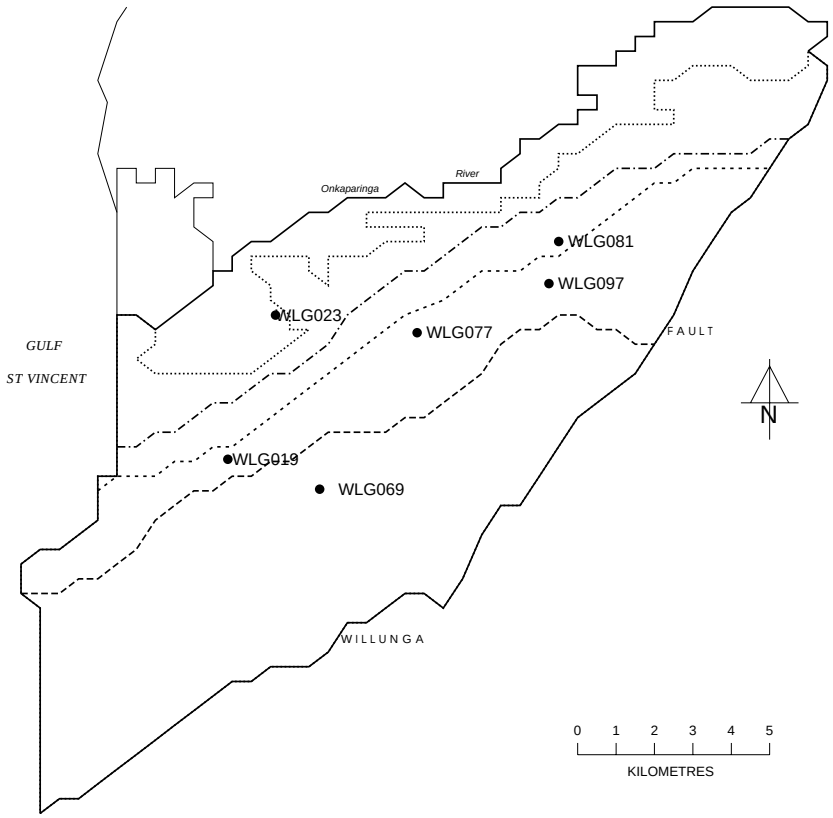

Figure 5.11: *Location of the observation wells used for the validation of the forward model using the parameter values estimated by the response function method.*

forward model using the parameter values estimated by the response function method. Figures 5.12–5.13 show a comparison between the modelled and observed piezometric head at two locations for each of the aquifers within the Willunga Basin. From these figures it can be seen that a poor match has been obtained for most of the wells.

Calibration of the steady–state model using the response function method produced a good match between the modelled and recorded piezometric heads. However for the transient model a poor calibration has been obtained. It is believed that the poor calibration is not the result of the response function method performing poorly but to inaccuracies in the transient model.

Some of the possible causes for these inaccuracies are that the data relating to the

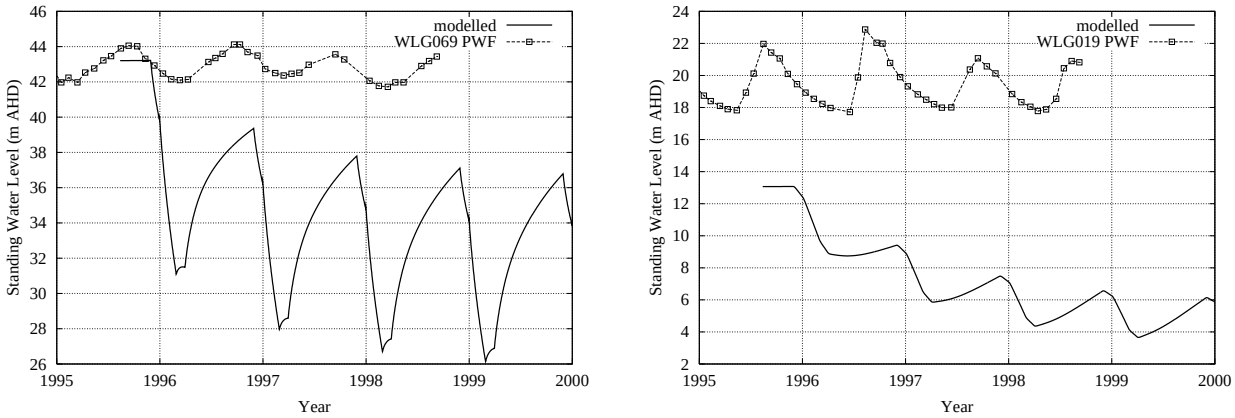

Figure 5.12: *The modelled and observed standing water levels at observation wells* (a) *WLG069 and* (b) *well WLG019 for the Port Willunga Formation aquifer.*

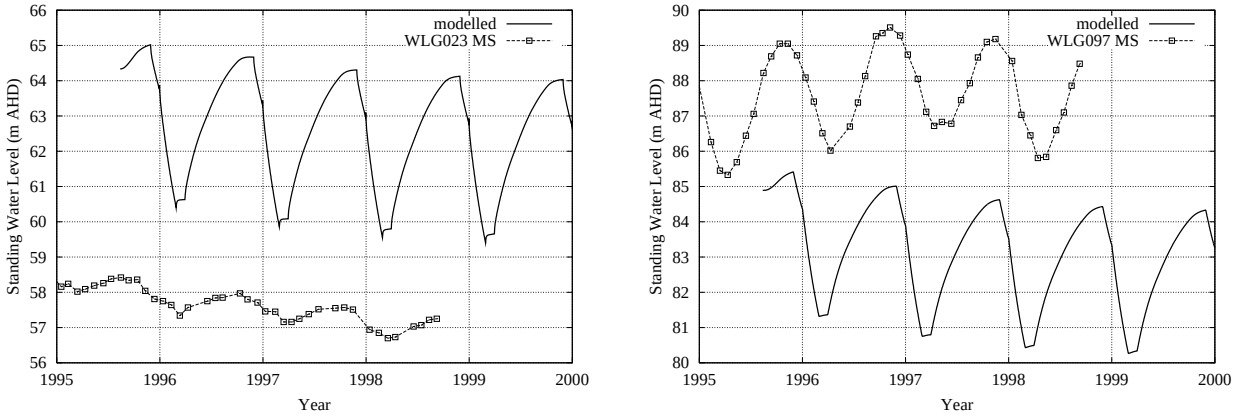

Figure 5.13: *The modelled and observed standing water levels at observation wells* (a) *WLG023 and* (b) *well WLG097 for the Maslin Sands aquifer.*

volume of water that is extracted from the production wells is likely to have been poorly estimated rather than metered. It has been suggested [26, 29] that many of the major irrigators did not have meters attached to their wells for the 1995–1996 extraction period. Also no definitive study has been made as to which of the extraction wells extract water from a particular aquifer. This has been approximated based on the production well's spatial location without knowledge of the screen depth of each well.

However some of the results are qualitatively accurate. The annual oscillations estimated by the forward model and shown in Figure 5.14(a), 5.15(a) and 5.15(b) seem quite

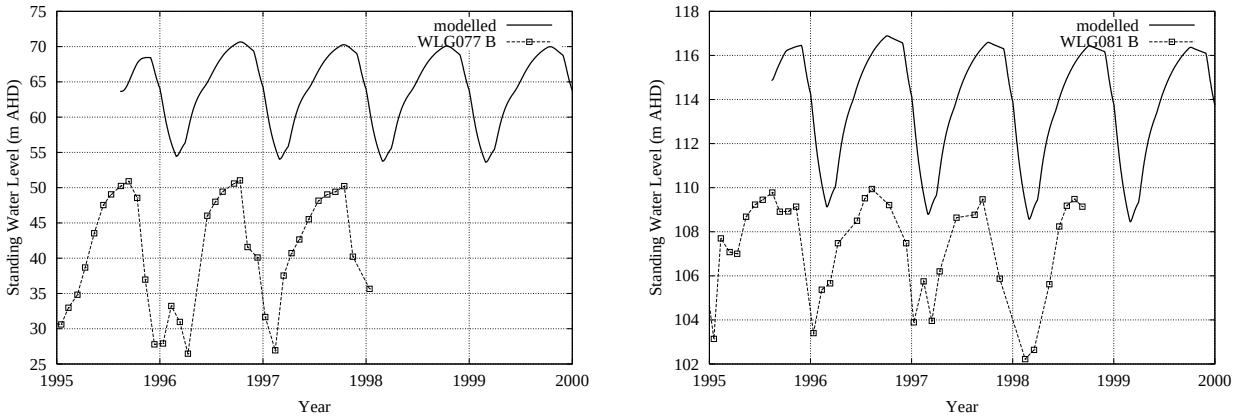

Figure 5.14: *The modelled and observed standing water levels at observation wells* (a) *WLG077 and* (b) *well WLG081 for the Basement aquifer.*

accurate, although the average standing water levels are inaccurate. The decreases in average water levels at well WLG023 (Figure 5.14(a)) also seem to be very consistent. In other aspects, though, the results must be considered to be inaccurate.

The overall goal of this thesis has been to develop a calibration technique that is an improvement over existing techniques. The application of the response function method to the steady–state model of the Willunga Basin has shown a definite improvement in calibration over an application of the trial and error method. If the prime objective of this research was to develop the optimal calibrated and validated groundwater flow model of the Willunga Basin, then additional work would be needed to improve the current transient model. As this is not the case, the author feels that the development of the response function technique (the primary objective), its comparison with other existing techniques (the secondary objective) and its application to the Willunga Basin (the third objective) justifies not spending additional time on improving the transient model.

Chapter 6

Sustainable Yield for the Willunga Basin

6.1 Introduction

The sustainable yield of a groundwater system is the amount of groundwater that can be safely withdrawn over a yearly cycle without exceeding the natural yearly recharge rate [17]. While this definition is appropriate for a groundwater system that has previously been in steady–state (i.e. before extraction has occurred), some consideration should also be given within this definition to include the restoration of previously degraded groundwater levels to steady–state levels. From the literature it has been suggested that 5700 ML/yr of groundwater are sustainable for the Willunga Basin [17].

6.2 Estimating sustainable yield

From data obtained from PIRSA [32], 5057 ML, 1295 ML and 563 ML of groundwater were extracted from the Port Willunga Formation, Maslin Sands and Basement aquifers respectively for 1995–1996, giving a total of 6915 ML (although, as suggested in Section 4.3, this is highly questionable). The forward model developed in Chapter 5 has been used to estimate the piezometric head levels in the basin resulting from an annual extraction volume of 6915 ML/yr for the time period of 1996–2010. The boundary conditions, the regime of extraction of groundwater from the basin and the rainfall recharge are as described in Chapter 5, with the initial conditions taken to be the steady–state levels as of 14/8/1995. Figure 6.1 shows modelled hydrographs for observation wells within the

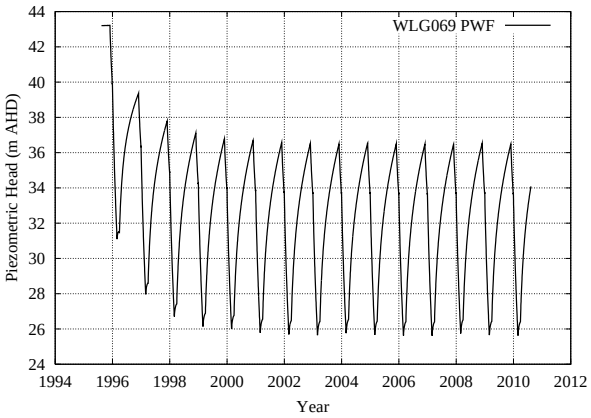

(a) Hydrograph for WLG069

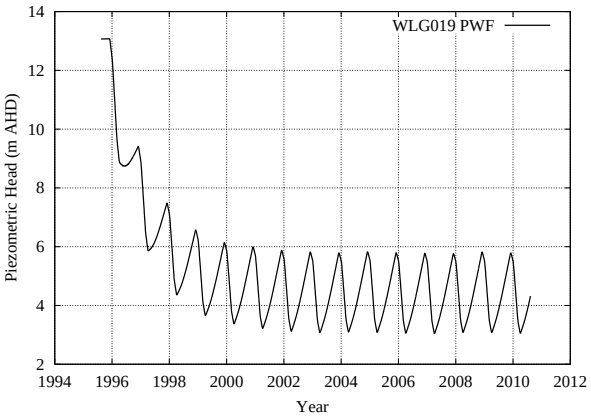

(b) Hydrograph for WLG019

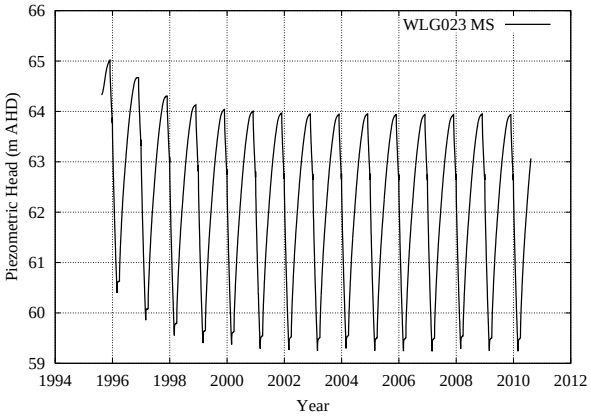

(c) Hydrograph for WLG023

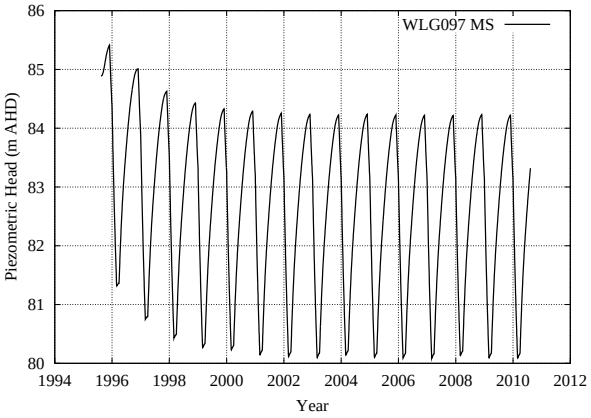

(d) Hydrograph for WLG097

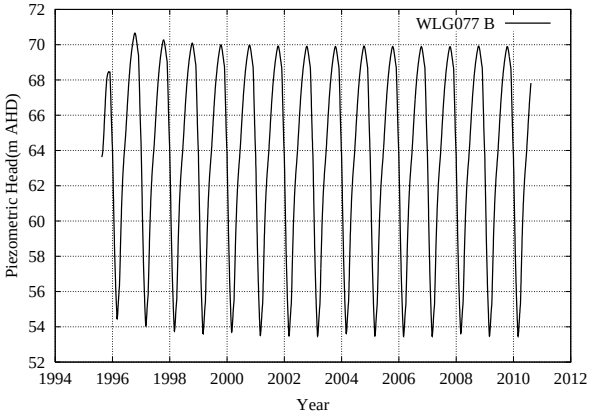

(e) Hydrograph for WLG077

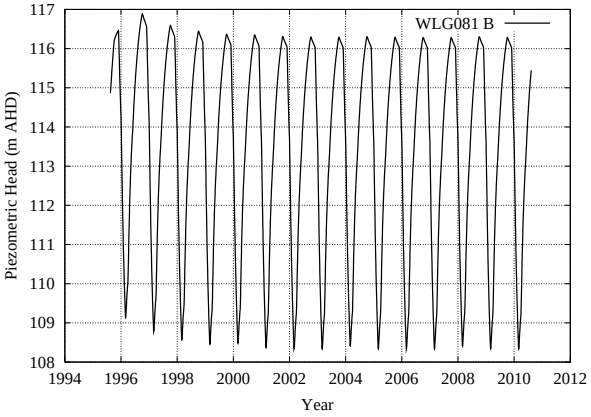

(f) Hydrograph for WLG081

Figure 6.1: *The modelled piezometric head at observation wells (a) WLG069 and (b) WLG019 for the Port Willunga Formation aquifer, (c) WLG023 and (d) WLG097 for the Maslin Sands aquifer and (e) WLG077 and (f) WLG081 for the Basement aquifer using an annual extraction rate of 6915 ML/yr.*

Willunga Basin with these wells being located as shown in Figure 5.11. From Figure 6.1 it can be seen that the piezometric head at each of the observation wells declines initially until reaching a steady–annual oscillation. This figure also shows that an extraction volume of 6915 ML/year would significantly reduce the piezometric head levels in the basin in comparison to the steady–state levels at 14/8/1995; however, these reduced piezometric head levels would be maintained (although it is likely that this steady oscillation is a result of the prescribed boundary conditions).

6.2.1 Modifying extraction rates

By assuming the same distribution of extraction wells and relative extraction rates as in Figure 5.10, a multiplication factor of 0.8242 was applied to the 1995–1996 extraction rates for the years 2000–2010 for each production well to give an annual extraction rate of 5700 ML/year (the suggested sustainable yield [17]).

Figure 6.2 shows the hydrographs resulting from an extraction rate of 6915 ML/year for the years 1995 through to 1999 and an extraction rate of 5700 ML/year from 2000 until 14/8/2010. From this figure it can be seen that the piezometric head in each of the observation wells declines from 1996 to 2000 when the 6915 ML/year extraction rate has been applied, and there after increases until reaching a constant level resulting from the 5700 ML/year extraction rate. Although the groundwater extraction rates of 6915 ML/year and 5700 ML/year both ultimately result in "steady" piezometric heads for the Willunga Basin over a yearly cycle, the head levels over the basin are significantly lower than at steady–state on 14/8/1995 except for the Basement aquifer.

6.2.2 Using the inverse response function for optimised sustainable yield

A numerical experiment has been performed where the annual rate of extraction from the Willunga Basin has been sought for the years 2000 through to 2010, so that the observed piezometric head at observation well WLG019 on 30/11/2007 is 12.5 m. It has been assumed that 6915 ML/year of groundwater are extracted from 1996 to 1999. The same distribution of production wells as for the 1995–1996 season has also been assumed, with the volume of extraction of each well multiplied by a factor to increase or decrease the overall volume extracted from the basin. The initial value for the factor has been

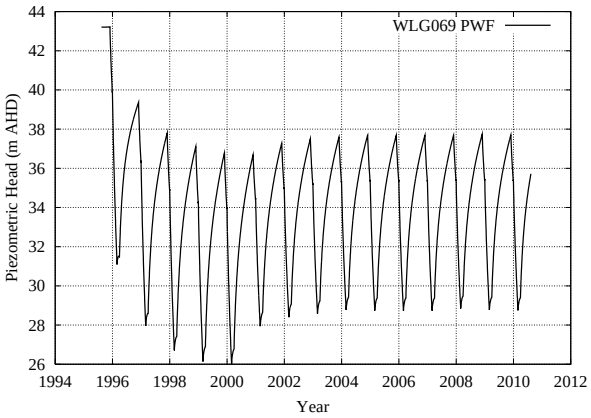

(a) Hydrograph for WLG069

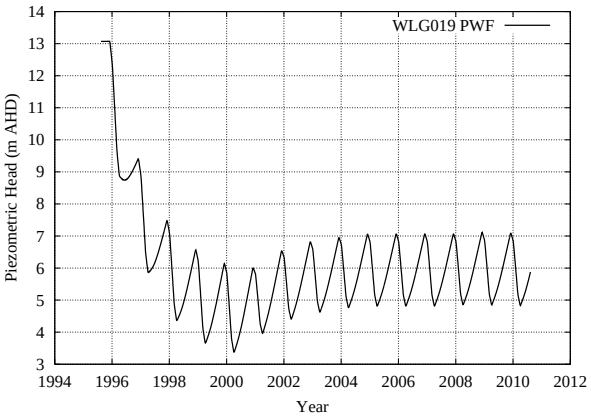

(b) Hydrograph for WLG019

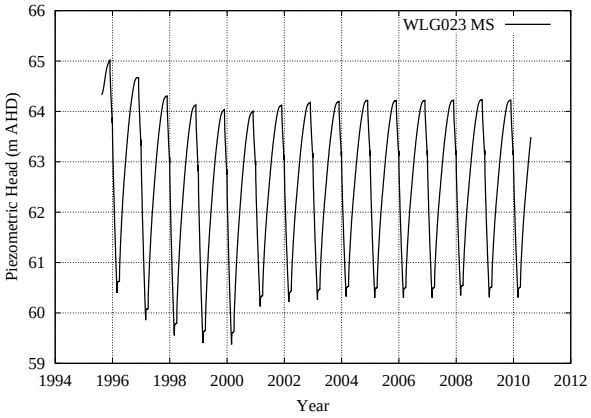

(c) Hydrograph for WLG023

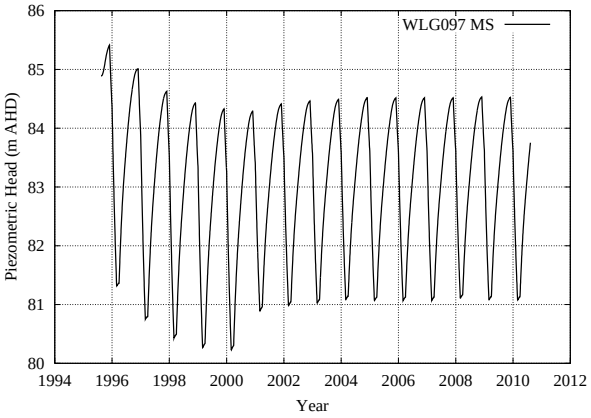

(d) Hydrograph for WLG097

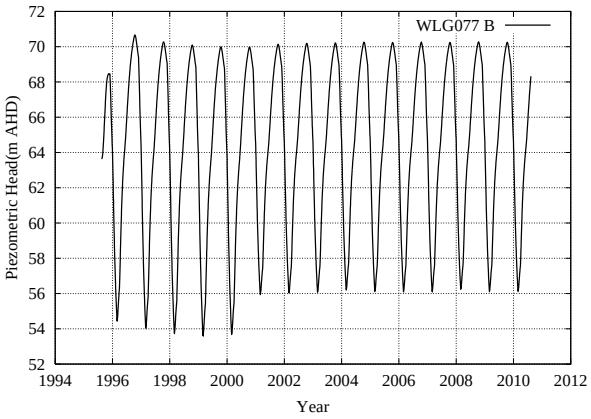

(e) Hydrograph for WLG077

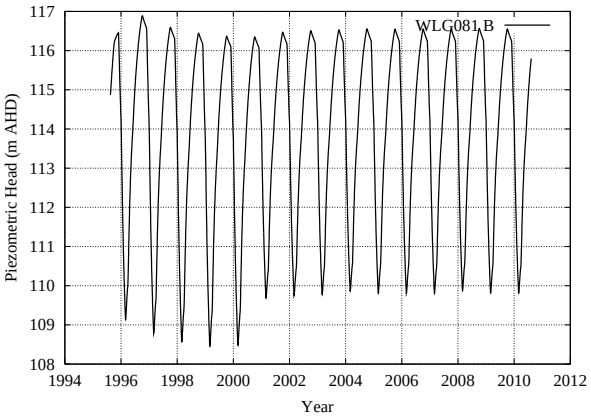

(f) Hydrograph for WLG081

Figure 6.2: *The modelled piezometric head at observation wells (a) WLG069 and (b) WLG019 for the Port Willunga Formation aquifer, (c) WLG023 and (d) WLG097 for the Maslin Sands aquifer and (e) WLG017 and (f) WLG081 for the Basement aquifer using an annual extraction rate of 5700 ML/year.*

chosen to be 0.7. This corresponds to approximately 4842 ML/year. A perturbed value of 0.77 corresponding to approximately 5324 ML/year has also been used. This initial value has been chosen as it can be assumed that the value must be lower than the 0.8242 factor which resulted in piezometric head levels of approximately 6 m for WLG019, as can be seen in Figure 6.2. With no analytic solution or previous experience in estimating parameters of this type, a linear response function has been assumed.

After applying the response function method, convergence for the error occurred in 1 iteration; in this case the response between the model output and the factor must be linear.

In order for the piezometric head at well WLG019 to return to 12.5 m on 30/11/2007, a factor of 0.088 is required. This equates to an extraction rate of only 600 ML/year.

Figure 6.3 shows the model output at the observation wells within the Willunga Basin using an extraction rate of 600 ML/year. In particular for observation well WLG019 (Figure 6.3(b)) it can be seen that the piezometric head has returned to the 12.5 m level on 30/11/2007.

Having applied the 6915 ML/year and 5700 ML/year extraction rates to the model of groundwater flow in the Willunga Basin, it can be concluded that groundwater levels would reach a steady–state in both cases. However, extracting groundwater at these rates reduces the overall piezometric head levels in the Willunga Basin significantly. The response function method has been applied to the problem of determining the rate of extraction so that a desired piezometric head is obtained. The response function method performed well with convergence achieved in one iteration. The results suggested that 610 ML/year should be extracted to return observation well WLG019 to 12.5 m by 2007. However, the very poor data regarding the assumed extraction rates as well as the imprecise evaluation of the distribution of the production wells to the aquifers renders this value of 610 ML/year suspect for water management but accurate for the given model. Once again, the primary objective here has been to develop, test, and apply the response function method. This section has shown that it can be applied to many different aspects associated with evaluating management alternatives for groundwater resources.

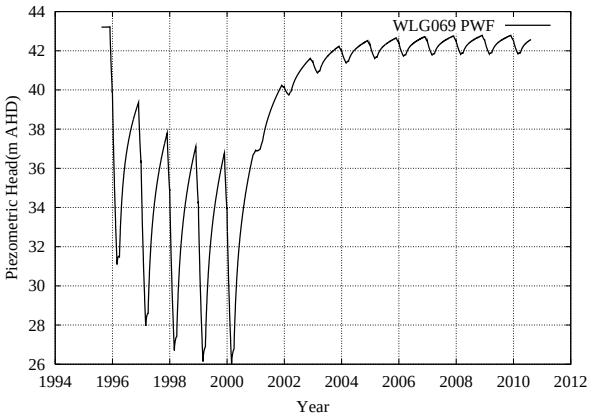

(a) Hydrograph for WLG069

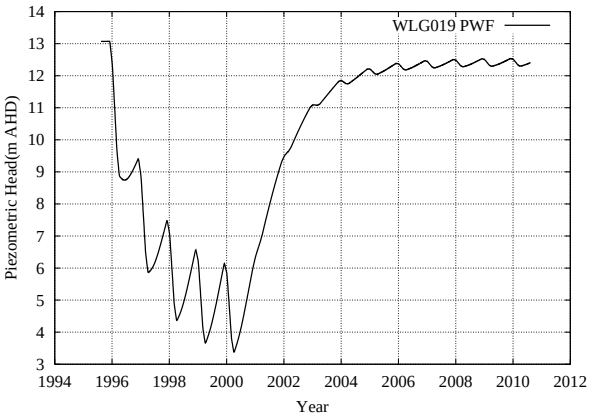

(b) Hydrograph for WLG019

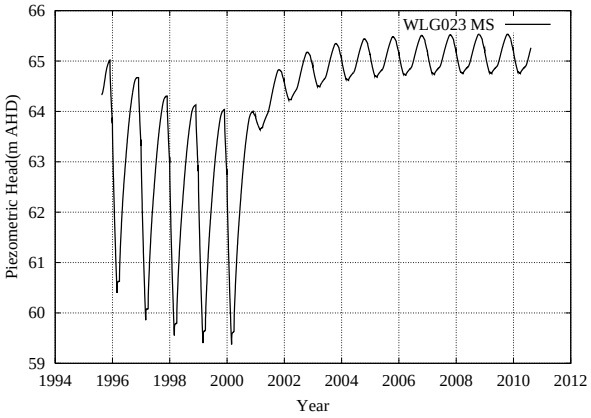

(c) Hydrograph for WLG023

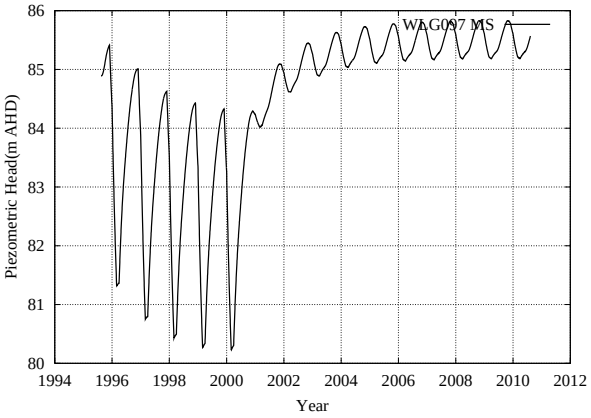

(d) Hydrograph for WLG097

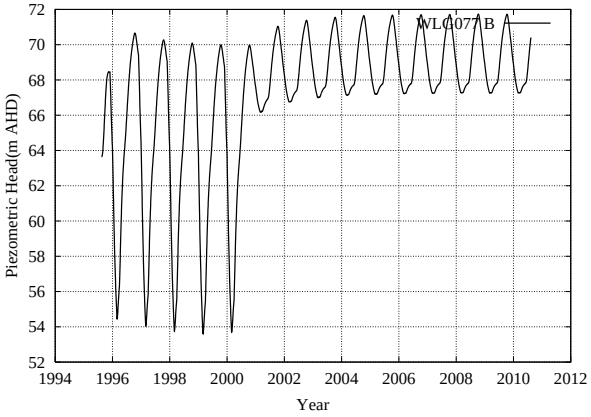

(e) Hydrograph for WLG077

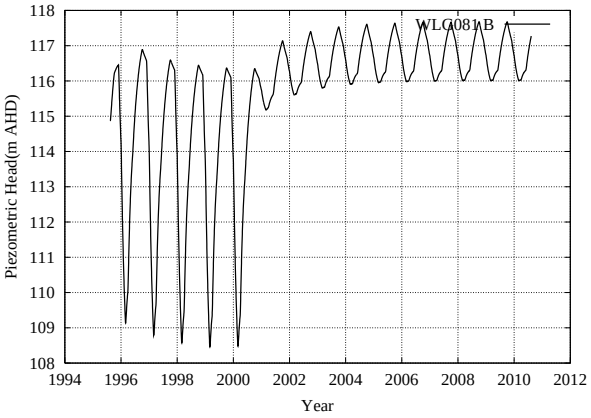

(f) Hydrograph for WLG081

Figure 6.3: *The modelled piezometric head at observation wells (a) WLG069 and (b) WLG019 for the Port Willunga Formation aquifer, (c) WLG023 and (d) WLG097 for the Maslin Sands aquifer and (e) WLG017 and (f) WLG081 for the Basement aquifer using an annual extraction rate of 610 ML/year.*

Chapter 7

Summary and Conclusions

Chapter 1 of this thesis discussed the flow of groundwater and introduced the process of numerical modelling. As part of the process of modelling, the governing equation of groundwater flow was presented and both analytical and numerical solutions discussed. In particular the numerical method used by the groundwater flow code PLASM was examined with regard to quasi–three dimensional flow within and between aquifers.

As part of the process of modelling, inverse methods for the calibration of numerical models have been examined. The process of calibration involves the varying of unknown parameters of a model so that a match is obtained between the output from the model and the recorded values. This process can be performed using the method of trial and error; however it is highly inefficient when a large number of unknown parameters are considered. Other calibration methods using inverse techniques are direct and indirect methods. Because of the nature of groundwater data (i.e. sparsely distributed), indirect inverse methods are more applicable to "real–world" groundwater models.

The indirect inverse techniques of steepest descent and non–linear least squares, as well as a new response function based method have been compared with application to idealised calibration problems. These problems include a two–dimensional function of one parameter, an idealised steady–state model and an idealised transient model. Using these, the response function method gave accurate estimations in the least amount of iterations.

To further test the response function method for calibrating groundwater flow models the Willunga Basin in South Australia, an area used extensively for the production of grapes, almonds and olives, has been examined.

To develop a numerical model of groundwater flow in the Willunga Basin, it was

necessary to estimate some of the unknown parameters of the groundwater model. This has been initially performed under steady–state conditions using the method of trial and error and the response function method. The response function method performed very well and reduced the error between the recorded data and the model output significantly. Following the steady–state calibration, a transient calibration has also been applied using the response function calibration method. Although convergence of the response function method was obtained, the subsequent water levels from the transient model were poor when compared to the recorded data. It is suggested that this is not in a function of the response function method but due to some underlying error in the forward model. The possible sources of the error are the extraction rates that have been applied. Also, no qualitative analysis has been performed to determine which of the production wells extract water from which of the aquifers. This has been approximated using the spatial location of the production wells in the Willunga Basin and has not included the screen depth. It is also possible that homogeneous transmissivity and storativity distributions which have been assumed, may not represent heterogeneous variability which may actually be present in the aquifer.

Although the model has not been validated successfully, the response function method has been used for examination of the sustainable yield within the basin. An extraction volume from the 1995–1996 year and a value from the literature were both used in the model to estimate the piezometric head levels in the basin. It has been found that both extraction volumes are sustainable by the Willunga Basin; however, they cause a continued decrease in groundwater levels in the basin. The response function method has been used to estimate the amount of annual extraction that would lead to a return to a previous piezometric head value in a particular well. This would required a significant reduction in the annual extraction volume from the Willunga Basin, and while the value is questionable for the purposes of management of groundwater resources in the Willunga Basin, the value obtained by the response function method successfully simulated the desired levels.

The response function method is an improved method for the calibration of numerical models and can also be applied to problems of optimisation for management purposes.

Appendix A

Hydrographs of Observation Wells from the Port Willunga Formation Aquifer.

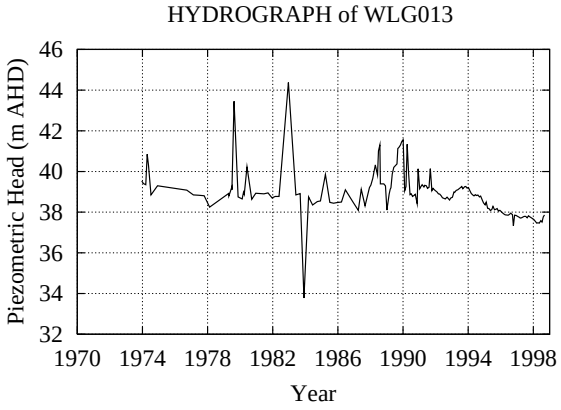

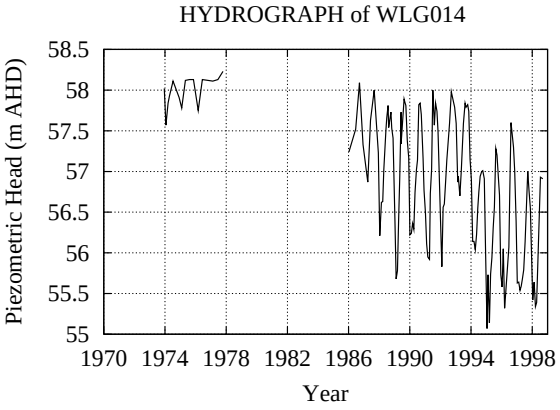

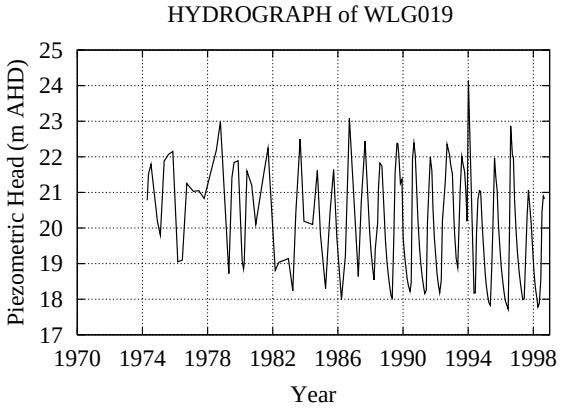

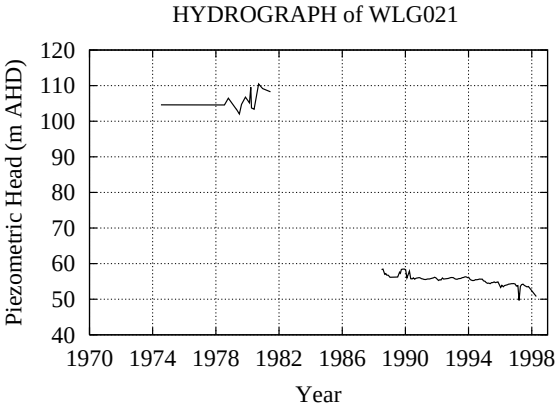

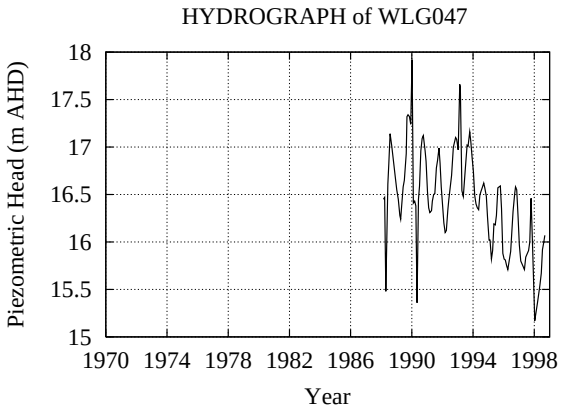
HYDROGRAPH of WLG047
Piezometric Head (m AHD)
18
17.5
17
16.5
16
15.5
15
1970 1974 1978 1982 1986 1990 1994 1998
Year

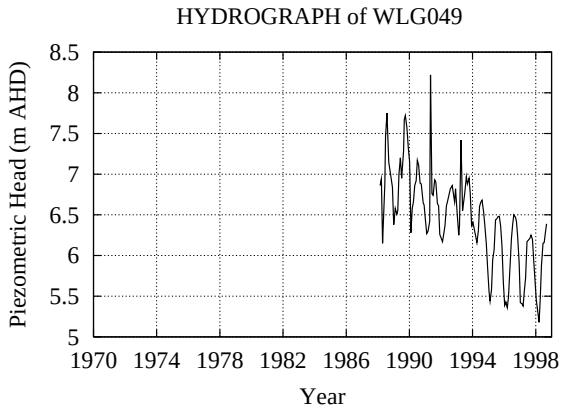
HYDROGRAPH of WLG049
Piezometric Head (m AHD)
8.5
8
7.5
7
6.5
6
5.5
5
1970 1974 1978 1982 1986 1990 1994 1998
Year

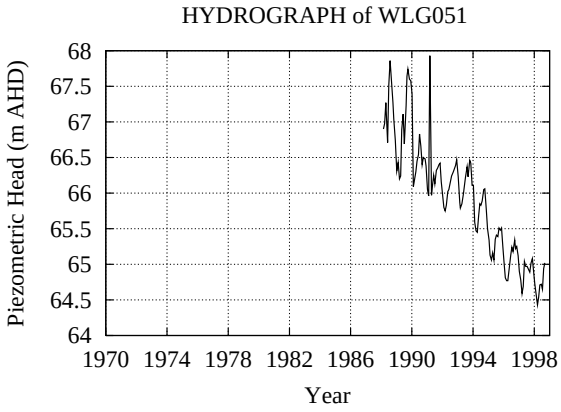
HYDROGRAPH of WLG051
Piezometric Head (m AHD)
68
67.5
67
66.5
66
65.5
65
64.5
64
1970 1974 1978 1982 1986 1990 1994 1998
Year

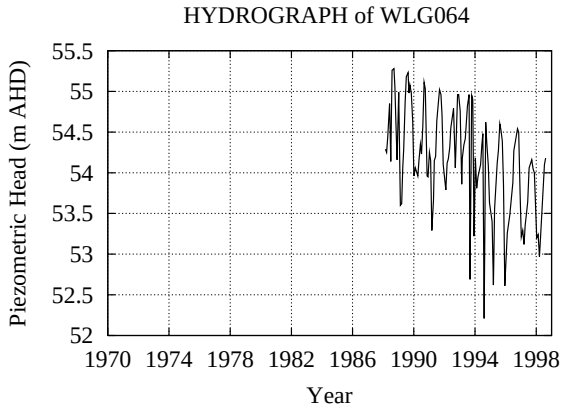
HYDROGRAPH of WLG064
Piezometric Head (m AHD)
55.5
55
54.5
54
53.5
53
52.5
52
1970 1974 1978 1982 1986 1990 1994 1998
Year

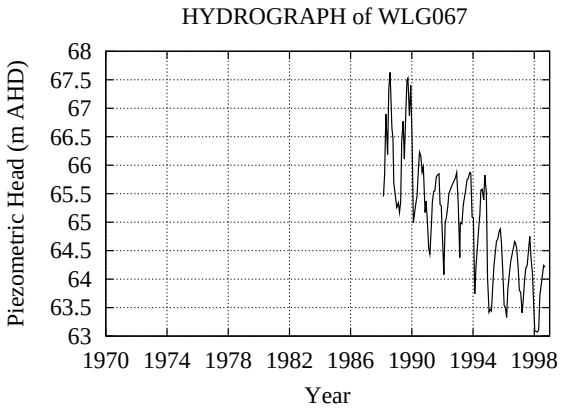
HYDROGRAPH of WLG067
Piezometric Head (m AHD)
68
67.5
67
66.5
66
65.5
65
64.5
64
63.5
63
1970 1974 1978 1982 1986 1990 1994 1998
Year

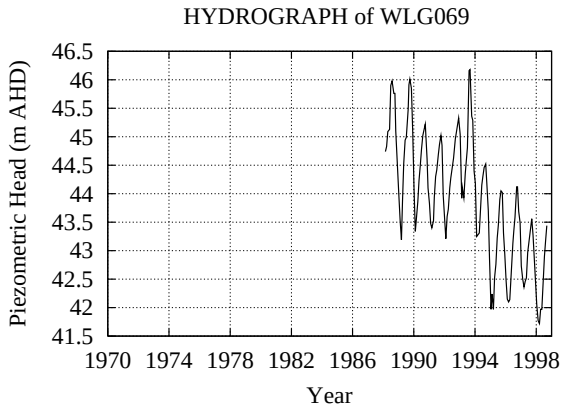
HYDROGRAPH of WLG069
Piezometric Head (m AHD)
46.5
46
45.5
45
44.5
44
43.5
43
42.5
42
41.5
1970 1974 1978 1982 1986 1990 1994 1998
Year

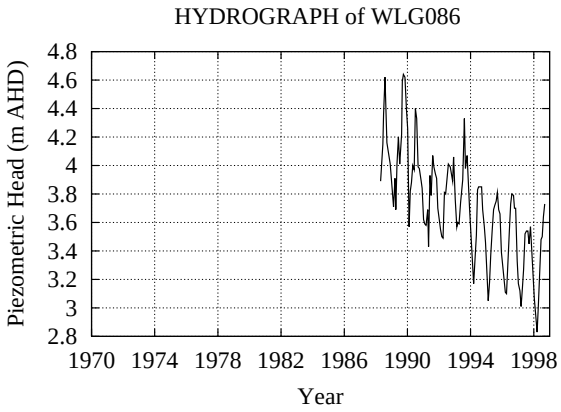
HYDROGRAPH of WLG086
Piezometric Head (m AHD)
4.8
4.6
4.4
4.2
4
3.8
3.6
3.4
3.2
3
2.8
1970 1974 1978 1982 1986 1990 1994 1998
Year

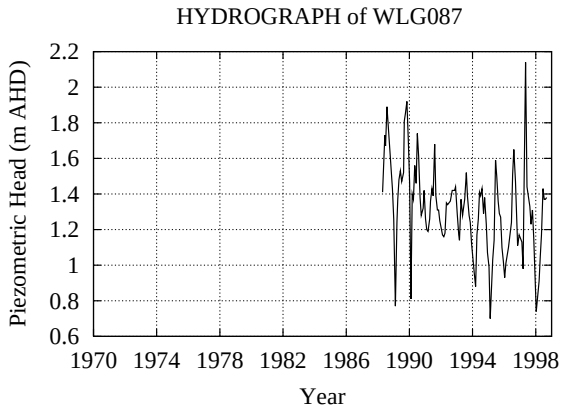
HYDROGRAPH of WLG087
Piezometric Head (m AHD)
2.2
2
1.8
1.6
1.4
1.2
1
0.8
0.6
1970 1974 1978 1982 1986 1990 1994 1998
Year

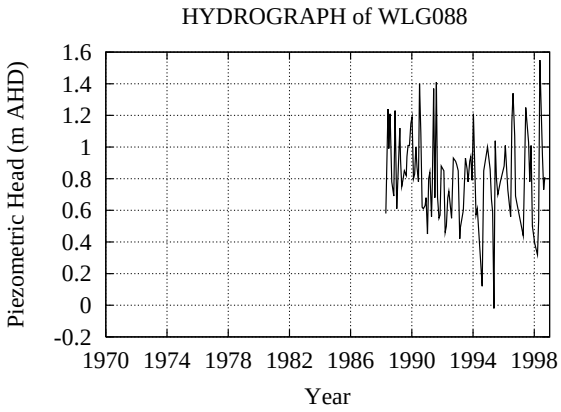
HYDROGRAPH of WLG088
Piezometric Head (m AHD)
1.6
1.4
1.2
1
0.8
0.6
0.4
0.2
0
-0.2
1970 1974 1978 1982 1986 1990 1994 1998
Year

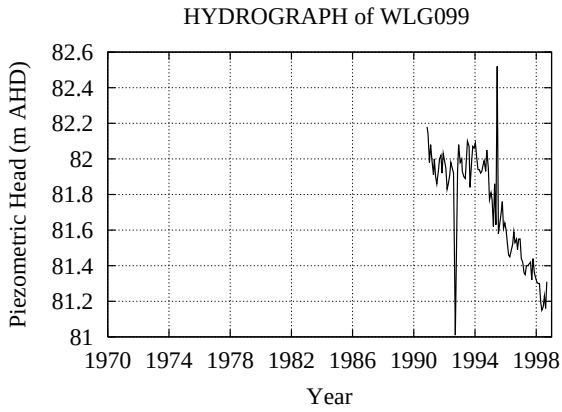
HYDROGRAPH of WLG099
Piezometric Head (m AHD)
82.6
82.4
82.2
82
81.8
81.6
81.4
81.2
81
1970 1974 1978 1982 1986 1990 1994 1998
Year

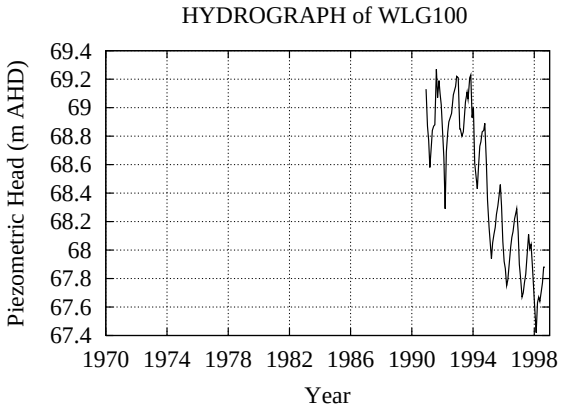
HYDROGRAPH of WLG100
Piezometric Head (m AHD)
69.4
69.2
69
68.8
68.6
68.4
68.2
68
67.8
67.6
67.4
1970 1974 1978 1982 1986 1990 1994 1998
Year

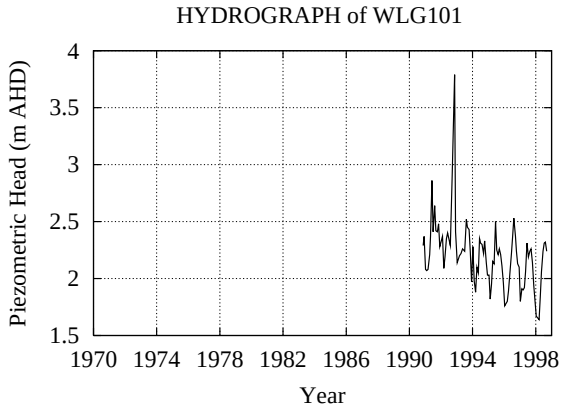
HYDROGRAPH of WLG101
Piezometric Head (m AHD)
4
3.5
3
2.5
2
1.5
1970 1974 1978 1982 1986 1990 1994 1998
Year

Appendix B

Hydrographs of Observation Wells from the Maslin Sands Aquifer.

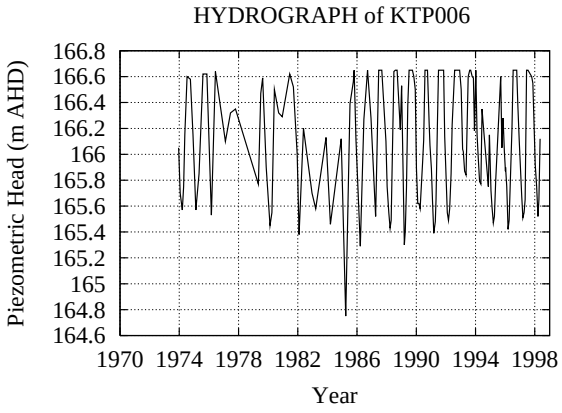

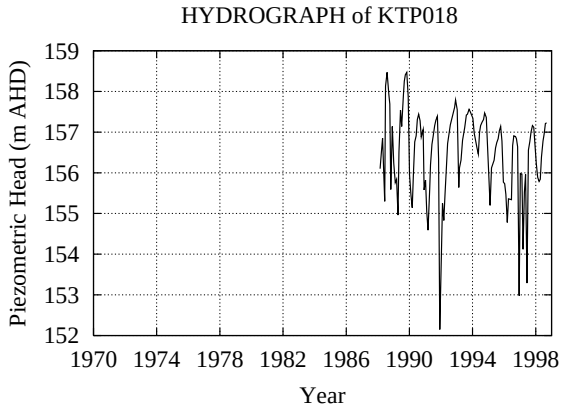

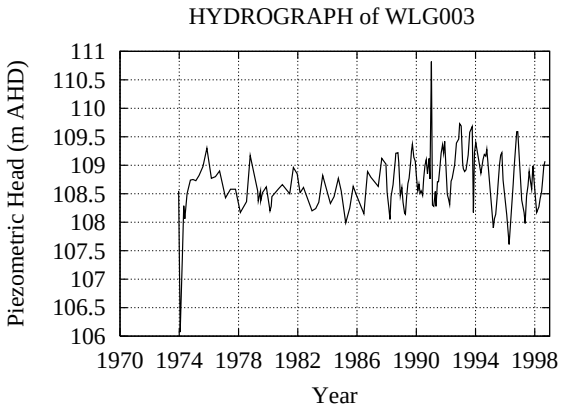

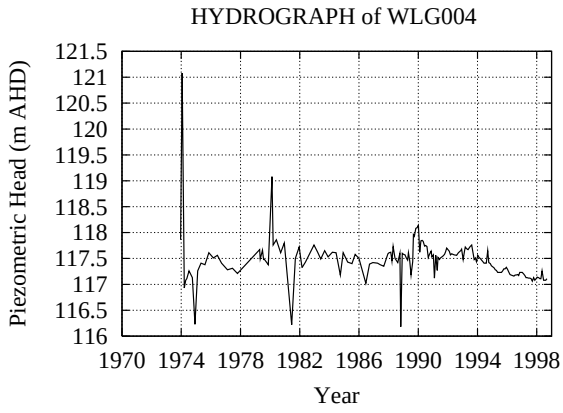

HYDROGRAPH of WLG023

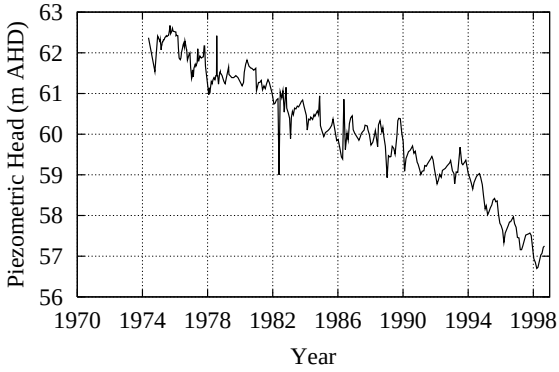

HYDROGRAPH of WLG038

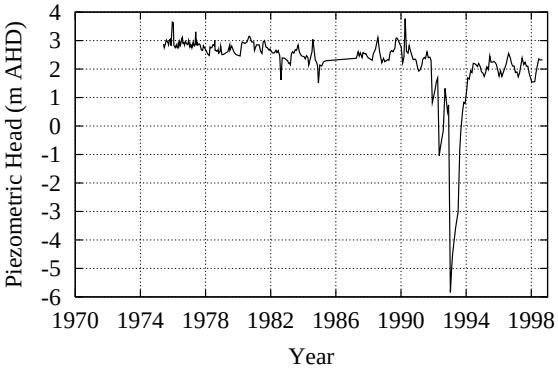

HYDROGRAPH of WLG044

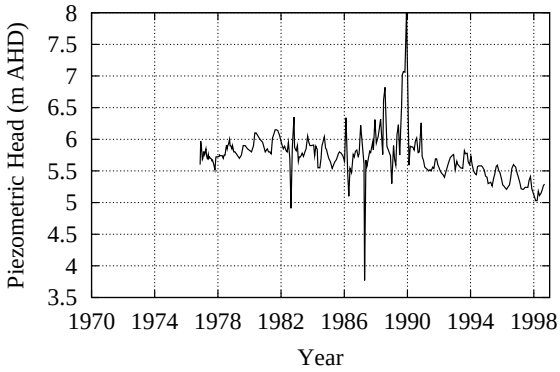

HYDROGRAPH of WLG048

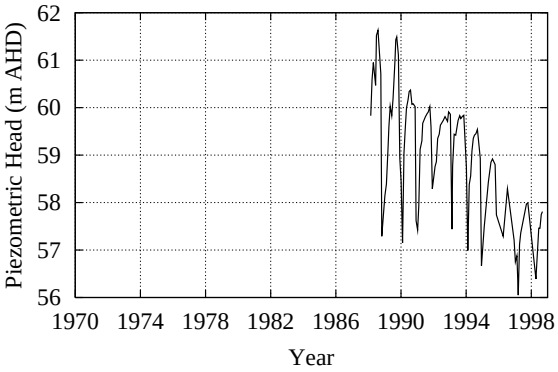

HYDROGRAPH of WLG056

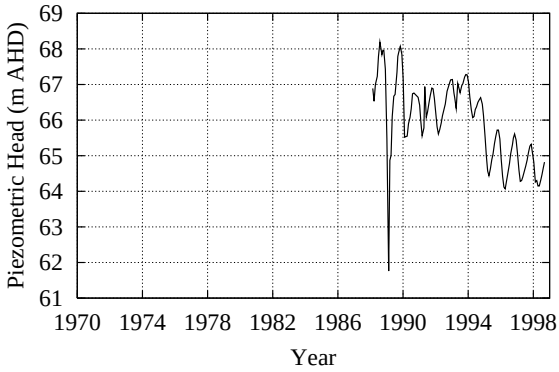

HYDROGRAPH of WLG075

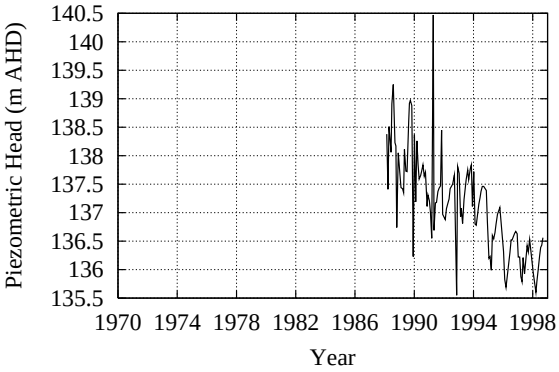

HYDROGRAPH of WLG079

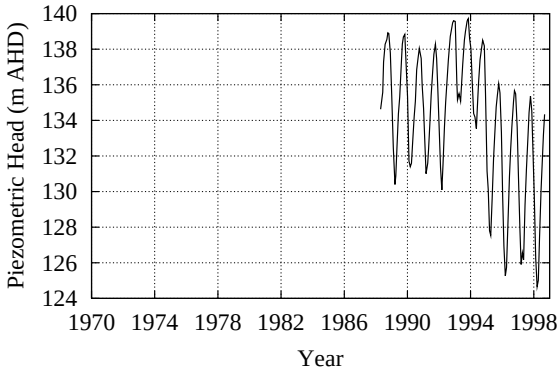

HYDROGRAPH of WLG092

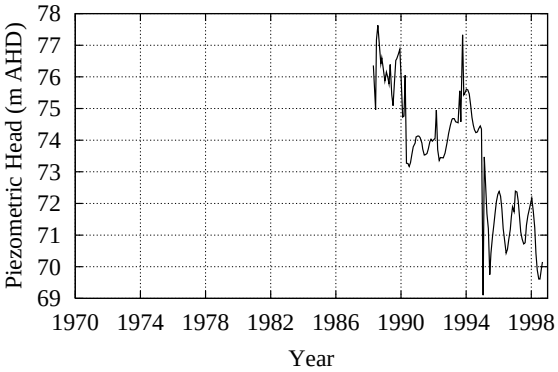

HYDROGRAPH of WLG093

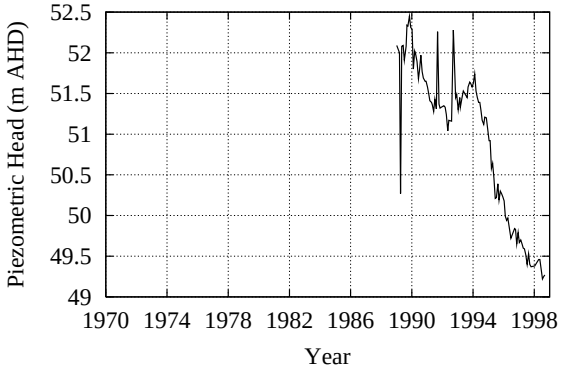

HYDROGRAPH of WLG096

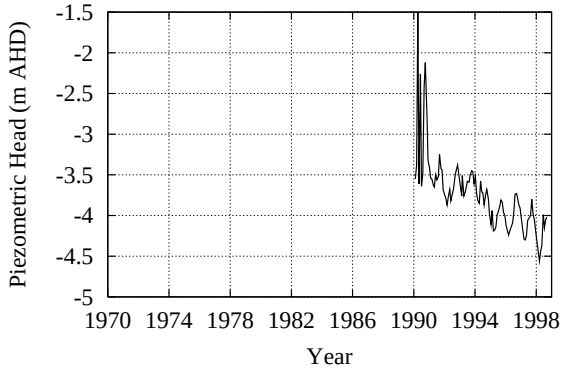

HYDROGRAPH of WLG097

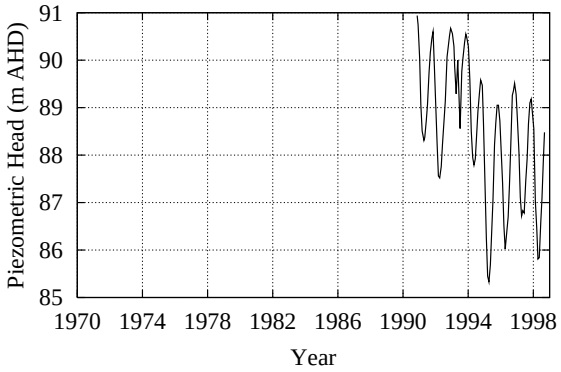

HYDROGRAPH of WLG098

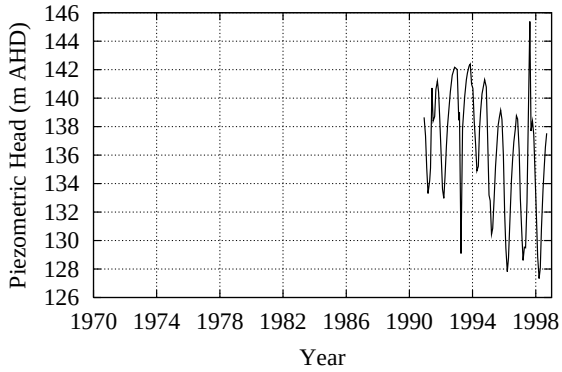

Appendix C

Hydrographs of Observation Wells from the Basement Aquifer.

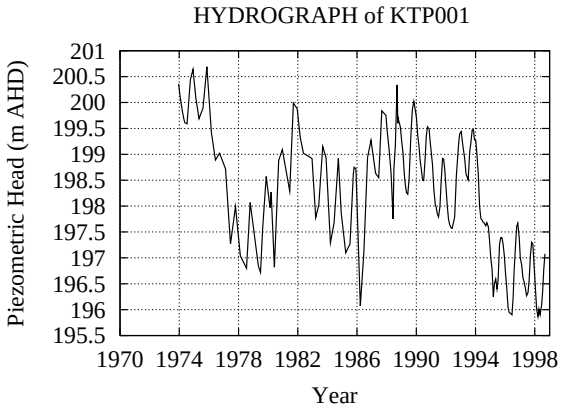

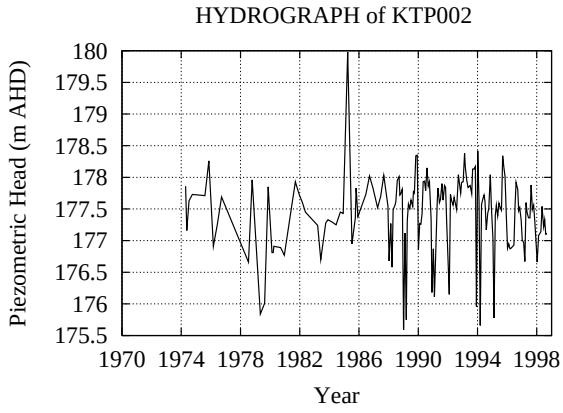

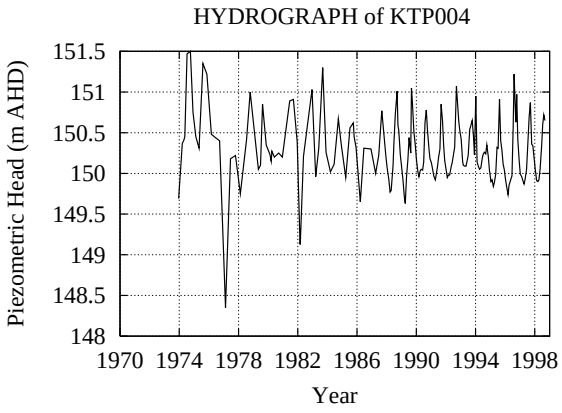

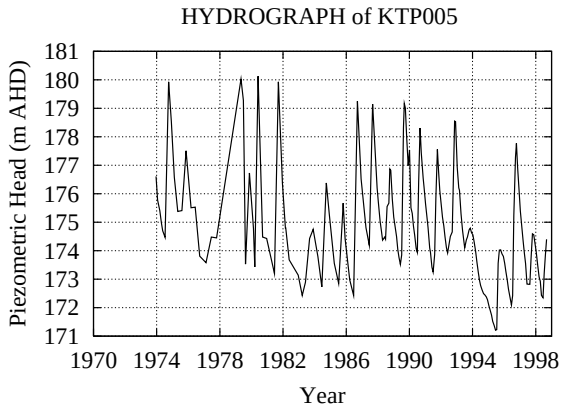

HYDROGRAPH of KTP007

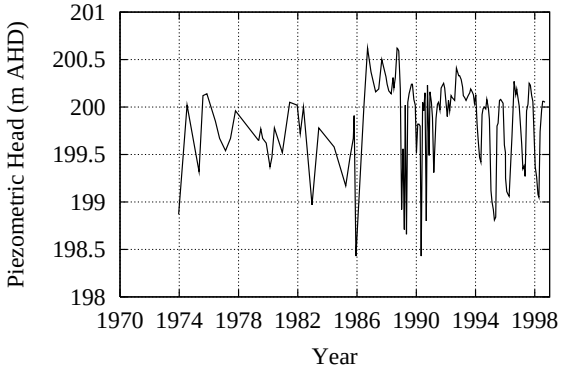

HYDROGRAPH of WLG005

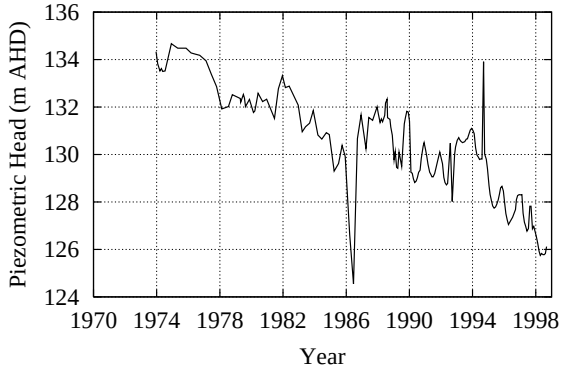

HYDROGRAPH of WLG010

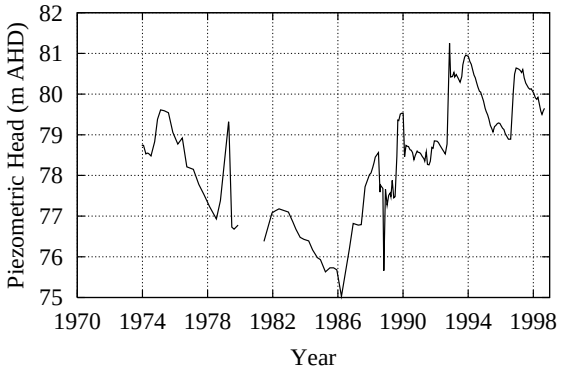

HYDROGRAPH of WLG011

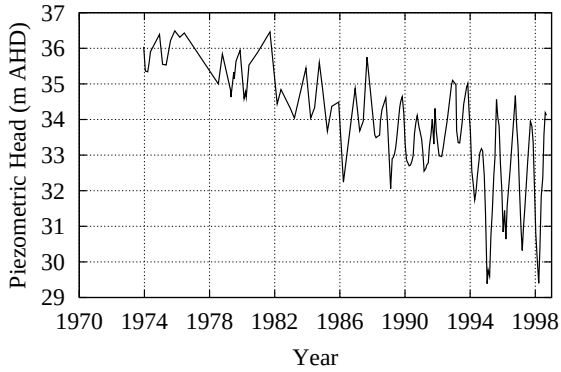

HYDROGRAPH of WLG017

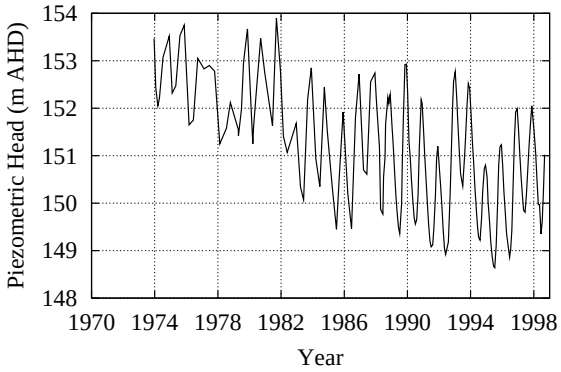

HYDROGRAPH of WLG024

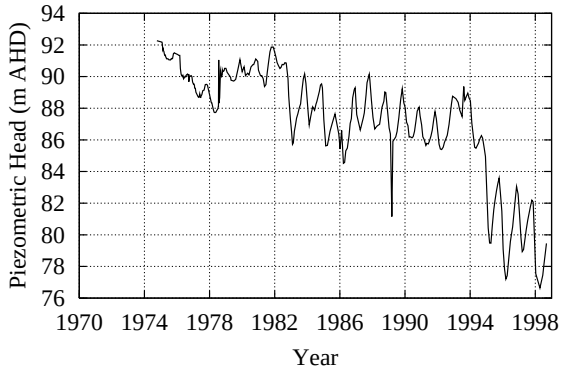

HYDROGRAPH of WLG077

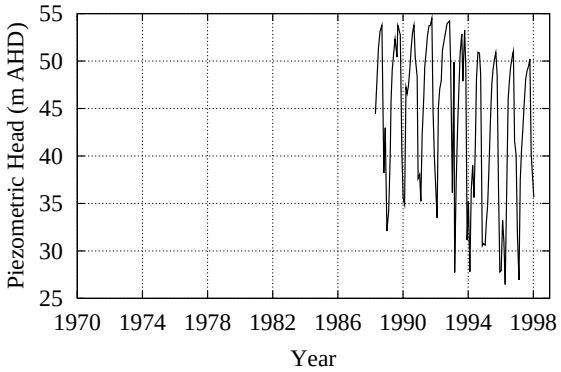

HYDROGRAPH of WLG081

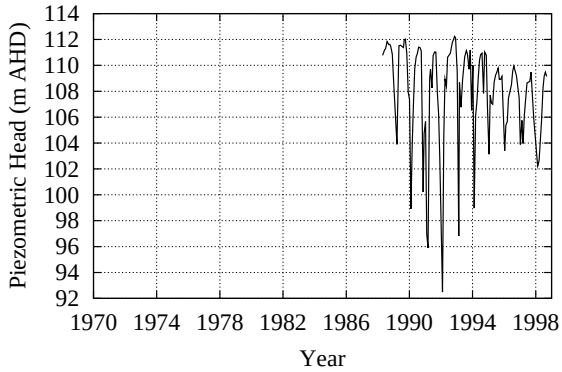

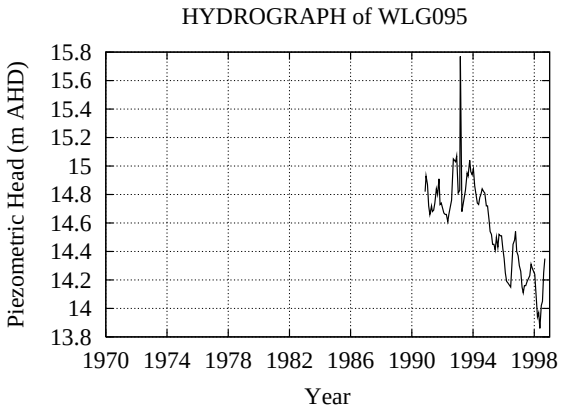
HYDROGRAPH of WLG095
Piezometric Head (m AHD)
15.8
15.6
15.4
15.2
15
14.8
14.6
14.4
14.2
14
13.8
1970
1974
1978
1982
1986
1990
1994
1998
Year

Bibliography

[1] M.P. Anderson and W.W. Woessner. *Applied Groundwater Modelling: Simulation of Flow and Advective Transport*. Academic Press, Inc., 1994.

[2] J. Carrera and S.P. Neumann. Estimation of aquifer parameters under transient and steady state conditions, 2, uniqueness, stability, and solution algorithms. *Water Resources Research*, 22(2):211–227, 1986.

[3] P.M. Clifton and S.P. Neumann. Effects of kriging and inverse modelling on conditional simulation of the Aura Valley in Southern Arizona. *Water Resources Research*, 18(4):1215–1234, 1982.

[4] D.K. Cresswell. Willunga basin integrated water resources study. Technical report, Department of Environment and Natural Resources, South Australia, 1994.

[5] F.A. D'Agnese, C.C. Faunt, M.C. Hill, and A.K. Turner. Death Valley regional ground–water flow model calibration using optimal parameter estimation methods and geoscientific information systems. *Advances in Water Resources*, 22(8):777–790, 1999.

[6] G.F. Feeman and N.R. Grabios. *Linear Algebra and Multivariable Calculus*. McGraw–Hill, 1970.

[7] R. Fletcher. *Practical Methods of Optimization*. John Wiley & Sons, 1980.

[8] R.A. Freeze and J.A. Cherry. *Groundwater*. Prentice Hall, 1979.

[9] A.W. Harbaugh and M.G. McDonald. *User's Documentation for MODFLOW–96, an update to the U.S. Geological Survey Modular Finite–Difference Ground–Water Flow Model*. U.S. Geological Survey, Reston, Virginia, Open–File Report 96–485, 1996.

[10] M.C. Hill. Methods and guidelines for effective model calibration: U.S. Geological Survey Water-Resources Investigations Report 98-4005. Technical report, U.S. Geological Survey, 1998.

[11] S. Howles. Personal communication, 1998.

[12] M. Inoue, J. Simunek, S. Shiozawa, and J.W. Hopmans. Estimation of aquifer parameters under transient and steady state. *Advances in Water Resources*, 23:677–688, 2000.

[13] E. Kreyszig. *Advanced Engineering Mathematics.* John Wiley and Son, 7th edition, 1999.

[14] L. Lapidus and G.F. Pinder. *Numerical Solutions of Partial Differential Equations in Science and Engineering.* J. Wiley & Sons, 1982.

[15] H. Li and Q. Yail. A least squares penalty algorithm for inverse problems of steady–state aquifer models. *Advances in Water Resources*, 23:867–880, 2000.

[16] D.W. Marquardt. An algorithm for least–squares estimation of non–linear parameters. *J. Soc. Indust. Appl. Math.*, 11(2):431–441, 1963.

[17] R.R. Martin. Willunga Basin–status of groundwater resources 1998. Technical Report Book 98/28, Department of Primary Industries and Resources SA, 1998.

[18] E.P. Poeter and M.C. Hill. Inverse Models - A Necessary Next Step in Ground-Water Modelling. *Ground Water*, 35(2):250–260, 1997.

[19] T.A. Prickett and C.G. Lonnquist. *Selected Digital Computer Techniques for Groundwater Resource Evaluation.* Illinois State Water Survey, Urbana, Bulletin 55, 1971.

[20] P.E. Rasser and M.D. Teubner. Groundwater model of the Willunga Basin using automated calibration. In B.J. Noye, M.D. Teubner, and A.W. Gill, editors, *Computational Techniques and Applications: CTAC–97*, pages 569–576. World Scientific, 1998.

[21] J. Rodert and M.D. Teubner. Groundwater modelling of the Wanilla Catchment using flownets. In *Water 99*, pages 637–642. The Institute of Engineers, Australia, 1999.

[22] A. Sciortino, T.E. Harmon, and W.W-G. Yeh. Inverse modelling for location of dense nonaqueous pools in groundwater under steady flow conditions. *Water Resources Research*, 36(7):1723–1735, 2000.

[23] J. Segerlind. *Applied Finite Element Analysis*. John Wiley and Son, 1984.

[24] N-Z Sun. *Inverse Problems in Groundwater Modelling*, volume 6. Kluwer Academic, 1994.

[25] M.D. Teubner. Personal communication, 1995.

[26] M.D. Teubner. Personal communication, 2001.

[27] M.D. Teubner, P.E. Rasser, and B.J. Noye. Systematic approach to calibrating hydrodynamic numerical models. In R.L. May and A.K. Easton, editors, *Computational Techniques and Applications: CTAC–95*, pages 763–770. World Scientific, 1996.

[28] D.K. Todd. *Groundwater Hydrology*. John Wiley and Son, 1980.

[29] V. Vasarelli. Personal communication, 2001.

[30] N.L. Watkins. Personal communication, 1996.

[31] N.L Watkins. Personal communication, 1997.

[32] N.L. Watkins and A.L. Telfer. Willunga Basin review of hydrogeology and water budget. Technical Report Book 95/4, Department of Mines and Energy SA, 1995.

[33] W.W. Yeh. Review of parameter identification procedures in groundwater hydrology: The inverse problem. *Water Resources Research*, 22(1):95–108, 1986.